TAMPEREEN TEKNILLINEN YLIOPISTO
TAMPERE UNIVERSITY OF TECHNOLOGY

SUVI SUOJANEN

DEVELOPMENT OF CONCENTRATED SOLAR POWER AND CONVENTIONAL POWER PLANT HYBRIDS

Master of Science thesis

Examiners: prof. Jukka Konttinen
pm. Yrjö Majanne
Examiners and topic approved by the Faculty Council of the Faculty of Natural Sciences
on 04th November 2015

ABSTRACT

SUVI SUOJANEN: Development of concentrated solar power and conventional power plant hybrids
Tampere University of technology
Master of Science Thesis, 140 pages, 13 Appendix pages
March 2016
Master's Degree Programme in Environmental and Energy Engineering
Major: Energy and Biorefining Engineering
Examiners: professor Jukka Konttinen and project manager Yrjö Majanne

Keywords: concentrated solar power (CSP), hybrid, direct steam generation (DSG), dynamic modelling and simulation (DMS), Apros

CSP hybrids are one of the possible technical solutions in order to increase the share of renewable energy and decrease greenhouse gas emission levels as well as fuel consumption. The main objectives of the thesis are to research state-of-the-art technologies in concentrated solar power (CSP) and conventional power plants, to comprehensively study the possible integration options and to develop one CSP hybrid configuration by using Advanced Process Simulator (Apros), which is a dynamic modelling and simulation tool for industrial processes. Furthermore, the objectives are to develop control strategy for the hybrid and demonstrate the operation of the hybrid under steady state and transient conditions in order to find challenges of hybrid systems and future development requirements. The theory is based on the available scientific literature for CSP, conventional power plants and CSP hybrids as well as on the information available from companies and organizations working with the technologies. The model development is based on the theoretical background as well as the know-how of VTT about Apros.

Based on the simulations, solar steam fed to the joint high pressure turbine increases thermal efficiency and changes the thermal balance of the steam cycle. In addition, attainable solar shares are studied, in which design values of live steam and reheated steam temperatures of steam boiler are reached. Furthermore, as the steam generation is decreased from the solar field, transients can be seen in steam mass flows to turbines, power output of the turbines and steam temperatures and pressures. However, the modelled transients could be compensated with the steam boiler and the transients are acceptable for turbines. Based on the conducted research, the main challenges of the hybrid system are identified. These are, for example, attainable solar shares, design of the steam parameters in solar field and steam boiler and combination of the two steam lines, imbalance between turbines and heat surfaces, optimization of heat surfaces and operation of steam boiler under fluctuating solar irradiation conditions.

The developed and modelled CSP hybrid seems to be technically feasible at least with smaller solar shares. However, the hybrid system requires more research. Thus, future development requirements include, for example, improvement of the control engineering of the hybrid, research on the optimal hybrid configuration and on the possibilities to reach higher solar shares, transient simulations with higher solar shares and conducting exergy and economic analyses for the hybrid system. As a conclusion, the achieved results and the developed model in this thesis provide viable information for the future development of CSP hybrids.

TIIVISTELMÄ

SUVI SUOJANEN: Keskittävän aurinkovoiman ja perinteisen voimalaitoksen hybridin kehitys
Tampereen teknillinen yliopisto
Diplomityö, 140 sivua, 13 liitesivua
Maaliskuu 2016
Ympäristö ja energiatekniikan diplomi-insinöörin tutkinto-ohjelma
Pääaine: Energia- ja biojalostustekniikka
Tarkastajat: professori Jukka Konttinen ja projektipäällikkö Yrjö Majanne

Avainsanat: keskittävä aurinkovoima (CSP), hybridi, suora höyryntuotanto, dynaaminen mallinnus ja simulointi, Apros

CSP hybridit ovat yksi mahdollisuus lisätä uusiutuvan energiantuotannon osuutta ja vähentää kasvihuonekaasupäästöjen määrää sekä alentaa fossiilisten polttoaineiden kulutusta. Diplomityön tavoitteena on tarkastella keskittävän aurinkovoiman ja perinteisten voimalaitosten teknologioita, vertailla kattavasti laitosten mahdollisia integrointiratkaisuja ja kehittää yksi hybridikonfiguraatio käyttäen Aprosta, joka on dynaaminen mallinnus- ja simulointiohjelma teollisille prosesseille. Lisäksi tavoitteena on kehittää hybridilaitoksen säätötekniikkaa ja simuloida laitoksen toimintaa useilla testitapauksilla, jotta hybridilaitoksen haasteet saadaan selville ja jatkotoimenpiteet voidaan määritellä. Teknologiatarkastelut perustuvat saatavilla olevaan tieteelliseen kirjallisuuteen keskittävästä aurinkovoimasta, perinteisistä voimalaitoksista ja hybridiratkaisuista. Lisäksi työssä hyödynnetään alan toimijoilta saatavissa olevaa informaatiota. Mallin kehitys puolestaan pohjautuu teoreettiseen taustaan sekä VTT:n tietotaitoon Apros-ohjelmasta.

Simulaatioiden perusteella aurinkohöyryn syöttäminen yhteiseen korkeapaineturbiiniin nostaa laitoksen hyötysuhdetta ja muuttaa höyrypiirin sisäistä tasapainoa. Lisäksi työssä on tutkittu saavutettavia aurinko-osuuksia, joissa tuorehöyryn ja välitulistetun höyryn lämpötilojen suunnitteluarvot saavutetaan. Höyryntuotannon alentuessa aurinkokentällä gradientteja ilmenee höyryn massavirroissa turbiinille, laitoksen sähkötehossa sekä höyryn lämpötiloissa että paineissa. Mallinnetut gradientit ovat kuitenkin kompensoitavissa höyrykattilalla ja ne ovat turbiinille sallituissa raja-arvoissa. Lisäksi hybridilaitoksen olennaiset haasteet on tunnistettu tehdyn tutkimuksen perusteella. Näitä ovat esimerkiksi saavutettavat aurinko-osuudet, aurinkokentän ja höyryvoimalaitoksen höyrynarvojen yhteensovittaminen ja höyryvirtojen yhdistäminen, höyrylaitoksen lämpöpintojen optimointi ja höyrykattilan toiminta vaihtelevissa säteilyolosuhteissa.

Kehitetty ja mallinnettu hybridilaitos näyttäisi olevan teknisesti toteutettavissa ainakin pienillä aurinko-osuuksilla. Toimivan hybridilaitoksen kehittäminen vaatii kuitenkin jatkotutkimusta, joten tulevaisuuden kehitystoimenpiteitä ovat esimerkiksi hybridilaitoksen säätötekniikan kehitys, optimaalisen hybridilaitoksen ja suurempien aurinko-osuuksien tutkimus, transienttisimulaatiot suurilla aurinko-osuuksilla ja exergia-analyysin sekä taloudellisten analyysien teko. Johtopäätöksenä voidaan todeta, että työssä saavutetut tulokset ja suunniteltu malli antavat hyvän pohjan CSP hybridilaitoksien jatkokehitykselle.

PREFACE

The Master thesis "Development of concentrated solar power and conventional power plant hybrids" has been conducted for VTT Technical Research Centre of Finland under the project called "Combination of Concentrated Solar Power with Circulating Fluidized Bed Power Plants". The research of the thesis was conducted from June 2015 to December 2015. First of all, the topic of the thesis was a dream come true, as one of the special interests of mine is the addition of renewable energy technologies in order to prevent climate change. In addition, the researcher exchange during the Master thesis at the German Aerospace Centre was another dream come true. Thus, I would like to express my greatest gratitude towards the staff of VTT at Jyväskylä, Finland as well as towards the staff at the line focus department of DLR at Stuttgart, Germany for this amazing possibility, which was very rewarding.

In addition, I would like to especially express my gratitude towards the people, who have supported and given me instructions during the thesis. First of all, I would like to express my warmest gratitude towards my supervisors at VTT, Matti Tähtinen and Elina Hakkarainen, for the daily support, instructions and comments of the work. In addition, I would also like to express my warmest gratitude towards my supervisor at DLR, Jan Fabian Feldhoff, for the daily support and guidance during my stay at DLR. Furthermore, I am grateful of the guidance given by the examiners of this thesis, professor Jukka Konttinen and project manager Yrjö Majanne. Moreover, I would like to direct special thanks to Hannu Mikkonen, Jouni Hämäläinen, Teemu Sihvonen and Tomi Thomasson at VTT for all the help and support during this project.

As one door is closed, at least two more are opened. The five years spent at Tampere University of technology have been full of new people and friendships, unforgettable moments and finding my professional interests. Therefore, I would also express my gratitude towards friends and faculty met at TUT for the joy, support and guidance throughout my studies. Most of all, I would like to thank my loving family from the bottom of my heart for all the caring and support in good times and in bad times. Especially, I would like to thank my grandmother, Soile, for all the support during my studies. I really don't know what I would have done without it. And last but not least, I would like to thank my loving boyfriend, Vesa, for being my rock for all these years.

Sometimes I'm quite astonished about the journey that has brought me to this day, but I wouldn't change a single day of it.

Jyväskylä, January 31st, 2016

Suvi Suojanen

CONTENTS

LIST OF ABBREVIATIONS AND SYMBOLS

Abbreviations

2DS	2 °C Scenario created by IEA
6DS	6 °C Scenario created by IEA
Apros	Advanced Process Simulator
BFB	bubbling fluidized bed
CC	combined cycle
CCS	carbon capture and storage
CFB	circulating fluidized bed
CFD	computational fluid dynamics
CLFR	compact linear Fresnel reflector
CRH	cold reheating line
CSP	concentrated solar power
CO_2	carbon dioxide
DISS	European Direct Solar Steam
DLR	Deutsche Zentrum für Luft- und Raumfahrt, *engl.* German Aerospace Center
DMS	dynamic modelling and simulation
DNI	direct normal irradiance
DSG	direct steam generation
DUKE	Development and demonstration of once-through concept
EIB	European Investment Bank
EPA	the United States Environmental Protection Agency
EPS	emission performance standard
ETP 2014	Energy Technology Perspectives 2014
EU	European Union
FBC	fluidized bed combustion
FC	forced circulation
FCL	flow control loop
FIC	flow indication and control
FT	flow transmitter
FWH	feedwater heater
FWHBOS	feedwater heating, in which superheated steam from solar field is fed into bled of steam line
FWHFL	feedwater heating, in which solar field produces heated feedwater
hi-Ren	high renewable scenario created by IEA
HP	high pressure
HTF	heat transfer fluid
IEA	International Energy Agency
IP	intermediate pressure
IRENA	International Renewable Energy Agency
LC	level control loop
LCOE	levelized costs of electricity
LFR	linear Fresnel reflector
LIC	level indication and control
LP	low pressure
LT	level transmitter

M	motor
MIC	multiple variable indication and control
Mtoe	megaton oil equivalent
MY	multiple variable calculating function
NC	natural circulation
NO_x	nitrogen oxide
OT	once-through
O&M	operation and maintenance
PC	pressure control loop
PCC	pulverized coal combustion
PD	parabolic dish
PDC	pressure drop control loop
PDT	pressure drop transmitter
PE1	Puerto Errado 1 power plant
PE2	Puerto Errado 2 power plant
PIC	pressure indication and control
PID	proportional-integral-derivative
PT	pressure transmitter
PTC	parabolic trough collector
PV	photovoltaics
R&D	research and development
RH 1	primary reheater
RH 2	secondary reheater
s	set point
SaSBD	saturated steam from solar field is fed into the boiler drum
SaSBDFWH	saturated steam from solar field is fed into the boiler drum combined with feedwater heating
SC	supercritical
SH 1	primary superheater
SH 2	secondary superheater
SH 3	tertiary superheater
SO_2	sulphur dioxide
STC	solar tower collector
STE	solar thermal energy
SuSCRH	superheated steam from solar field is fed into cold reheat line after HP turbine
SuSHP	superheated steam from solar field is fed into the inlet of HP turbine
SuSIP	superheated steam from solar field is fed into the inlet of IP turbine
TC	temperature control loop
TIC	temperature indication and control
TSE1	Thai Solar Energy 1 power plant
TT	temperature transmitter
TY	temperature calculating function
USC	ultra-supercritical
USD	United States dollar

Subscripts

0	design value
e	electric
i	inlet
I	first
j	source
o	outlet
st	isentropic
th	thermal

Symbols

E_i	energy entering the system	[J]
E_o	energy leaving the system	[J]
h	specific enthalpy	[J/kg]
$\dot{m}$	mass flow	[kg/s]
Q	heat transfer to the system	[W]
$\dot{Q}_{th}$	thermal power	[W_{th}]
p	steam pressure	[bar]
T	temperature	[°C]
W	net work done by the system	[W]
x_{solar}	thermal solar share	[%]
η_I	first law efficiency	[-]
η_{st}	isentropic efficiency	[-]
η_{th}	thermal efficiency	[-]

1. INTRODUCTION

Concentrated solar power (CSP) focuses solar irradiation in order to transfer energy from the irradiation to the heat transfer fluid (HTF), which is then applied to a power cycle in order to produce electricity. CSP has been attracting more and more attention due to the characteristics of solar irradiation as a clean, free and non-exhausting source of energy. However, solar irradiation has relatively low intensity, intermittency and periodicity, the costs of CSP production are still high (Figure 1) and the share of CSP is relatively small compared to fossil fuels as a primary energy source. On the other hand, conventional power plants are still the main alternative in the electricity production, but their environmental impacts are being criticized, such as pollutions, greenhouse gas emissions and reduction of fossil fuel resources. The integration of CSP and conventional power plants could reduce the costs of CSP plants while helping the conventional power plants to meet their carbon dioxide (CO_2) emission limits. (Hong-juan et al. 2013, p.710) In the following Chapter 1.1, the background for the thesis is presented. Based on the background, the research questions, objectives and delimitations are defined (Chapter 1.2). Then, the research methodology and materials as well as the structure of the thesis are presented (Chapter 1.3 and Chapter 1.4) before the introduction of the companies related to the conduct of the thesis (Chapter 1.5 and Chapter 1.6).

1.1 Background

According to International Energy Agency (IEA), almost all existing CSP plants use back-up power stations. IEA calls these plants as CSP hybrids in addition to the power plants, in which CSP and conventional power plants are co-operated parallel through a joint power cycle in order to produce electricity. (International Energy Agency 2014a, p.14) In this thesis, the term CSP hybrid is associated with co-operative parallel power plants. Currently, there are nine operational CSP hybrids, as shown in Appendix A. According to CSP World Map, seven of these plants are integrated with a combined cycle (CC) power plant, one with a biomass-fired power plant and one with a coal-fired power plant. In addition, there are at least three CSP hybrids under construction, from which two are integrated with CC plant and one with a coal-fired power plant. Furthermore, there are at least seven CSP hybrids under development or planned, from which six are integrated with CC plants and one is integrated with a gas and coal fired-unit. (CSP World 2015) There are numerous aspects, which affect the utilization of CSP in conventional power plants. These are, for example, the current use of CSP and fossil fuels and their future perspectives (Chapters 1.1.1 and 1.1.2) as well as current legislation, emis-

sion performance standards (EPS) and the needed reduction of CO_2 emission level (Chapter 1.1.3).

1.1.1 The use of concentrated solar power and future perspectives

Solar irradiation is the largest available carbon-neutral energy source, as one hour of solar irradiation on the surface of Earth corresponds to the energy consumption of one year (Zhang et al. 2013, p.467). However, CSP plants can exploit only direct normal irradiance (DNI) of solar irradiation, which is the solar irradiation on surface perpendicular to the sun beam (International Energy Agency 2014a, p.10). The annual average DNI levels around the world can be seen from the map in Appendix B. DNI is sensitive to atmospheric absorption caused by clouds and aerosols as well as to the scattering caused by the surface of earth. Therefore, areas with high DNI level can be found in hot and dry regions with clear skies and low aerosol optical depths, as can be seen from Appendix B. (International Energy Agency 2014a, p.10) Typically, stand-alone CSP plants require annual average DNI level over 2000 kWh/m^2/year, and the most promising areas locate on the "solar belt" between 20 to 40 degrees latitude north and south (Petrov et al. 2012, p.2). These are, for example, the North African desert, South Africa, Central and Western Australia, the Southwest United States and Southern Spain. In the case of CSP hybrids, even broader areas may be considered, as the power production is supported by the conventional power plant. CSP hybrids can be located in areas where the annual average DNI level is over 1700 kWh/m^2/year. (Peterseim et al. 2013, p.521)

Currently, CSP presents only a fraction of the consumed total primary energy supply. In June 2015, there was 4.4 GW of installed CSP capacity in the world, as shown in Appendix C (SolarPACES 2015). The installed CSP capacity is approximately 0.07% of the world's installed power generation capacity (World Energy Council 2013, p.10), and about 40 times less than the installed capacity of photovoltaic (PV), which was 177 GW at the end of 2014 (International Energy Agency 2015a, p.4). The low share of CSP is mainly due to a gradual learning curve of the technology (Petrov et al. 2012, p.2), expensive costs of the technology (Peterseim et al. 2013, p.520) and the current economic and financial crisis. The costs of different power plants can be compared with each other by using levelized costs of electricity (LCOE), which consists of fixed and variable costs of a certain power generating technology per unit of produced electricity. Thus, the LCOE is often expressed as United States dollar per megawatt hour (USD/MWh). The International Renewable Energy Agency (IRENA) represents that the LCOE of CSP in utility-scale was in the range of 170 to 280 USD/MWh in 2014. On the other hand, the LCOE of fossil fuel-fired power plants was in the range of 45 to 140 USD/MWh, and the LCOE of PV was in the range of 60 to 400 USD/MWh, as can be seen from Figure 1. (IRENA 2015, p.12) However, the LCOE does not represent the overall economic balance of power plants, as the site-specific aspects are not included in

the LCOE value. These are, for example, local markets, quality and availability of local infrastructure, distance between the power plant and the existing infrastructure and local labour rates (IRENA 2015, p.14).

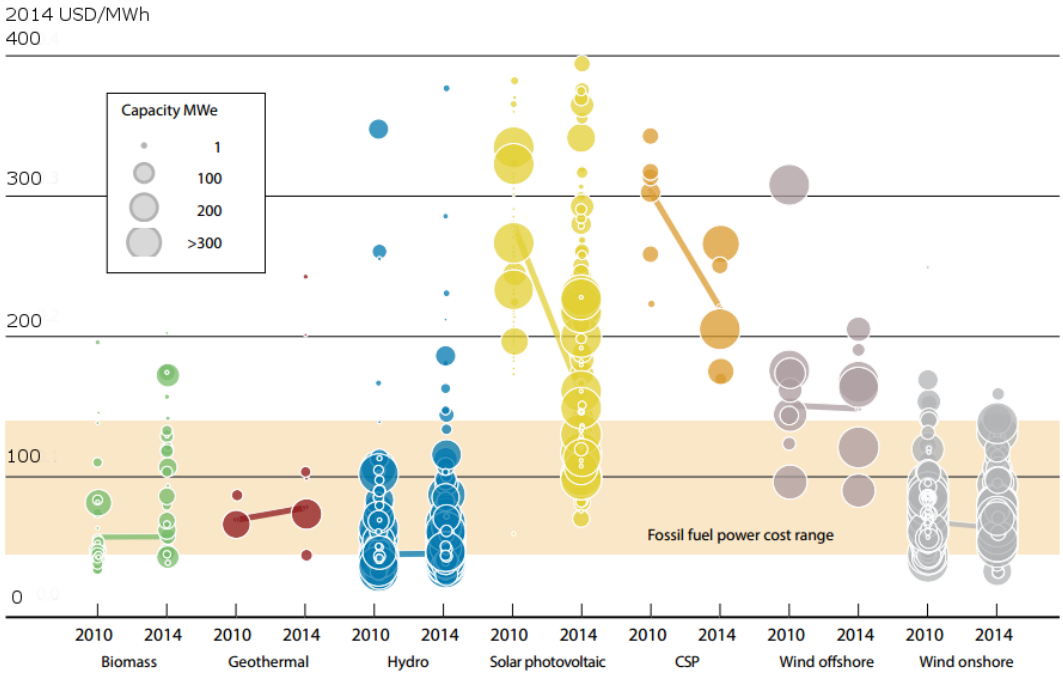

Figure 1. *The LCOEs from utility scale-renewable technologies in 2010 and 2014. Adapted from IRENA 2015, p.12.*

On the other hand, the capacity of installed CSP has grown over 10-fold from 2004 to the end of 2014 (Figure 2). The market leaders are clearly Spain (2.3 GW) and the United States (1.63 GW), but CSP capacity is especially growing in India, Middle East, North Africa, Australia, South Africa, Chile and China. (International Energy Agency 2014a, p.9) Currently, there is 1.39 GW of capacity under construction and 4.3 GW is being developed, as shown in Appendix C (SolarPACES 2015).

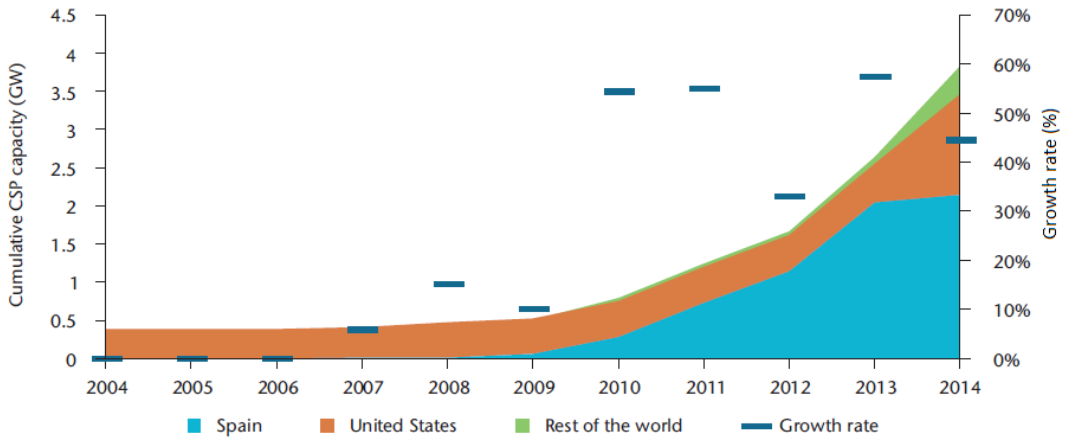

Figure 2. *The installed global capacity of CSP from 2004 to 2014 (International Energy Agency 2014a, p.9).*

The extensive growth of CSP capacity in the recent years is due to activities in research and development, test and prototyping. In addition, the capacity has grown due to admitted financial incentives, such as feed-in-tariffs, tax reliefs and capital cost grants. (Behar et al. 2013, p.16) However, the exploitation of CSP faces challenges, such as comparatively high investment costs for stand-alone CSP power plants and rapid deployment and decreased costs of PV. In addition, the exploitation of CSP does not happen overnight, since investment decisions are usually made for decades. On the other hand, CSP is considered to be competitive, since it can generate dispatchable energy. (Peterseim et al. 2013, p.520) Furthermore, World Energy Council estimated in 2012, that the LCOE of CSP could be reduced to 120-150 USD/MWh over the ten year period from 2012 to 2022, if the technology is widely deployed (World Energy Council 2013, p.22). In addition, the IEA estimates in their high renewables scenario (hi-Ren) that CSP could represent about 11% of total electricity generation in 2050. This means that the capacity of installed CSP should be increased from 4.4 GW to 980 GW if the costs of CSP technology can be lowered. (International Energy Agency 2014a, p.19-21) However, according to the study conducted by Lappeenranta University of Technology and by the German organization Energy Watch Group, the IEA has underestimated the growth of renewable energy. For example, the estimation of the solar PV capacity conducted in 2010 for the year 2024 was reached in the beginning of 2015. (Metayer et al. 2015, p.6 & p.23)

1.1.2 The use of fossil fuels, the level of CO_2 emissions and future perspectives

In 2012, about 81.7% of world's primary energy was produced with fossil fuels. The share of coal was 29%, oil 31.4% and natural gas 21.3%. About 70% of electricity was produced with fossil fuels, and the share of coal was 40.4%, oil 5% and natural gas 22.5%. (International Energy Agency 2014b, p.6 & p.24) From these energy sources,

the use of coal as energy source is still increasing (Figure 3), as it is a more delocalized and inexpensive energy source than oil and natural gas (Franco et al. 2009, p.348-349). In addition, coal consumption increases as industrializing countries, like China and other Asian countries, need to increase their energy production capacities (International Energy Agency, 2014b, p.45). Therefore, coal is likely to remain as a source of primary energy for a long time.

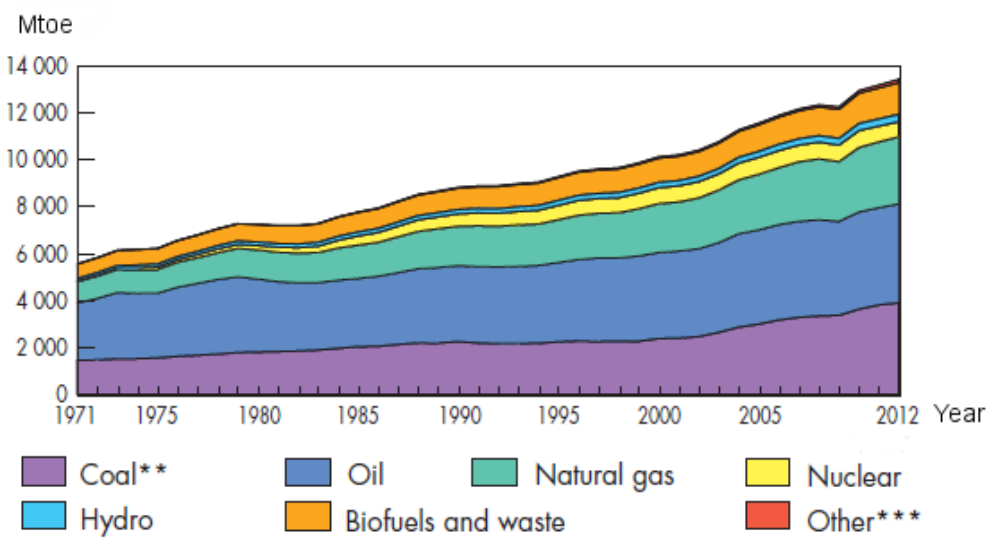

Figure 3. *Total primary energy supply from 1971 to 2012 by fuel as megaton oil equivalent (Mtoe). Figure includes also aviation and international marine bunkers. Coal** includes peat and oil shale and Other*** consists of geothermal, solar, wind etc. (International Energy Agency, 2014b, p.6).*

On the other hand, the CO_2 emission level has doubled from the 1971 to 2012 (Figure 4). In 2012, the CO_2 emissions from coal combustion were 13,930 $MtCO_2/a$, from oil combustion 11,200 $MtCO_2/a$, from natural gas combustion 6,400 $MtCO_2/a$, and from others 160 $MtCO_2/a$ (International Energy Agency 2014b, p.44).

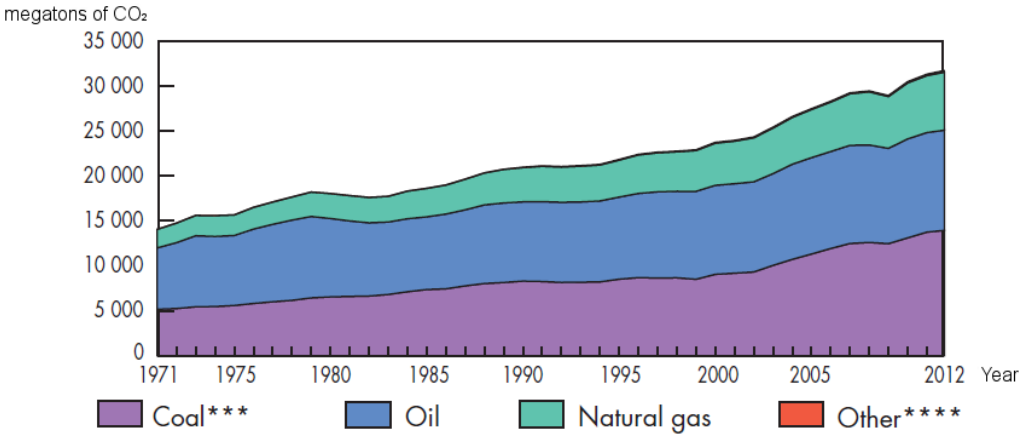

Figure 4. *CO_2 emissions from 1971 to 2012 by fuel. The figure includes also aviation and international marine bunker. CO_2 emissions are calculated for only combustion fuels and using IEA's energy balances. Coal*** includes peat and oil shale and Others **** industrial waste and non-renewable municipal waste (International Energy Agency 2014b, p.44).*

The CO_2 emission level is still increasing according to Energy Technology Perspectives 2014 (ETP 2014) done by the IEA. The ETP 2014 includes three different scenarios, which are the 6 °C Scenario (6DS), the 2 °C Scenario (2DS) and the hi-Ren Scenario. The 6DS is the base-case scenario, in which energy demand would increase by more than two-thirds between 2011 and 2050. This would increase the global mean temperature up by 6 °C. In the 2DS, the increase of global mean temperature is limited to 2 °C due to changes in energy production, which include, for example, the deployment of renewable energy systems. In the hi-Ren scenario, even larger share of renewables are deployed, such as PV, solar thermal energy (STE) and wind energy. In the 6DS, the annual CO_2 emissions would be about 22,000 $MtCO_2$/year in 2050, which is nearly double the amount in 2012. On the contrary, the amount of annual CO_2 emissions could be decreased to 1,000 $MtCO_2$/year according to the hi-Ren scenario, in which IEA estimates that 9% of CO_2 emission reductions in the power sector over the next 35 years can be achieved by exploitation of STE from CSP plants. (International Energy Agency 2014a, p.19-20) In addition to ETP 2014, The United Nations conference on climate change was held from November 30th to December 11th 2015 in Paris. The conference confirmed a target, in which the rise of the global temperature should be kept under 2 °C. Thus, it set a new target to limit the temperature rise to 1.5 °C instead of 2 °C. (United Nations 2015)

1.1.3 Legislation emission performance standards and needed reductions of CO_2 emissions

The use of different energy sources can be controlled, for example, through legislation and emission performance standards (EPS). One example of the legislation is conducted by the European Union (EU), which is working hard to cut down its greenhouse gas

emission levels. The directive 2009/28/EC of the European Parliament and of the Council set the targets known as "20-20-20" targets, which include three key objectives for 2020. First target considers the share of renewable energy, which should cover 20% of the EU's energy consumption. Secondly, the energy efficiency has to be increased to 20%, and final target is the reduction of CO_2 emission level by 20% from the 1990 level. In addition, each EU member state had to establish a national renewable energy action plan, in which the technical pathways are identified in order to reach the "20-20-20" targets. Since EU is well on track to reach "20-20-20" targets, the European Council has set a framework for climate and energy policy for the period 2020-2030. This framework presents three targets for 2030. Firstly, the domestic greenhouse gas emissions need to be reduced at least 40% from the 1990 level. Secondly, renewable energy should cover 27% of the EU's energy consumption. Finally, the energy efficiency needs to be increased to 27%. The EU's framework aims to ensure a cost-effective track towards a low-carbon economy in 2050, as in long term the EU is aiming to reduce its greenhouse gas emissions by 80-95% from the 1990 level. (European Commission 2015, p.2)

In addition to legislation, many EPSs have been presented in order to reduce the CO_2 emission level. The European Investment Bank (EIB) has approved on July 23rd 2013 an EPS for new energy projects, which prevents banks from lending to producers which emit more than 550 gCO_2/kWh. (European Investment Bank 2013) In addition, the United States Environmental Protection Agency (EPA) has also presented on August 1st 2014 two different limits for CO_2 emissions of new fossil fuel-fired power plants. The first limit is 500 gCO_2/kWh gross over a 1-operating year period and the second is 454-476 gCO_2/kWh gross over a 7-operating year period. (The United States Environmental Protection Agency, p.1447-1448) The EPA has also presented on June 2nd 2014 a proposal for CO_2 emission reductions from existing power plants. The goal is to cut CO_2 emission level by 30% from the 2005 level. In addition, soot and smog pollution should be reduced by 25% from the 2005 level. (The United States Environmental Protection Agency 2014b, p. 34832) Furthermore, Canada has also presented an EPS limit of 420 gCO_2/kWh for new and old fossil fuel-fired units (Canadian Environmental Protection Act 2012, p.8).

The presented EPSs indicate a CO_2 emission level of 420-550 gCO_2/kWh (Figure 5). As a result, CO_2 emission level has to be reduced at least 33% in a reference plant, which combusts 100% coal with a net efficiency of 44%. However, the required CO_2 emission level reduction is even greater for a current average coal-fired power plant, in which net efficiency is 36%. For the average plant, the CO_2 emission level has to be reduced over 40%.

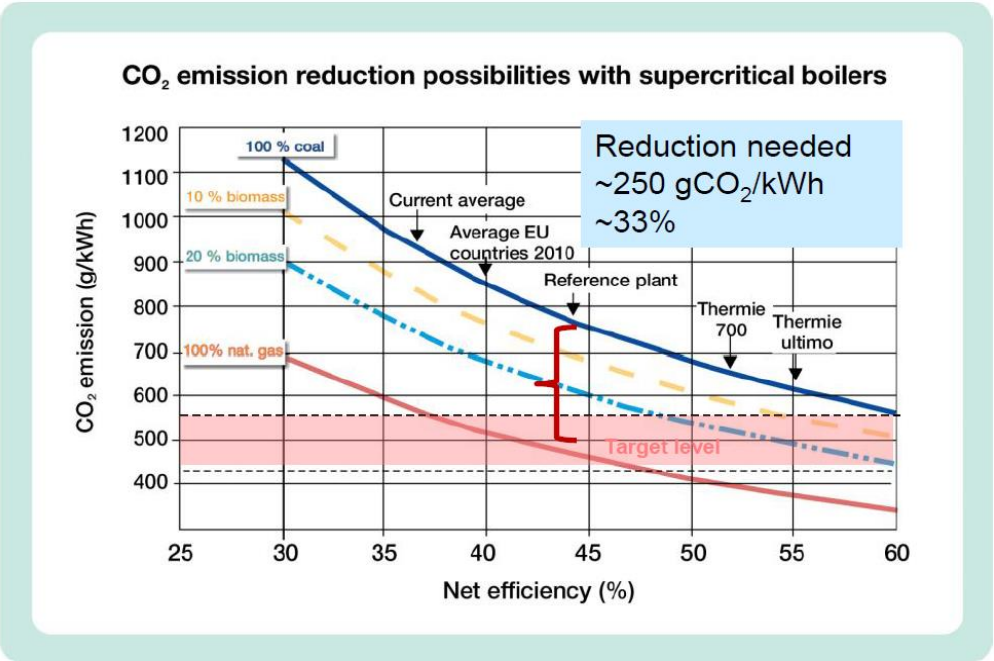

Figure 5. *The needed CO_2 emission reduction due to emission performance standards (VTT 2014).*

There are at least three possible methods for the reduction of CO_2 emission level. These are development of new high-efficient power plants, addition of renewable and nuclear energy, and development of carbon capture and storage (CCS) (Miller 2011, p.251). By developing new high-efficient power plants, their net efficiencies can be increased, which decreases the coal consumption rate and CO_2 emission level (Bugge et al. 2006, p.1439). However, pollutants and greenhouse gases are still generated. Another option is the addition of nuclear energy, but its exploitation is currently affected by the accident in Fukushima Daiichi nuclear power plant as well as by the current economic and financial crisis. However, the prospects for further exploitation of nuclear energy seems positive in the medium to long term. (International Energy Agency 2015b, p.5) Although CCS is technically viable, it creates challenges considering costs and energy consumption. The loss of power output ranges from 19% to 22% of the original power output due to the solvent regeneration and the auxiliary systems of the CCS. (Parvareh et al. 2015, p.508) Furthermore, the earliest commercial deployment of CCS technology is not expected before 2025 (International Energy Agency 2012, p.6 & p.16). Another option is the addition of renewable energy, which includes for example biomass, wind, STE and PV power plants. One possible technical solution to increase the share of renewable energy is the integration of CSP with conventional power plants.

1.2 Research questions, objectives and delimitations

CSP hybrids seem to be one possible solution for the problems of stand-alone CSP and conventional power plants, since they are capable of lowering the LCOE of CSP technology and provide a technical pathway to reach lower CO_2 emission level demanded

by the EU and EPSs. However, there are only few operational CSP hybrids. The research questions for this thesis originate from this situation:

- What are the state-of-the-art technologies in CSP and conventional power plants?
- Which are the possible integration options available between the CSP and conventional power plant technologies?
- How the possible integration options compare to each other?
- What are the process requirements and restrictions, and the achievable thermal parameters for both plants?
- What kind of solar shares can be reached with the hybrid system?
- What are the automatic control strategies and the main control loops of CSP and conventional power plants?
- How the control engineering of the hybrid power plant can be arranged?
- How the system operates at steady state with different solar field and boiler loads?
- How the system operates under transient solar irradiation conditions?

As a conclusion from the research questions, the main objectives of the thesis are:

- Research state-of-the-art technologies in CSP and conventional power plants.
- Comprehensively study the possible integration options between the CSP and conventional power plants.
- Work out process and control engineering for one hybrid plant configuration.
- Develop control mechanisms for the hybrid power plant.
- Demonstrate the operation of the hybrid system under typical boundary conditions by means of Advanced Process Simulator (Apros).
- Find challenges, process requirements and restrictions within the hybrid system and future development requirements for the hybrid system.

The results include simulation results of steady-state and transient simulations with the selected and modelled CSP hybrid. Thus, the results include steady state results with different loads of solar field and boiler as well as transient results of the hybrid system under fluctuating solar irradiation conditions. In addition, challenges of the hybrid system are discussed based on theory and simulations results. Furthermore, possible solutions and future development requirements are defined.

The thesis includes many limitations. First of all, the reader of the thesis is assumed to have basic knowledge about power plant and control engineering. Thus, the basics of thermodynamics and control engineering are excluded from the theory, which focuses on the state-of-the-art technologies of CSP and conventional power plants in recent years and in the near future. In addition, CSP plants can use different kinds of collectors and HTFs. In this thesis, the focus is on line-focusing collectors with direct steam gen-

eration, since they offer good conditions for direct integration of steam cycle and solar field. Any other collector type and heat transfer fluid are excluded. On the other hand, solar fields can be connected to different kinds of conventional power plants, which use different kinds of combustion technologies. The chosen host power plant scenario in this thesis is conventional steam power plant with atmospheric fluidized bed combustion. Thus, any other power plant and combustion technology is excluded. Furthermore, the theoretical and operational experience data of this kind of CSP hybrids is limited, as sufficient research data can only be found from feedwater preheating process arrangement, in which the solar field produces preheated feedwater for the steam power plant. Furthermore, only two CSP hybrids are operational and another one under construction, in which line-focusing collectors with direct steam generation are integrated with conventional steam power plants. The operational plants are Liddell Power Station in Australia (National Renewable Energy Laboratory 2013) and Sundt Solar Boost in Tucson, USA (Tucson Electric Power 2016; Tucson local media 2014). The CSP hybrid under construction is Kogan Creek plant in Australia (CS Energy 2015).

The focus of the thesis is on the development of the process and control engineering of the CSP hybrid plant in order to find challenges and limitations in the process and control engineering of the selected CSP hybrid configuration. In other words, only one CSP hybrid configuration is designed and modelled and economic analyses are excluded from the thesis. Energy analysis is conducted for different hybrid process configurations in order to select one configuration for the CSP hybrid plant. Exergy analysis is excluded, which can be used in later work in order to optimize the operation of the hybrid plant, as energy analysis can be conducted in order to analyse the quality of the process.

For the development of the hybrid configuration, the solar field is designed and modelled in order to produce steam with certain steam parameters correspond to the selected hybrid configuration. The thermal power and outlet steam mass flow of the solar field can be altered by changing the size of the solar field or the available DNI level in order to analyse the operation of the hybrid under different loads of the solar field. The optimal size of solar field for the hybrid system is not analysed, as it requires information about the location of the hybrid plant, such as the typical consumption curves for electricity and annual variation of the DNI level and weather conditions, which are excluded from this thesis. Furthermore, the simulations are conducted with peak DNI level of the selected location in order to demonstrate the operation of the hybrid plant under peak irradiation conditions. In other words, the hybrid is located in southern Spain and the steady state and transient simulations are conducted on June 21st at 12.00. a.m. Any other location, season or time are excluded from the thesis. Moreover, the start-up and shutdown procedures of the CSP hybrid are excluded from this thesis.

1.3 Research methodology and materials

The research methodology and materials are different for the theoretical and practical parts of the thesis. The theoretical part is based on literature available from line-focusing collectors with direct steam generation, from conventional steam power plants, and from CSP and conventional steam power plant hybrids. The references mainly consist of books and scientific articles. In addition, information is gathered from some web pages and publications of organizations and companies working with renewable energy, line-focusing collectors with direct steam generation and with CSP hybrids. The practical part of the thesis consists of selecting and modelling one process and control engineering configuration for hybrid plant, which is used for dynamic simulations. The selection of the hybrid configuration is performed by conducting an energy analysis, which is based on first law of thermodynamics and conservation of mass and energy. The model is configured based on the data gathered in the theoretical part of the thesis, and the modelling and simulations are carried out with Apros dynamic simulation software. Furthermore, in the practical part, the deep know-how of VTT about the Apros software and about dynamic modelling in general is utilized.

The research for the thesis was carried out from June 2015 to December 2015. Part of the work was conducted at VTT Technical Research Centre of Finland in Jyväskylä, Finland under the research group for combustion processes. Another part was conducted at Deutsche Zentrum für Luft- und Raumfahrt (DLR, *engl.* German Aerospace Center) in Stuttgart, Germany under the department for Line Focus Systems. The visit to DLR was carried out after the sections of thesis considering theory, model definition and set-up, definition of test cases, and the beginning of the control implementation, was conducted at VTT. The aim of the researcher exchange was to obtain better understanding of the control issues in hybrid system, to improve the control of the hybrid system, and to implement test case simulations to the model. The researcher exchange at DLR was conducted from October to December 2015.

1.4 Structure of the thesis

The structure of the thesis includes theoretical background, development of the model, conducted simulations, discussion and analysis as well as conclusions. The theoretical background is presented in Chapter 2, the development of the model is presented in Chapter 3 and conducted simulations are presented in Chapter 4. Chapter 5 includes the discussion and analysis based on the conducted research, and Chapter 6 includes the conclusions.

Chapter 2 consists of the theoretical background for CSP hybrids. Thus, it includes the theory of CSP with direct steam generation (Chapter 2.1), the theory of conventional steam power plants (Chapter 2.2) and the theory of CSP and steam power plant hybrids (Chapter 2.3). The theory of CSP with direct steam generation as well as the theory of

steam power plants consists of state-of-the-art power plant technologies focusing on the process and control engineering of power plants. The theory of CSP and steam power plant hybrids consists of the description of operation modes for the hybrid systems, a comprehensive study of different process arrangements of the hybrid systems and the process requirements and restrictions of the hybrid systems.

Chapter 3 consists of the theoretical background of dynamic modelling and simulation as well as the descriptions of the developed model and conducted simulation cases. Thus, it includes the description of Apros as dynamic modelling and simulation tool (Chapter 3.1) and the descriptions of previously developed Apros models (Chapter 3.2) used as reference models in this thesis. Based on theoretical background, the selection of the reference setup for the hybrid system is described (Chapter 3.3) by conducting an energy analysis. Furthermore, the developed hybrid model is described in Chapter 3.4, which consists of the description of process and control engineering of the hybrid system as well as the modifications of the steam power plant model based on the process and control engineering of the hybrid. Furthermore, the test cases are defined (Chapter 3.5) for steady state and transient simulations.

Chapter 4 includes the results from the simulated steady state cases (Chapter 4.1) under different loads of solar field and steam power plant. In addition, the Chapter 4 includes the results from the simulated transient state cases (Chapter 4.2), as the load of the solar field is changed by conducting step changes to the DNI level. In Chapter 5, based on the theoretical background, the simulation results are discussed and analysed and the challenges and the future development requirements of the hybrid system are defined. Chapter 6 includes the conclusions of the thesis.

1.5 VTT Technical Research Centre of Finland

VTT Technical Research Centre of Finland is the leading research and technology company in the Nordic countries. The company was established in 1942. At the end of 2014, the amount of personnel was 2,375, and the turnover was 251 million Euros. (VTT 2015a) VTT has identified six areas of research and technology, which address global challenges and provide prospects for new business and growth. These are: bioeconomy, low carbon and smart energy, people's wellbeing, resource-efficient industries, clean globe, and digital world. (VTT 2015b) The research of hybrid solar power systems locates under the low carbon energy area as a future technology and system for renewable energy production (VTT 2015c).

VTT carries out the research, develops the technology and assists in the commercialization of novel technologies. This thesis was commissioned by VTT under the project "Combination of Concentrated Solar Power with Circulating Fluidized Bed Power Plants", which is financed by Tekes – the Finnish Funding Agency for Innovation. There are three key drivers in this project. First one is to increase the capacity of CSP

production, which can operate with base and peak loads, utilize existing infrastructure and balance the distributed intermittent production. The second key driver is to meet the new EPS limits with combination of biomass, solar and gas with coal. The last key driver is to increase the share of intermittent renewable energy production, while calling for better load change capabilities with maximal efficiency and low emissions throughout the whole load range of conventional power plants. (VTT 2014)

1.6 DLR the German Aerospace Centre

DLR, the German Aerospace Centre, is Germany's research centre of aeronautics and space. The organization was established in 1907, and it has 8,000 employees in 16 locations in Germany. In the year 2013, the budget for research and operations amounted to roughly 846 million Euros. This does not yet cover the space budget of the German government. A great deal of the conducted research at DLR includes space, followed by aeronautics. In addition, DLR carries out research in the fields of energy, transport, and security. DLR has three mains goals in the energy sector. The first one is more efficient conversion of energy resources into power. The second one is the introduction of renewable energy sources to replace fossil fuels, and the last one is the reduction of energy demand through more efficient utilization. (DLR 2014, p.6 & p.12-13)

One subject of the energy research is the development of solar thermal power plants. This includes particularly research on components for parabolic and tower plants based on DLR's own research platforms, new measuring and qualification technologies, and simulation tools. DLR has conducted solar energy research for more than 30 years, and currently the solar research of DLR locates under the roof of the DLR Institute of Solar Research, which was founded in 2011. Its employees work at DLR's headquarters in Cologne, at the sites in Jülich and Stuttgart, and also at Europe's largest test centre for CSP technologies – the Plataforma Solar de Almeria in Spain, operated by DLR's Spanish research partner CIEMAT. The activities at the Institute of Solar Research can be divided into five departments: Point Focus Systems, Line Focus Systems, Qualification, Solar chemical engineering and facilities and Solar materials from which Line Focus Systems is presented in more detail. The research activities of Line Focus Systems concentrate on improvements of the technology and its exploitation on new applications, such as the use of industrial process heat and co-generation of heat and electric power. The main research topics of the department of Line Focus Systems at the moment are optimization of direct steam generation in terms of live steam parameters, process and control technology, investigation of alternative heat transfer fluids, exploitation of cost reduction potentials, demonstration of new technologies at relevant scale, and consulting services to support technology transfer in commercial project development and demonstration activities. (Institute of Solar Research 2015)

2. CONCENTRATED SOLAR POWER INTEGRATION TO CONVENTIONAL POWER PLANTS

Concentrated solar power (CSP) plants can be integrated with conventional power plants, which include conventional steam power plants and combined cycle power plants (Peterseim et al. 2013. p.528). Furthermore, different kinds of CSP plants can be integrated with conventional power plants. In this thesis, CSP plants with direct steam generation as well as conventional steam power plants are chosen for the development of CSP and conventional power plant hybrids, and any other power plant type is excluded. In the following chapters, the theoretical background of CSP with direct steam generation (DSG) is presented (Chapter 2.1) as well as the theoretical background of the conventional steam power plants (Chapter 2.2). Furthermore, the theoretical background of concentrated solar power and conventional power plant hybrids is presented (Chapter 2.3).

2.1 Concentrated solar power with direct steam generation

CSP is based on reflectors, which redirect and focus large amounts of solar irradiation into a small receiving area called as a receiver. The solar irradiation is redirected and focused with reflectors, which track the sun throughout its daily course in order to maintain the maximum solar flux at their focus. The reflectors can be either mirrors or lenses. By focusing the solar irradiation onto the receiver, solar energy is transferred to heat transfer fluid (HTF), which flows to the power block in order to generate electricity. The amount of heat collected by the solar field follows the daily DNI level (Figure 6). In addition, an energy storage system or another back-up system can be applied in order to enhance the performance and increase the capacity of the CSP plant. (Barlev et al. 2011, p.2704; Behar et al. 2013, p.15; Zhang et al. 2013, p.467-468)

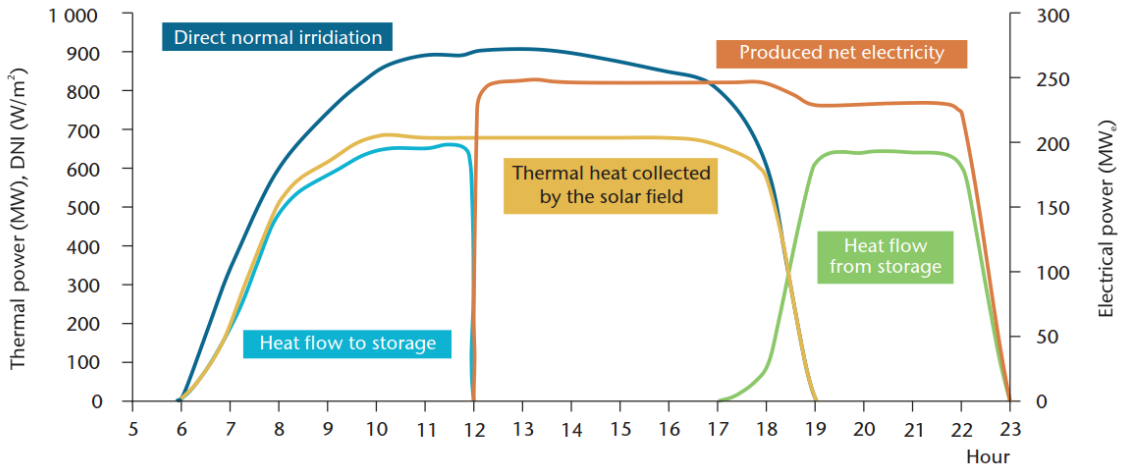

Figure 6. *Thermal and electrical power production from solar field with energy storage system (International Energy Agency 2014a, p.14).*

CSP collectors can be divided into four types: linear Fresnel reflectors (LFR), parabolic trough collectors (PTC), solar towers (ST) and parabolic dishes (PD), as shown in Figure 7 (Barlev et al. 2011, p. 2705; International Energy Agency 2014a, p.12). All the four main types use mirrors as reflectors, and they are applied in high-temperature applications in order to generate solar thermal energy and produce electricity. The first three are used commonly in utility-scale Rankine cycles, whereas PDs are often used in 1-30 kW_e sized modular power generation systems with a Stirling or Brayton engine. (Zhu et al. 2014, p.639) Currently, PTCs represent over 95% of the installed applications, STs approximately 3%, LRFs approximately 1% and PDs under 1% (Vignarooban et al. 2015, p.384).

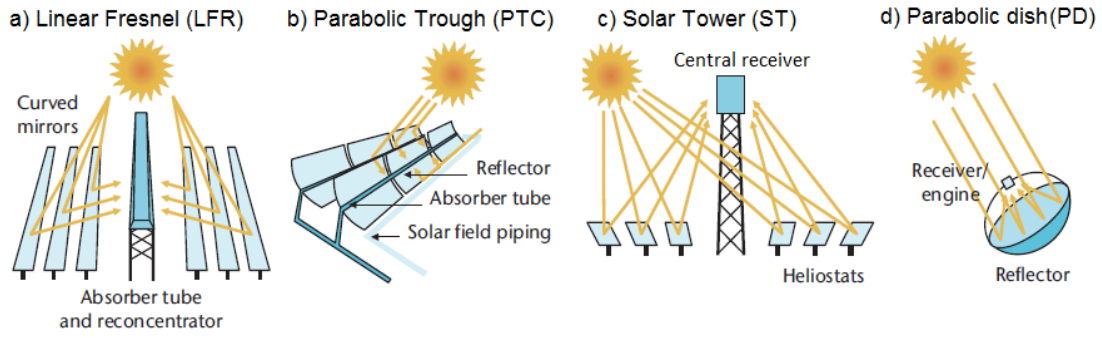

Figure 7. *Main CSP technologies: a) Linear Fresnel (LFR), b) Parabolic trough (PTC) c) Solar Tower (ST), and d) Parabolic dish (PD). Adapted from International Energy Agency 2014a, p.12.*

Furthermore, CSP collectors can be categorized by focus and receiver types (Figure 7). The focus types are point-focusing and line-focusing collectors, whereas the receiver type can be either fixed or mobile. (International Energy Agency, p.12)

Receiver type \ Focus type	**Line focus** *Collectors track the sun along a single axis and focus irradiance on a linear receiver. This makes tracking the sun simpler.*	**Point focus** *Collectors track the sun along two axes and focus irradiance at a single point receiver. This allows for good receiver efficiency at higher temperatures.*
Fixed Fixed receivers are stationary devices that remain independent of the plant's focusing device. This eases the transport of collected heat to the power block.	Linear Fresnel reflectors	Towers
Mobile Mobile receivers move together with the focusing device. In both line focus and point focus designs, mobile receivers collect more energy.	Parabolic troughs	Parabolic dishes

Figure 8. *Classification of CSP collector types (International Energy Agency 2014a, p.12).*

The focus types can be clearly distinguished by the concentration ratio, which stands for the aperture area of the solar field divided by the area of receiver. In point-focusing systems, the concentration ratio ranges from about 500 to several thousands, whereas in line-focusing systems the concentration ratio is about 50 to 100 (Lovegrove et al. 2012, p.16). As a result, the point-focusing collectors can generate higher temperatures than line-focusing collectors (Yan et al. 2011, p.910). STs and PDs are considered as point-focusing collectors, which track the sun along two axes and focus irradiance at a single point receiver. On the other hand, PTCs and LFRs are considered as line-focusing collectors, which track the sun along single axis and focus the solar irradiation on a linear receiver. Furthermore, the receiver types can be either fixed or mobile. Fixed receivers are stationary devices and apart from reflectors, which eases the transport of collected heat to the power block. On the contrary, mobile receivers are physically connected with reflectors and move along with the reflectors. Thus, they collect more energy than fixed receivers. LFRs and STs have fixed receivers, whereas PTCs and PDs have mobile receivers. (International Energy Agency 2014a, p.12)

In this thesis the focus is on line-focusing collectors with DSG. Therefore, the included collector types are PTCs and LFRs, and the STs and PDs are excluded. In addition, the HTF of the solar field is water, and CSP systems using any other HTF are excluded. In the following chapters, water as HTF is presented (Chapter 2.1.1) before the technical descriptions of parabolic trough collectors (Chapter 2.1.2) and linear Fresnel reflectors (Chapter 2.1.3). Furthermore, the currently considered operation concepts for line-focusing solar fields with DSG are presented (Chapter 2.1.4) as well as the basic principles of control engineering in line-focusing solar fields with DSG (Chapter 2.1.5).

2.1.1 Water as heat transfer fluid

The overall performance and efficiency of the CSP plant are highly dependent on the HTF, which is commonly thermal oil, molten salt, organic fluid or water. Air and other gases as well as liquid metals can also be used as HTFs, but currently they are relatively uncommon. A desired HTF has high boiling point, high thermal stability, high thermal conductivity, high heat capacity, low melting point, low vapour pressure at high temperatures, low corrosion with metal alloys, low viscosity, and low costs. Water as HTF has high thermal stability, high heat capacity, low melting point, low corrosion, low viscosity and low costs, but its downsides are low boiling point, low thermal conductivity and high vapour pressure at high temperatures. (Vignarooban et al. 2015, p.385-388 & p.393)

Despite of the downsides, water has attracted economic and energetic attention, as it has some advantages over the other HTFs. First of all, water can be used as HTF in all CSP collector types (Lovegrove et al. 2012, p.17). Compared to other HTFs, there is no need for extra heat exchanger between the solar field and power block, as the working fluid is the same in both parts. This increases the net efficiency of the plant, simplifies the plant configuration and lowers investment costs. Compared to thermal oils, water has no environmental risks. In addition, higher temperatures than 400 °C can be reached, as water does not degrade like thermal oils, which start to degrade around 400 °C. (Fernández-García et al. 2010, p.1710) Compared to molten salts, water is less corrosive than molten salts with metal alloys (Vignarooban et al. 2015, p.386). In addition, water can be used in direct thermal storage systems, whereas molten salts are applied to indirect thermal storage systems, which require an additional heat exchangers between the steam cycle and storage system (Birnbaum et al. 2010, p.1). However, thermal storage systems based on molten salts are applied to CSP plants (Vignarooban et al. 2015, p.385), whereas thermal storage systems based on water are being developed (Laing et al. 2011, p.627). Furthermore, the operation and maintenance costs are reduced, since water is less expensive than other HTFs, and there is no need for auxiliary heating system for water, as it is needed for thermal oils and molten salts (Fernández-García et al. 2010, p.1710). Moreover, Feldhoff et al. (2010) presented that LCOE of DSG system is 11% less than in thermal oil based system. The lower LCOE is mainly due to less pumping effort in the solar field, higher efficiency, and direct integration without extra heat exchanger. (Feldhoff et al. 2010, p.41001)

On the other hand, water has also some disadvantages as HTF. Due to its high vapour pressure at high temperatures, the stress on the receiver tubes is higher than using other HTFs. Therefore, sufficient cooling of the receiver tubes and a moderate pressure drop between inlet and outlet of a collector may help moderate the stress, reduce corrosion and promote tube lifetime. (Barlev et al. 2011, p. 2706; Alguacil et al. 2014, p.26) Furthermore, water may freeze (Fernández-García et al. 2010, p.1710), and stratified flow regime should be avoided in the evaporation zone. In DSG applications, the preferred

flow regime is annular flow, where a thin layer of water flows at the inside wall of the tube, and steam flows in the middle of the tube. (Hirsch et al. 2014 p.260) Due to the two-phase flow and different thermodynamic properties of water and steam, the required control systems are more complex and expensive than in homogenous HTF systems (Fernández-García et al. 2010, p.1710). In addition, a large-scale thermal storage system is currently not commercially available for DSG systems, since the storage technology is immature and not cost-effective (Feldhoff et al. 2012, p.530). However, the storage technology for DSG power plants is being developed by DLR together with Ed. Züblin AG within the project ITES (Laing et al. 2011, p.627). Feldhoff et al. (2012) conclude that the development and market introduction of storage technology is the one of the main research topics for DSG plants. Due to the disadvantages of water, it is relatively uncommon as HTF in CSP systems, although research on collectors using water as HTF has begun in the 1980s when the first alternatives to thermal oils have been investigated (Vignarooban et al. 2015, p.386-389).

2.1.2 Parabolic trough collectors (PTC)

Parabolic trough collectors consist of a group of parabolic reflectors, which are assembled as long troughs. These troughs are assembled in parallel to form a solar field. The reflectors are usually coated with silvered acrylic, and the shape of the reflector focuses sunbeams onto a receiver tube, which is mounted in the focal line of the parabola (Figure 9). The receiver tube is a black metal pipe, which is encased within a glass pipe in order to limit heat loss by convection. A vacuum is placed between the casings in order to also prevent heat loss by convection. The metal tube is covered with a selective coating, which enhances high solar absorbance and low thermal emittance. In addition, the glass tube is covered with an anti-reflective coating, which enhances transmissivity. (Barlev et al. 2011, p.2705)

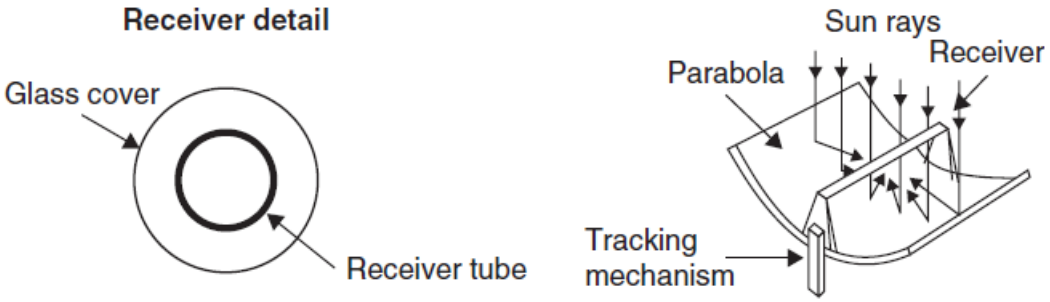

Figure 9. *Schematic of PTC collector (Kalogirou 2014, p.143).*

In PTCs, the reflector and receiver tube move in tandem with the sun in order to keep solar irradiation focused on the receiver tube throughout the day. PTCs are mounted on a single-axis sun-tracking system, which is oriented either east-west or north-south. The east-west oriented field tracks the sun from south to north, whereas the north-south oriented field tracks the sun from east to west. The choice of tracking mode depends on the

need of energy during winter and summer, and also on the application. The annual output is more constant in east-west oriented fields, which collect more energy in winter and less in summer than north-south oriented fields. However, north-south oriented fields provide slightly more thermal energy annually than east-west oriented fields, and maximize the yearly production (Barlev et al. 2011, p.2706; Kalogirou 2014, p.70 & p.143).

Major advantage of PTCs is the maturity of the technology. PTCs are the most mature of the CSP collector designs (Barlev et al. 2011, p. 2705; Kalogirou 2014, p.143), since considerable experience of the collectors can be found, and the systems are produced and marketed by a small commercial industry. However, PTCs have some challenges. One challenge is the exposure to wind drag. As a result, the tracking system needs to be robust enough to account for wind loads and prevent deviations from normal incidence angle between the solar irradiation and the reflector (Barlev et al. 2011, p. 2706). Therefore, investment costs are higher than using flat reflectors. Another challenge associated with PTCs is thermal uniformity in the receiver tube. The heat input of the receiver tube is asymmetric, which causes a temperature difference between the heated and nonheated side of the receiver tube. The temperature difference induces thermal stress on the wall of the receiver tube. This problem concerns especially DSG applications due to the two-phase flow and evaporation inside the tube. In addition, the operating pressure inside the receiver tube superposes the thermal stress especially in the joints between the collectors. Furthermore, as the one-sided heat flux is combined with annular flow regime of the water, it leads to large differences in heat transfer coefficients of wetted and non-wetted areas. The amount of overall stress depends on the wall thickness and on the chosen material, and needs to be considered at the design phase of the system. (Hirsch et al. 2014, p.260)

Despite of the challenges with DSG systems, there are currently few operational test and commercial PTC plants with DSG, as can be seen from Appendix D. The test facilities are the European Direct Solar Steam (DISS) facility and Eureka GDV facility. The DISS facility is the first test facility concerning DSG in PTCs (Figure 10). It was built in 1997 at Plataforma Solar de Almería, Spain (Feldhoff et al. 2014, p.1766) and at its beginning it applied PTC LS-3 type, which was capable of producing steam up to 400 °C and 100 bar. (Eck et al. 2003, p.342) Since then, the DISS facility has been extended with Eurotrough ET-100 collectors developed by European Commission EuroTrough I project and with SL 4600+ collectors manufactured by Solarlite. In addition, the receivers of the collectors have been replaced with SCHOTT PTR®70 receiver model manufactured by SCHOTT. Currently, the DISS plant is capable of producing steam up to 500 °C and 110 bar, and according to SCHOTT the coating of the receiver tube is stable up to 550 °C. (Feldhoff et al. 2014, p.1767-1770)

Figure 10. *PTC collectors at the DISS facility (Institut für Solarforschung 2015).*

The other test facility called Eureka GDV locates at Sanlucar la Mayor Solar Platform, Spain. In the Eureka GDV plant, Abengoa Solar has built, operated and evaluated successfully a 8 MW_{th} demonstration plant, in which PTCs with DSG are studied in order to achieve an operating temperature of around 550 °C. The system has proven a great stability at 550 °C and a large thermal inertia during the shutdown of the plant. (Alguacil et al. 2014, p.21 & p.26)

The first commercial and currently only operational large-scale PTC plant with DSG is the Thai Solar Energy 1 power plant (TSE1) in Kanchaburi, Thailand. The operation of the plant has started in the beginning of 2012, and the TSE1 plant has an electrical output of 5 MW_e. The collectors are Solarlite's SL 4600, which deliver steam up to 340 °C and 30 bar. The TSE1 is owned and operated by Thai Solar Energy Co. Ltd. (National Renewable Energy Laboratory 2013) The experience of the operation from the first year is published by Krüger et al. (2012), who conclude that DSG is a good and technically viable solution for CSP plants, since the temperatures and mass flows can be well controlled in order to avoid any damage to receivers. In addition, the live steam pressure and temperature can also be controlled well in order to avoid damage to the steam turbine. (Krüger et al. 2012, p.7) Furthermore, the experiences of the operation during the first two years are also published by Khenissi et al. (2015), who moreover conclude that the TSE1 plant has proven the reliability of PTCs with DSG under not ideal operation conditions (Khenissi et al. 2015, p.1607-1609).

In addition to the operational test and commercial plants, Hittite Solar Energy is developing PTCs which can deliver steam up to 500 °C and 140 bar (Hittite Solar Energy 2015). As a conclusion, PTCs with DSG are possibly capable of producing steam up to 550 °C and 140 bar in the near future. These steam parameters correspond almost to the live steam parameters of subcritical steam power plants, which are approximately 160-180 bar and 535-565 °C (Miller 2011, p.256).

2.1.3 Linear Fresnel reflectors (LFR)

Linear Fresnel reflectors are similar to the PTCs, since several LFRs can be used to approximate the parabolic shape of PTCs. LFR consists of large amount of flat reflectors, which concentrate sun rays onto a receiver tube (Figure 11). The receiver tube locates on a tall tower above and along the arrays of reflectors. (Barlev et al. 2011, p. 2711; Kalogirou 2014, p. 148) LFRs have not reached their full industrial maturity as only a few of the existing and planned CSP plants use LFRs as collectors. However, all current LFR plants use water as HTF (International Energy Agency 2014a, p.13), and the technical improvements of the collector have made LFRs suitable for high-temperature CSP applications to generate electricity at utility scale. The US Department of Energy has identified CSP plants with LFRs to be the potential pathway to reach the level of LCOE, which can be cost-competitive with conventional power plants without any incentives or government subsidies. (Zhu et al. 2014, p.646) This means that on average the LCOE of CSP needs to be approximately reduced from 225 USD/MWh to 90 USD/MWh (Figure 1).

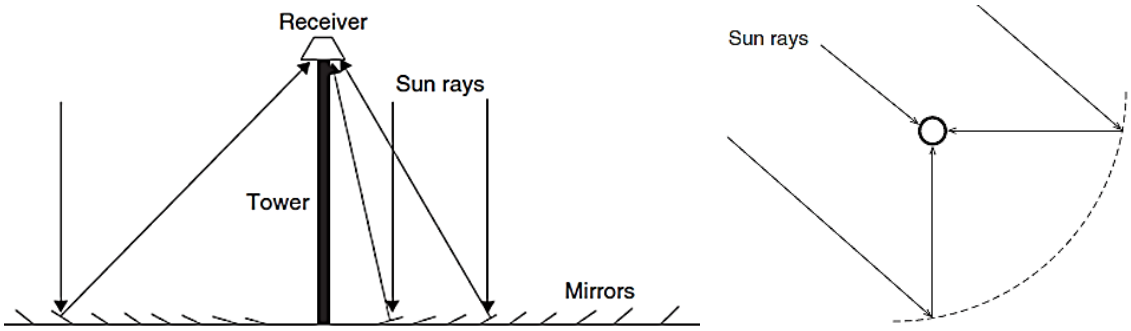

Figure 11. *Schematic of LFR field and the receiver. Adapted from Kalogirou 2014, p.148-149.*

LFRs have some advantages over the PTCs. One advantage is the fixed receiver unit, which does not track the sun. Therefore, only the flat reflectors track the sun, which makes tracking simpler, more accurate and more efficient than with mobile receivers. (Barlev et al. 2011, p. 2711) Another advantage is the lower price due to the flat and elastic reflectors, which are cheaper to produce than parabolic troughs. Furthermore, the reflectors can vary by size and by arrangement, and the concentration ratio can be increased without increasing the wind load due to the flexible architecture of LFRs. This provides a variety of different applications with different target temperatures. (Zhu et al. 2014, p.639 & p.650) In addition, LFRs have lower land requirement and cleaning water consumption than other CSP technologies, which lowers the costs even further (Peterseim et al. 2013, p.526). LFRs can also withstand higher operation pressures and temperatures than PTCs due to their fixed receiver configuration, which reduces the need for heat and pressure resistant joints (Popov 2011, p.346).

The disadvantage of the LFRs is larger optical losses than PTCs. The optical efficiency of LFR is decreased due to shading and blocking of solar irradiation between adjacent reflectors. Thus, the LFRs have lower annual thermal power output than PTCs especially in early mornings and late afternoons, and also in winter. However, the optical losses can be compensated by increasing the concentration ratio and the size of solar field or by building a taller receiver tower, but these modifications increase costs. (Zhu et al. 2014, p.640 & p.650) One solution for the shading and blocking has been developed by Mills and Morrison at Sydney University, Australia (Kalogirou 2014, p.148-149). The developed compact linear Fresnel reflector (CLFR) uses at least two receiver towers, which allows the individual reflectors to focus sunbeams on either one of the towers (Figure 12). Thus, closely packed reflectors avoid shading and blocking, and the size of the solar field and the height of the receiver tower can be reduced. Furthermore, CLFR field decreases the investment costs, which include ground preparation, array substructure, tower structure and steam lines. In addition, the thermal losses from steam lines are smaller. CLFR provides maximum system output with limited ground area if the technology is applied to urban area or next to an existing power plant. However, a more sophisticated tracking mechanism has to be applied to the CLFR field than to the LFR field, and the maintenance costs of CLFR field are higher than LFR field. (Zhu et al. 2014, p.640)

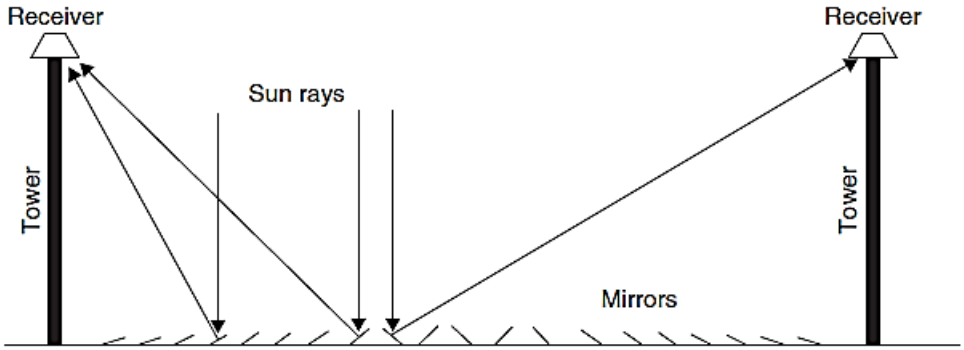

Figure 12. *Schematic of CLFR field (Kalogirou 2014, p. 150).*

In addition to CLFR, some other innovations have been made in order to compensate the lower optical efficiency. One innovation is the use of secondary reflector whilst using a single receiver tube (Figure 13). This increases the optical performance of the collector, but the design of the secondary reflector is difficult to optimize. (Zhu et al. 2014, p.644) Another innovation is the addition of an inverted cavity receiver with a planar array of boiling tubes (Figure 13). This trapezoidal multi-tube receiver use non-vacuumed receiver tubes, and sidewall insulation is added to reduce thermal loss. However, thermal loss could be very significant from this kind of receiver whilst producing steam temperature higher than 400 °C (Zhu et al. 2014, p.641). Furthermore, by reforming the platform of the solar field into a wave-shaped one, the blocking and shading can be reduced, and the layout density of the field maximized. Moreover, individual shape

adjustments can be made on single reflectors, but it increases the costs. All the reflector and receiver innovations have further reduced costs of LFRs. (Barlev et al. 2011, p.2712)

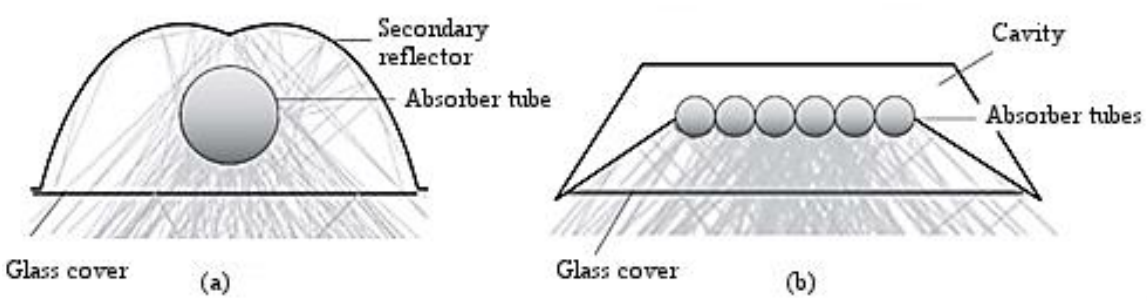

Figure 13. *The two main types of LFR receiver design a) single tube cavity receiver with secondary reflector and b) multi-tube trapezoidal cavity receiver. Adapted from Lovegrove et al. 2012, p.490.*

Even though LFRs are not fully mature industrial technology, there are few operational LFR plants with DSG, as can be seen from Appendix E. In addition, few test and commercial plants are under construction. These plants can be roughly categorized by the manufacturer of LFRs. The two major manufactures, which have produced commercial, state-of-the-art high-temperature LFRs with DSG, are Novatec Solar and AREVA Solar. Currently, Novatec Solar is named as Frenell GmbH (FRENELL 2015) and continues its operation, whereas AREVA Solar has announced its exit from CSP market in August 2014 due to weak sales and falling revenues across nuclear and renewables businesses (Reuters 2014).

Novatec Solar has constructed LFR fields in the test plant Puerto Errado 1 (PE1), in the commercial plant Puerto Errado 2 (PE2), and half of the Liddell Power Station as the first half was constructed by AREVA Solar (CSP World 2015). Novatec Solar has two collector models: NOVA-1 and Supernova. NOVA-1 has a single non-vacuum receiver tube (Novatec Solar 2015a), and it can generate saturated steam up to 270 °C and 55 bar (Novatec Solar 2015b). On the other hand, the Supernova collector is designed for superheating of the steam, as it uses single vacuumed receiver tube instead of non-vacuumed tube. The Supernova can generate steam temperatures up to 550 °C (Novatec Solar 2015c). In the PE1 plant (Figure 14), Novatec Solar demonstrates their NOVA-1 and Supernova LFRs with steam parameters up to 500 °C and 55 bar, and the PE1 has electrical output of 1.4 MW_e. On the other hand, the commercial PE2 plant uses only the NOVA-1 technology. The operation of the PE2 plant has started in early 2012, and it produces live steam at 270 °C and 55 bar with a peak electrical output of 30 MW_e. A fact worth of mentioning is that the mirror surface of the PE2 is 302,000 m^2, which makes the PE2 world's largest operational CSP plant based on LFRs. (Novatec Solar 2015b)

The solar fields at the Liddell Power Station are integrated with a 2000 MW_e coal-fired power plant. The combined thermal power of the solar fields is 18 MW_{th} and electric power is 6 MW_e. (CSP World 2015) Thus, the solar share is only 0.3% of the installed electric power capacity. The solar fields heat the feedwater from 140 °C to steam at 270 °C and 55 bar, and the steam is fed into feedwater preheating of the coal-fired power plant. The last stage of the solar fields was commissioned in 2012 (National Renewable Energy Laboratory 2013) and hybrid system replaces 5,000 tons of CO_2 per year. However, this is only equivalent to 2.8 hours of full-load operation of the coal-fired power plant. In addition, the coal-fired power plant was commissioned in 1971 so the environmental and economical aspect of the hybrid system is questionable. (Peterseim et al. 2014, p.179)

Figure 14. *Novatec Solar's LFR field at the PE1 facility (Novatec Solar 2015d).*

AREVA Solar has constructed CLFR fields at the Kimberlina test plant and in the Sundt Solar Boost project. Furthermore, it is currently building the commercial Dhursar and Kogan Creek plants even though its exit from the CSP markets. The CLFR technology of AREVA Solar is capable of producing steam up to 482 °C and 165 bar (AREVA Solar 2015a). In the Kimberlina plant, AREVA Solar demonstrates their CLFR technology with steam parameters up to 300 °C and 40 bar, and it can generate up to 5 MW_e of peak electricity (National Renewable Laboratory 2013). In the Sundt Solar Boost plant, the CLFR field boosts the 156 MW_e coal/gas-fired unit owned by the Tucson Electric Power by up to 5 MW_e. Thus, the solar share is approximately 3% of the installed electric power capacity. The unit of the host plant combusts mainly gas (Tucson 2014), and the hybrid is capable of offsetting the use of natural gas up to 46 million m^2 per year or use of coal up to 3,600 tons per year. As a result, it avoids annually 4,600 to 8,500 tons of CO_2 emissions. (AREVA Solar 2015b) The construction of the Sundt Solar Boost project has been delayed due to permitting issues (Tucson 2014), but the construction has been finished in end of 2014 (Tucson Electric Power 2016; Tucson local media 2014). However, any technical details of the produced steam parameters at solar field cannot be found as well as the exact process arrangement of the hybrid system remains unclear.

The construction of the Dhursar and Kogan Creek power plants are delayed, but for example the Kogan Creek plant is expected to be completed and in full commercial use at the end of 2016 (CS Energy 2015). The CSP plant at Dhursar is based on AREVA Solar's CLFR technology, which is going to deliver live steam at 390 °C and 90 bar. The Dhursar plant consists of two units with an electric power of 125 MW_e each (AREVA India 2013) and so far it is the largest CSP plant with DSG under construction. In the Kogan Creek plant, a 44 MW_e solar field is going to be integrated with a 750 MW_e coal-fired power plant. Therefore, the solar share is 5.9% of the installed electric power capacity. The feedwater is heated in the CLFR field from 186 °C to steam at 370 °C at 60 bar. (National Renewable Energy Laboratory 2013) The steam is injected to the cold reheat line after the high pressure turbine, and the addition of solar steam is going to increase the amount of steam available for the electricity production. (AREVA Solar 2015c) The coal-fired power plant was commissioned in 2007, and it is expected to be operational for the next 25-30 years (Peterseim et al. 2014, p.179; CS Energy 2015). After the solar field is commissioned, the hybrid avoids annually up to 35,600 tons of CO_2 emissions (AREVA Solar 2015c).

In addition to the two major manufacturers, Solar Euromed is merging to the CSP market. It develops LFRs, which can stand steam temperatures over 500 °C (Solar Euromed 2015a). Currently, Solar Euromed is providing LFRs for Alba Nova 1 plant, which produces live steam up to 500 °C and 65 bar with an electric power of 12 MW_e. (Solar Euromed 2015b) As a conclusion of the current status of LFRs, the state-of-the-art LFRs are possibly capable of producing steam up to 550 °C and 165 bars in the near future according to the development objectives of LFRs.

2.1.4 Currently considered operation concepts for direct steam generation in PTCs and LFRs

The currently considered operation concepts for DSG in PTCs and LFRs are based on research, which has started in the 1990's. Since the PTCs and LFRs can be considered as similar line-focusing collectors, the same operation concepts can be applied to both collectors (Muñoz-Antón et al. 2014, p.187). The first investigated basic operation concepts are: the recirculation concept, the once-through concept and the injection concept, as shown in Figure 15 (Eck et al. 2003, p.342).

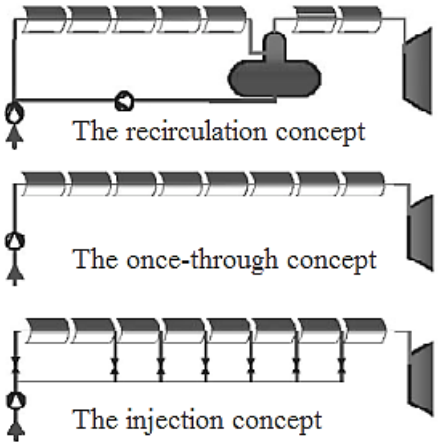

Figure 15. *The basic concepts for DSG in linear receivers. Adapted from Eck et al. 2003, p.342.*

In the recirculation concept, there are two sections in the solar field: one for feedwater preheating and evaporating, and one for superheating the steam. The amount of feedwater through the evaporation section is higher than the amount of generated steam, and the water-steam mixture from the evaporator section is fed to a phase separator tank. In this tank, saturated steam is separated from the water, the steam is fed to the superheating section and the excess water is fed to the inlet of the collector row. The amount of recirculation is expressed as recirculation ratio, which is defined as the ratio of the recirculated mass flux to the steam mass flux. If the recirculation ratio is zero, the process is identical with once-through operation concept, in which the total amount of feedwater is preheated, evaporated and superheated within one loop. In the injection concept, the loop is divided into subgroups, which consist of a collector, an attemperator and gauging equipment. (Eck et al. 2003, p.342 & p.347)

The basic operation concepts for DSG in PTCs were investigated and compared under real operation conditions in the DISS project, which was conducted at the DISS facility. The aim of the DISS project was to investigate the thermohydraulic behaviour of the DSG process, assess the different basic operation concepts, develop the control engineering for the basic concepts, and optimize and improve the operation strategy for the DSG collector loop. More tests were executed with the recirculation concept and once-through concept, and less with injection concept. (Zarza et al. 2004, p.640) The results of these tests are presented in Eck et al. (2003) and in Zarza et al. (2004). It is concluded that the DSG is feasible in PTCs and the recirculation concept is the most attractive operation concept for commercial DSG collector fields, since it has no bad performance in any of the assessment criterions, such as feasibility, investment costs, maintenance, controllability, reactive loads, and potential for improvements. On the contrary, the once-through concept has the lowest investment costs of the three concepts due to avoiding of attemperators and separation tank, but also the worst controllability. Furthermore, Eck et al. 2003 concludes that the injection concept has the highest investment costs due to multiple attemperators. (Eck et al. 2003, p.348-350)

Since the DISS project, the basic operation concepts have been adjusted and further developed. According to Feldhoff et al. (2012), as cited in Hirsch et al. (2014), the main three current operation concepts are identified: recirculation concept with a central separator, recirculation concept with distributed steam separators and once-through concept with additional injection lines (Figure 16).

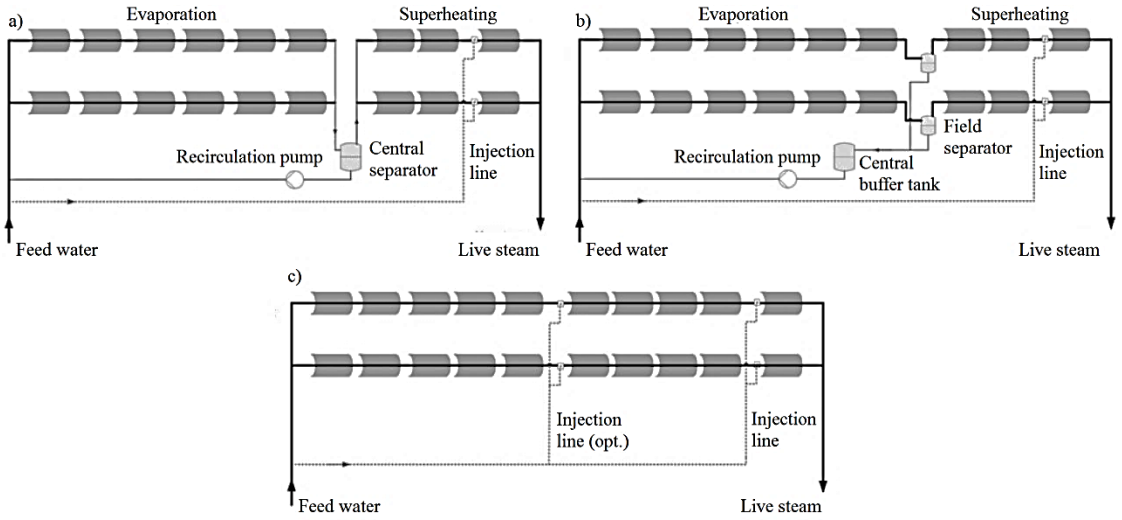

Figure 16. *The current concepts for DSG: a) recirculation with central separator b) recirculation with distributed steam separators and c) once-through with additional injection lines. Adapted from Hirsch et al. 2014, p.262.*

The basic recirculation operation concept can be arranged with central separator or with distributed field separators and a central buffer tank. In the recirculation with central separator, water-steam flux is collected from each evaporation loop into a central separator from which saturated steam continues to superheating section. This concept is also applied in the TSE1 power plant in Kanchanaburi, Thailand. (Hirsch et al. 2014, p.263) In the recirculation mode with distributed field separators, there is also a common central tank with buffering, but the steam is separated in the field separators and only water flows into the central buffer tank. This concept was considered in the first precommercial DSG plant in the INDITEP project (Zarza et al. 2006, p.1274). The use of distributed field separators aims to reduce thermal inertia, materials consumption and pressure loss over the whole loop as long as the size of field separators is kept small (Eck et al. 2007a, p.270). The driving force of the water from distributed field separators to central buffer tank is pressure difference. However, this allows partial evaporation along the line leading to larger pipe diameters. The pipe diameter can be lowered if water is injected in the line, which enters the buffer tank, but it results to higher heat losses in the recirculation loop. Both recirculation concepts have an additional attemperator before the last superheating collector in order to stabilize the outlet steam temperature of the collector loop. (Hirsch et al. 2014, p.263)

In the once-through mode with additional injection lines, up to two attemperators are applied to the collector loop. This improves the controllability of the process and en-

sures stable outlet steam temperature. As the amount of attemperators increases the investment costs, only two attemperators are installed in the collector row. One can be installed before the last superheating collector, and the optional second attemperator can be installed in the evaporation section. The previous controls the outlet temperature well, but it cannot control the behaviour between the inlet and the last collector. With the latter one, an earlier intervention in the process is possible, but it has a delayed influence on the outlet steam temperature. Better control is achieved, when both attemperators are applied. In addition to the problem with outlet steam temperature, there can be fluctuations in the end of the evaporation, where dry-out zones can occur and cause high thermal stress on the receiver tubes. Hence, more sophisticated control scheme has to be applied to the once-through concept than to recirculation concept. (Hirsch et al. 2014, p.263) The once-through concept is currently demonstrated and tested in the Development and demonstration of the once-through concept (DUKE) project under real solar conditions at the DISS facility. Therefore, it is not yet commercially available even though it is the most promising concept to further reduce the costs of line-focusing solar fields with DSG. (Feldhoff et al. 2014, p.1767)

2.1.5 Control engineering of line-focusing collectors with direct steam generation

As the PTCs and LFRs can be operated by similar operation concepts (see Chapter 2.1.4), the control can also be similar. Regardless of the operation concept, the main objective of control engineering in solar field is to maintain the produced steam at constant pressure and temperature at the outlet of the solar field (Valenzuela et al. 2006, p.5). As solar irradiation cannot be used as control variable for the process, the control of solar field has to be arranged by mass flow manipulation and by attemperators (Eck et al. 2007a, p.270). As a result, small disturbances of the solar irradiation affect the quantity of produced steam, but not on its quality. With greater disturbances, some fluctuations can be also seen on the outlet steam temperature. (Alguacil et al. 2014, p.24; Khenissi et al. 2015, p.1607-1609) The disturbances can appear slowly like variations of the solar irradiation on clear days and by dusty mirrors, or they can be fast and strong due to cloudy days or changes in the temperature and pressure of water entering the solar field. (Valenzuela et al. 2005, p.304)

The disturbances of the solar field can be observed from the mass flow and temperature point of views. From the mass flow point of view, the dynamics of disturbances through the whole collector loop is dominated by the evaporation section, which key parameters are the steam and liquid mass fractions at the end of the evaporation section. These parameters are used to design the phase separator and condensate drainage systems in the recirculation concept. (Eck et al. 2007a, p.272) In addition, a certain steam mass fraction has to be obtained at the outlet of the evaporation section in order to reduce the risk of superheating in the evaporation section. The desired steam mass fraction at the phase

separator inlet is 0.80 (Giostri et al. 2011, p.4), which guarantees sufficient cooling of the absorber tube during steady state conditions. However, the steam mass fraction should be lower than 0.80 during cloudy periods, where frequent transients are expected (Eck et al. 2006, p.1427). Eck et al. (2007a) observed that the disturbances in the solar irradiation causes much higher liquid loads to the phase separator and drainage system compared to steady state situation. These higher liquid loads needs to be taken into account, as the phase separator and drainage systems are designed.

From the temperature control point of view, Birnbaum et al. (2011) presents steam temperature stability of a collector field, which is equipped with attemperators in order to control the steam temperature at the outlet of solar field. Birnbaum et al. (2011) conclude that the steam mass flow through the solar field is linked to the solar irradiation conditions in evaporation section, whereas the steam temperature is mainly affected by solar irradiation conditions in the superheating section. The disturbances are related to whether the evaporation section, the superheating section, or both are affected. In addition, it has different impact if the evaporation section is disturbed before or after the superheating section. Birmbaum et al. (2011) researched these scenarios by modelling them with the software Dymola and conducting -50% step change to the irradiation conditions in the evaporator section after 10 minutes of simulation (Figure 17). The solar irradiation conditions were restored to its initial state of 550 W/m^2 after 10 minutes. Same kind of step change was conducted to superheating section before, after or at the same time with the evaporation section.

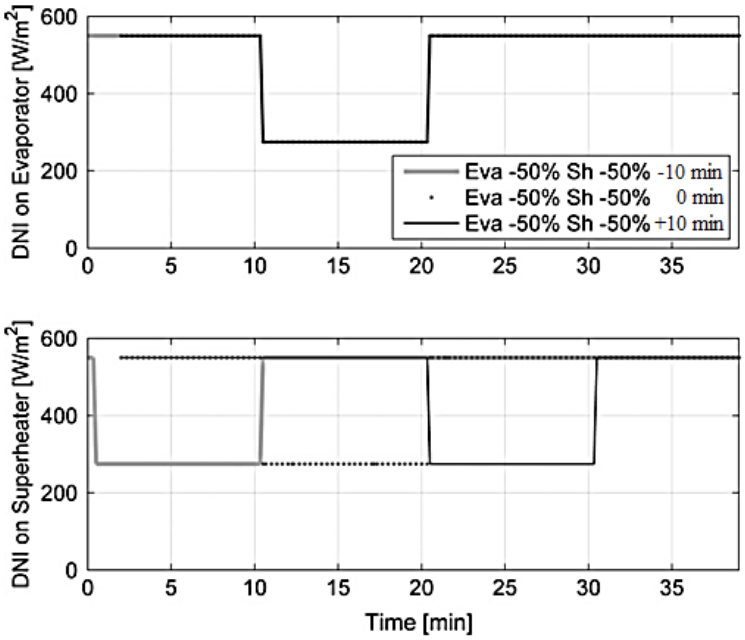

Figure 17. *-50% step changes in the solar irradiation conditions of evaporator and superheater. Adapted from Birnbaum et al. 2011, p.663.*

The steam mass flow from the solar field is steadily decreased during the first seven minutes after the step change in the DNI on evaporation section (Figure 18). The steady

decrease of steam mass flow is due to the thermal inertia of the collector row and applied control system of the power block. After the seven minutes, the steam mass flow from solar field is more rapidly decreased, as the control of the power block is changed from sliding pressure to fixed pressure mode. As the initial DNI level on evaporator is restored, the steam mass flow is steadily increased, and it overshoots slightly before reaching the initial state of 70 kg/s. (Birnbaum et al. 2011, p.662-663)

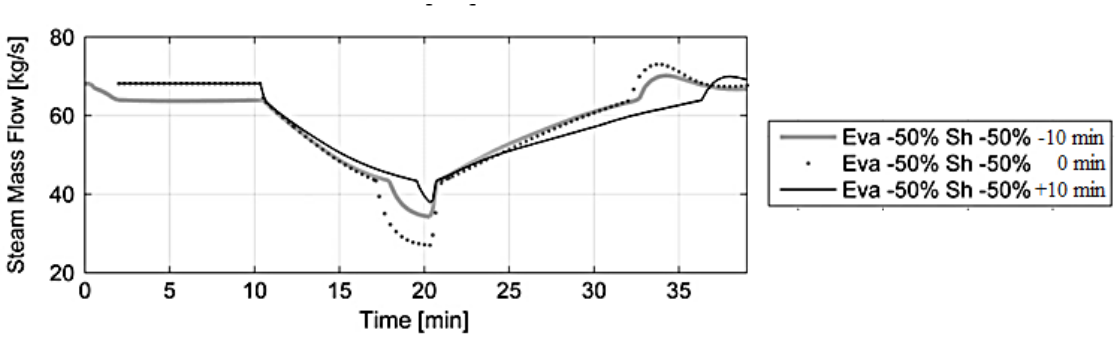

Figure 18. *Steam mass flow transients, as the DNI level is decreased by -50 % step change. Adapted from Birnbaum et al. 2011, p.663.*

If the superheating section is affected before the evaporator section, the steam mass flow stays almost stable, whereas the steam temperature is decreased shortly after the step change in the DNI level of the superheater section (grey line in Figure 19). On the contrary, if the superheating section is affected after the evaporator section, the steam mass flow is already decreased through superheating section, which first increases the steam temperature before the DNI on superheating section is decreased (black line in Figure 19). If both sections are affected at the same time (dotted line in Figure 19), the steam temperature and steam mass flow are decreased simultaneously, and the steam temperature is decreased less than in the other cases. In all three cases, the steam temperature overshoots before it reaches the initial temperature of 400 °C, as the steam temperature is more rapidly restored than the steam mass flow. Furthermore, the overshoot is the smallest, if the superheating section is affected after the evaporator section. (Birnbaum et al. 2011, p.662-663)

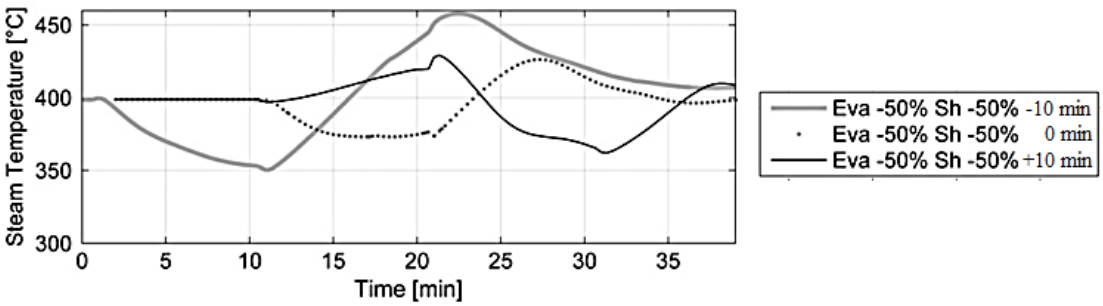

Figure 19. *Steam temperature transients, as the DNI level is decreased by -50 % step change. Adapted from Birnbaum et al. 2011, p.663.*

The applied control loops depend on the operation concept (see Chapter 2.1.4), as recirculation concept has phase separator tank and once-through does not have a phase separator tank. The basic control loops for recirculation concept and once-through concept are researched at the DISS facility together with the basic operation concepts, and the control loops are different for recirculation and once-through concepts. The main five control loops of the recirculation mode are (Valenzuela et al. 2005, p.305; Valenzuela et al. 2006 p. 6-7):

1. Outlet steam temperature control loop.
2. Outlet steam pressure control loop.
3. Liquid level of the separator tank control loop.
4. Feedwater pump control loop.
5. Recirculation pump control loop.

The first two control loops can be considered as the primary control loops for the control of steam quality at any instance, whereas the rest are secondary loops in order to improve the behaviour and the feasibility of the applied control system (Valenzuela et al. 2005, p.305). The outlet steam temperature loop keeps the outlet steam temperature at its design point by adjusting the spray water mass flow through attemperators before the inlet of the last collector. (Figure 20) One option is to use a cascade control loop, in which outer loop measures the outlet steam temperature after the final collector, and the inner loop measures the middle temperature of the final collector. (Birnbaum et al. 2011, p.661)

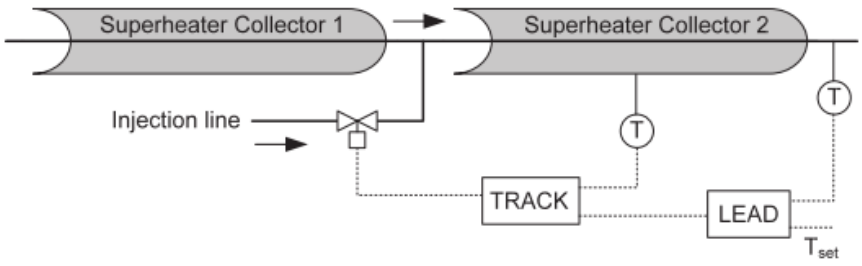

Figure 20. *Outlet steam temperature control loop (Birnbaum et al. 2011, p.661).*

If the power block of the solar field is operated on fixed pressure mode, the outlet steam pressure control loop keeps the outlet steam pressure constant by adjusting the position of outlet steam control valve (Figure 21). Thus, the steam pressure before the main steam valve is measured, and the position of the main steam valve is controlled accordingly. (Valenzuela et al. 2005, p.305) On the other hand, if the power block is operated on modified sliding pressure mode, the outlet steam pressure is directly proportional to the steam generation in solar field. Thus, the outlet main steam valve is kept almost fully opened and the outlet steam pressure is directly proportional to the thermal power of the power plant. (Joronen et al. 2007, p.158)

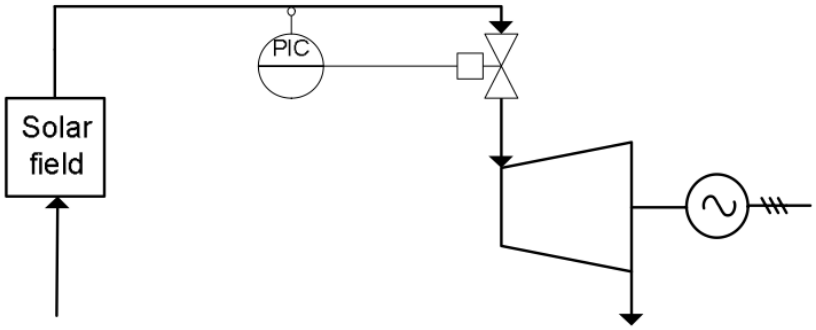

Figure 21. *Outlet steam pressure control loop. PIC= pressure indication and control. Adapted from Valenzuela et al. 2005, p.304.*

The liquid level of the separator tank is kept close to its nominal level by the feedwater valve and pump control loops (Figure 22). Thus, the feedwater inlet mass flow is adapted to the actual steam generation in the solar field (Birnbaum et al. 2011, p.661), as the objective is to keep the steam mass fraction after the evaporator section approximately at 0.80. The feedwater pump control loop adjusts the rotation speed of the pump in order to maintain constant pressure drop in the feedwater valve, which is used to control the inlet feedwater mass flow to the evaporation section. (Valezuela et al. 2005, p.305) Feedwater pump control loop could also be used to directly control the feedwater mass flow to the solar field due to frequency converters (Joronen et al. 2007 p.152). In addition, the liquid level of the feedwater tank is also affected by the recirculation pump

control loop, which maintains constant recirculation flow by adjusting the power input of the recirculation pump. (Valenzuela et al. 2005, p.305; Valenzuela et al. 2006 p.6-7)

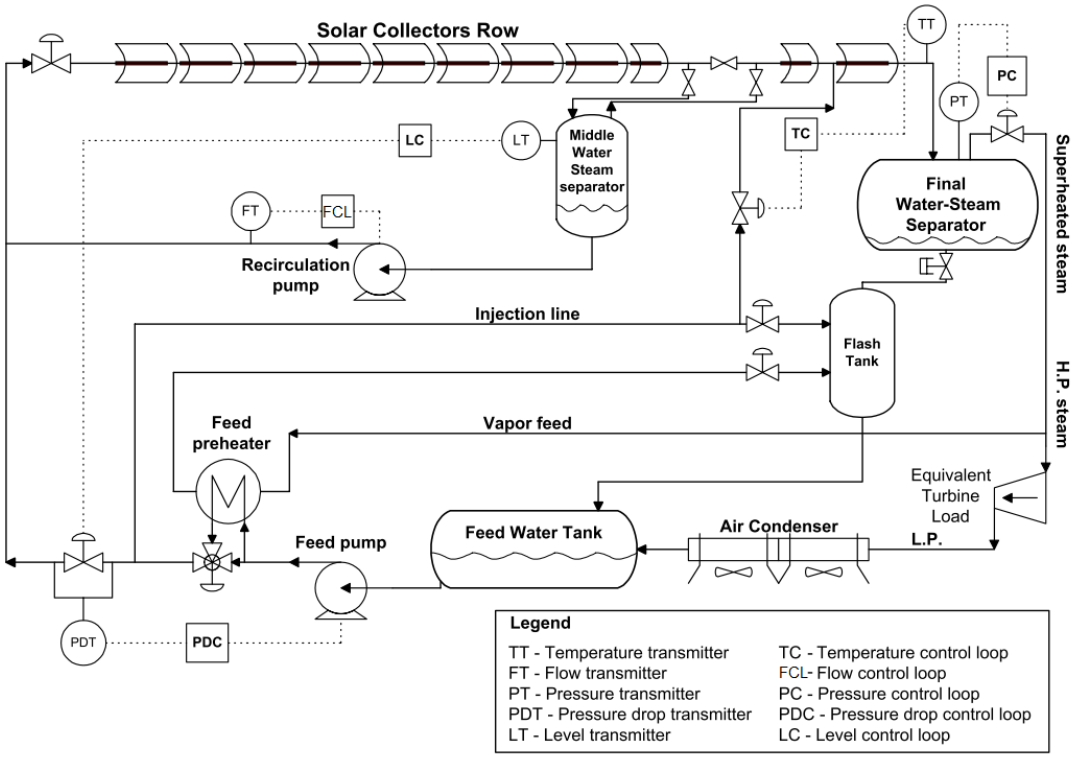

Figure 22. *Schematic of the recirculation concept at the DISS facility (Valenzuela et al. 2005, p.304).*

The main control loops in the once-through mode do not include control loops for recirculation pump and liquid level in the phase separator tank, as they are not included in the collector row. Thus, the main control loops for once-through concept are (Figure 23) (Valenzuela et al. 2005, p.305):

1. Outlet temperature control loops.
2. Outlet pressure control loop.
3. Feedwater pump control loop.

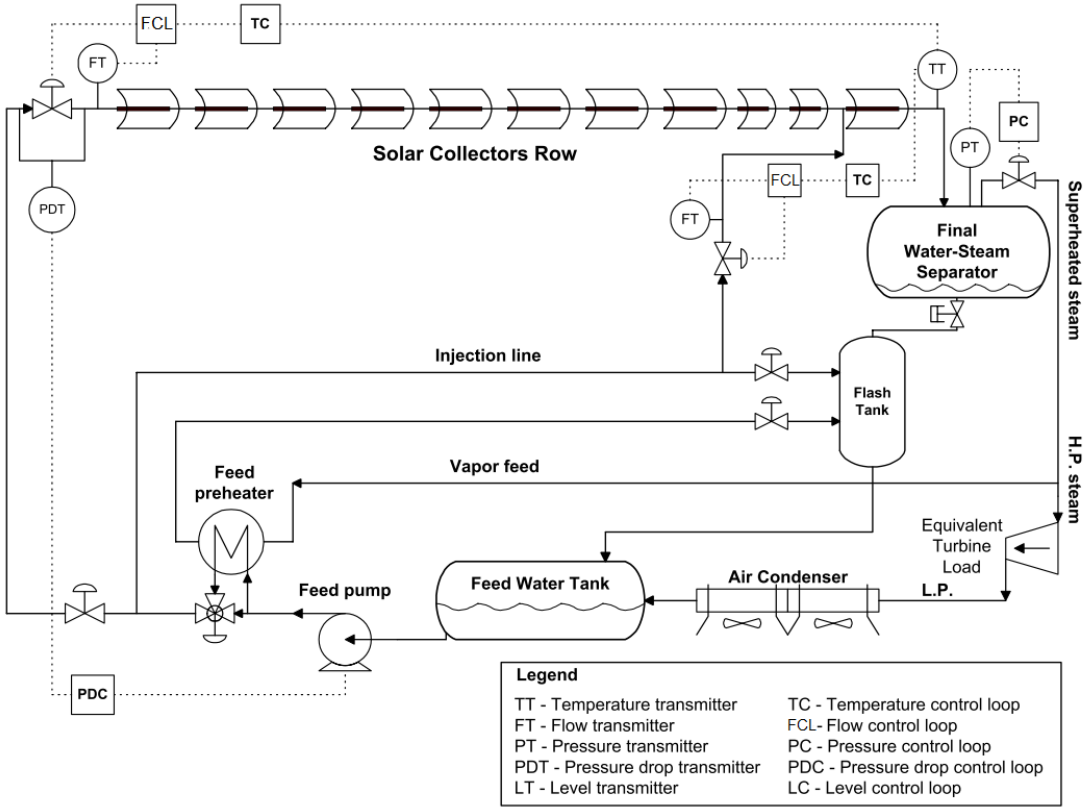

Figure 23. *Schematic of the once-through concept at the DISS facility (Valenzuela et al. 2005, p.306).*

In once-through concept, the outlet temperature control loops are designed to keep the outlet steam temperature at its design point by adjusting the inlet feedwater mass flow and spray water mass flow of attemperator in the superheating section. The former aims to control the inlet feedwater mass flow accordingly to the solar irradiation conditions, whereas the latter one aims to control the spray water mass flow of attemperator in case of sudden disturbances in the outlet steam temperature. The outlet steam pressure control loop operation is the same as in recirculation mode, and the feed pump control loop is basically the same as in recirculation mode, but the feedwater valve is designed differently than in recirculation mode, as the amount of feedwater entering the collector row is smaller than in recirculation concept. Furthermore, as all the feedwater is evaporated in once-through concept, the control engineering of once-through operation concept has to be based on feedforward action and be more sophisticated than in the recirculation concept. (Valenzuela et al. 2005, p.304-305)

2.2 Conventional steam power plants

Conventional steam power plant is chosen to be the host plant for the CSP integration. In conventional steam power plants, fuel is burnt in a steam boiler and electricity is generated through Rankine cycle. A typical conventional steam power plant is a subcritical unit, in which the live steam parameters are 160-180 bar and 535-565 °C, and the

net efficiency of the plant is 33% to 39%. (Miller 2011, p.256-257; Raiko et al. 2014, p.103-104) In order to increase the net efficiency of the plant and decrease pollution and fuel consumption, the combustion process of steam boilers is improved and the steam parameters are increased. If the steam parameters are increased over 221 bar, but they remain below 250 bar and 593 °C, the power plant is called a supercritical (SC) power plant. In ultra-supercritical (USC) plants, the pressure and the temperature are higher than 250 bar and 593 °C. The developed steam power plant technologies include atmospheric SC and USC pulverized coal combustion (PCC), pressurized PCC, atmospheric or pressurized fluidized bed combustion (FBC), combined cycle power plants, and externally fired combustion combined cycle (Miller 2011, p.251; Franco et al. 2009, p.351). In this thesis, the chosen power plant technology is the atmospheric FBC plants, and the other technologies are excluded. In addition, the power plant unit is chosen to be a typical subcritical steam power plant unit, which live steam parameters are close to the highest live steam parameters attainable from line-focusing solar field with DSG in the near future. Thus, the live steam parameters are approximately 160 bar and 550 °C. In the following chapters, fluidized bed combustion as an improved combustion technology is presented (Chapter 2.2.1). In addition, the basic process engineering principles of steam boilers (Chapter 2.2.2) and steam cycles (Chapter 2.2.3) are presented. Furthermore, the basic control engineering of steam power plants are presented (Chapter 2.2.4).

2.2.1 Fluidized bed combustion technology

Fluidized bed combustion represents the state-of-the-art technology of steam boilers, which are larger than stokers but smaller than PCC boilers. In the 1970s, many of the smaller units up to 100 MW_e were built to use stokers as boilers, but since the 1980s FBC has captured the market between small stokers and larger PCC boilers. Typically, only the small units up to 10 MW_e use stokers as boilers (Huhtinen et al. 1994, p.133) and FBC boilers are applied to units up to 500 MW_e (Teir 2002, p.8). FBC is an advanced combustion technology due to its advantages, which include in situ reduction of sulphur dioxide (SO_2) emissions, fuel flexibility and low nitrogen oxide (NO_x) emissions (Miller 2011, p.155-157; Teir 2002, p.7).

In FBC, the fuel is fed into the furnace, which contains limestone and inert bed material, such as sand or ash. The fuel, limestone and bed material are kept in a suspension due to stream of combustion air, which is distributed throughout the furnace floor. The bed material contains always excess amounts of limestone, which acts as a sorbent for SO_2. The amount of limestone depends on the sulphur content of the fuel, and it may cover up to 50% of the bed volume. The in situ control of SO_2 emissions is conducted by desulfurization during combustion process, which eliminates the need for separate and expensive flue gas desulfurization facilities. (Teir 2002, p.7)

The sand and ash in the bed material act as disperser for the fuel, and store a large amount of thermal energy, which ignites the fuel quickly. Due to effective mixing and

turbulence of the fluidized bed, heat transfer is enhanced, and the generation of heat inside the bed material is lower and more evenly distributed than in PCC boilers. (Miller 2011, p.160) In addition, the bed material provides adequate retention time to complete the combustion process (Huhtinen et al. 1994, p.143). Therefore, FBC enhances the use of different kinds of low-quality fuels, such as by-products of the forest industry, other residue biomasses and wastes.

The NO_x emissions are directly lowered by lower combustion temperature in the FBC boilers. (Teir 2002, p.7) The thermally induced NO_x begins to form, as the combustion temperature in the furnace reaches 1300 °C. However, in FBC boilers the temperature of the bed material is typically around 780-900 °C, which is well below the temperature range, where thermally induced NO_x production occurs. In addition, by staging the combustion air to different air zones in the furnace, the formation of fuel-bound NO_x can be minimized. (Huhtinen et al. 1994 p.84)

Depending on the velocity of the combustion air, the bed material acts in different kinds of fluid-like behaviour regimes (Figure 24). FBC boilers can be divided into bubbling fluidized bed (BFB) and circulating fluidized bed (CFB) boilers. The BFB refers to lower fluidizing velocity in the bed, which prevents solids to carry over from the furnace into the convective passes. Thus, the fluidizing velocity is between the minimum fluid velocity and the entrainment velocity, as can be seen in Figure 24. As the fluidizing velocity increases over the entrainment velocity, the BFB regime transforms into CFB regime, in which the particles are carried out from the furnace and circulated back to the furnace with a cyclone. In BFB boilers, the typical particle size of the bed material is 1-3 mm in diameter, and the fluidizing velocity varies between 0.7-2 m/s (Huhtinen et al. 1994 p.143). On the contrary, in CFB boilers the particle size of the bed material is 0.1-0.5 mm in diameter and the fluidizing velocity is 3-10 m/s (Huhtinen et al. 1994 p.145).

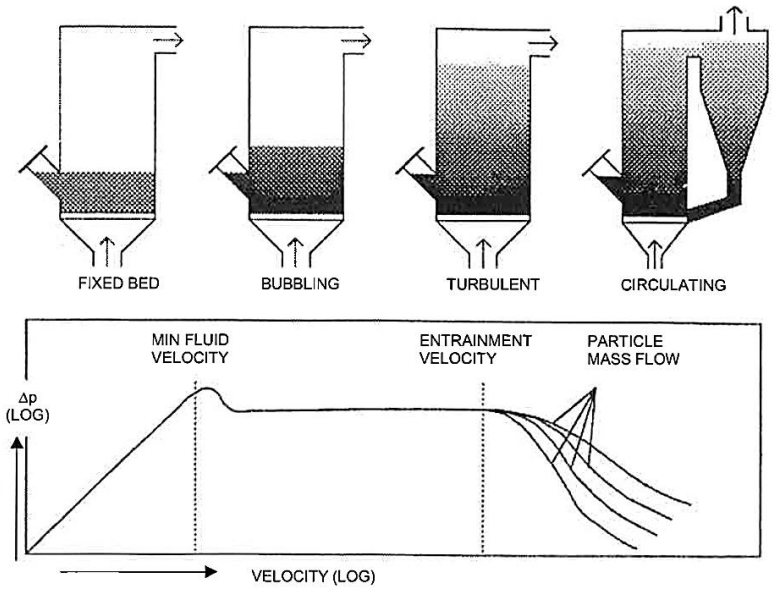

Figure 24. *Bed behavior regimes in FBC (Teir 2002, p.7).*

Typically, the power output of BFB boilers is lower than 100 MW_e, whereas the power output of CFB boilers is between 100 MW_e and 500 MW_e (Teir 2002, p.8). The BFB boilers are smaller in height than CFB boilers, contain less bed material, and require no cyclone. Therefore, the BFB boilers require less space in the boiler room and smaller ash-coolers. In addition, they require less fan power than CFB boilers due to smaller pressure drop across the bed material. Furthermore, erosion is also smaller in the furnace due to smaller gas velocity than in CFB boilers. (Miller 2011, p.264-265) Moreover, BFB boilers are typically used for combustion of waste materials, which have low calorific values (Koornneef et al. 2007, p.20).

On the contrary, CFB boilers have a number of advantages over BFB boilers. The combustion efficiency is higher and the consumption of limestone is lower in CFB boilers than in BFB boilers due to finer particles, more turbulent mixing and higher recycling rate. In addition, the CFB boilers need also smaller bed area and fewer fuel feed points. Furthermore, convective heat transfer coefficient in the heat surfaces is higher in CFB boilers than in BFB boilers. (Miller 2011, p.264-265) Currently, the development of FBC boilers aims to scale-up the units, achieve environmental compliance and wider fuel flexibility. In addition, the aim is to improve the construction and operation of the FBC plants, increase the efficiency and reduce investment and operational costs. (Koornneef et al. 2007, p.22)

2.2.2 Process engineering of steam boilers

All the steam boilers in conventional steam power plants are water-tube boilers, which can be divided into natural circulation (NC), forced circulation (FC), once-through (OT) and combined circulation boilers, which are basically a combination of FC and OT boilers. (Teir et al. 2002, p.6 & p.21) The NC and FC boilers can only be used in subcritical

units, whereas OT and combined circulation boilers are classified as universal boilers, which can operate also in supercritical units. Typically, the small and medium sized units apply NC or FC boilers, whereas OT boilers are used in larger units. (Teir et al. 2002, p.6 & p.17) One important design variable of steam boilers is the circulation number, which is defined as the ratio of the amount of water evaporating within the steam boiler and the total amount of water-steam mixture circulating in the evaporator. (Huhtinen et al. 1994, p. 110) In NC boilers, the circulation number is between 5 and 100, in FC boilers it is between 3 and 10, and in OT boilers it is 1. In other words, the feedwater circulates over five times in NC boilers before it is evaporated, whereas all the feedwater is evaporated in OT boilers. Thus, the amount of feedwater inside the boiler is the largest in NC boilers and smallest in OT boilers.

Natural and forced circulation boilers include a steam drum in order to separate the produced steam from water based on their density difference (Figure 25). The density difference between water and steam decreases, as the steam pressure increases and in the critical point (p = 221 bar) the density is same for water and steam. Therefore, NC and FC boilers are not suitable for supercritical units, as the steam drum cannot be operated in supercritical pressures. (Huhtinen et al. 1994, p.106) In addition, steam drum boilers are sensitive to pressure variations, as pressure decrease at the steam drum releases energy from the steam drum and vice versa. However, the steam drum can act as buffer to small load changes due to its capability to store energy on structure of the drum and its water volume. (Teir et al. 2002, p.7) In both boilers, the steam drum is also used to blow out some of the boiler water in order to prevent the formation of boiler scale (Huhtinen et al. 1994, p.103).

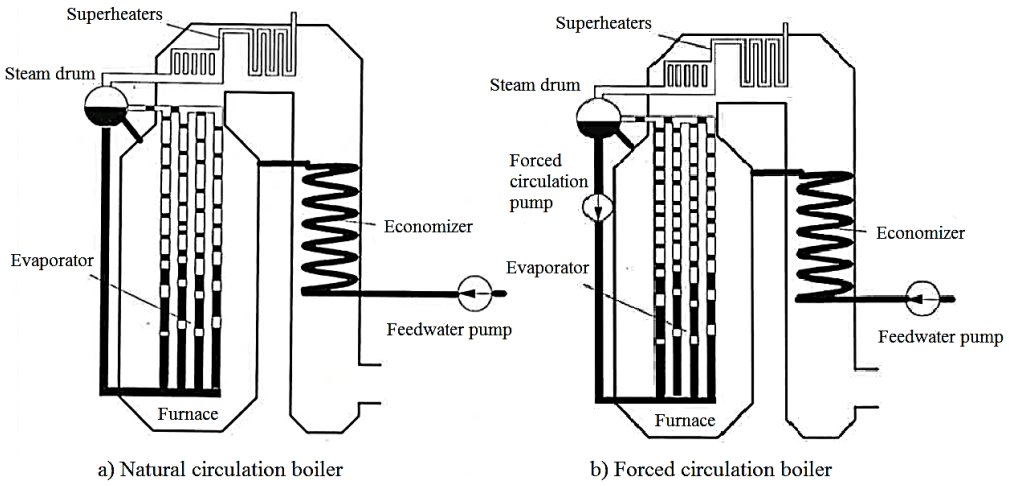

Figure 25. *Boilers with steam drum a) NC boiler and b) FC boiler. Adapted from Huhtinen et al. 1994, p.105 & p.111.*

In natural circulation boilers, the circulation between the steam drum and the evaporator is based only on density difference between the steam and water. Thus, the pressure of the live steam needs to be less than 170 bar. NC boilers are the oldest technique of water-tube boilers, which configuration is also simpler, and they are more tolerant to feedwater impurities than other water-tube boilers. Therefore, the investment costs and internal consumption of NC boilers are lower, and they are more reliable than other water-tube boilers. On the other hand, NC boilers are slower in start-ups and shutdowns than other water-tube boilers due to large volume of water inside the boiler. Furthermore, the pipes of the NC boilers are larger than in FC boilers. Thus, the NC boilers need to be accurately designed and the heat surfaces should be optimized in order to minimize the required amount of space and steel. (Teir et al. 2002, p.6-8)

In forced circulation boilers, the circulation between the steam drum and the evaporator is based on a circulation pump, which assures the circulation in the evaporator. Thus, the live steam pressure can be greater than 170 bar, but it still needs to be less than 190 bar, as the separation of steam and water in the steam drum is still based on density difference. The increased live steam pressure increases the attainable power output. However, the forced circulation pump needs to be installed directly under the steam drum in order to prevent cavitation in the pump. In addition, the circulation pump increases the internal consumption and the investment costs of the boiler. Furthermore, feedwater quality has to be higher in FC boilers than in NC boilers due to the circulation pump, which is sensitive to boiler scale. Moreover, the recirculation pump needs to be co-operated with the feedwater pump. Thus, the reliability of the FC boilers is lower than NC boilers. (Teir et al. 2002, p.14-15)

Once-through boilers do not include a steam drum. Thus, the amount of evaporated feedwater is directly proportional to the power output of the plant. In addition, the OT

boilers can be operated in supercritical pressures. The common OT boilers are Benson and Sulzer boilers (Figure 26).

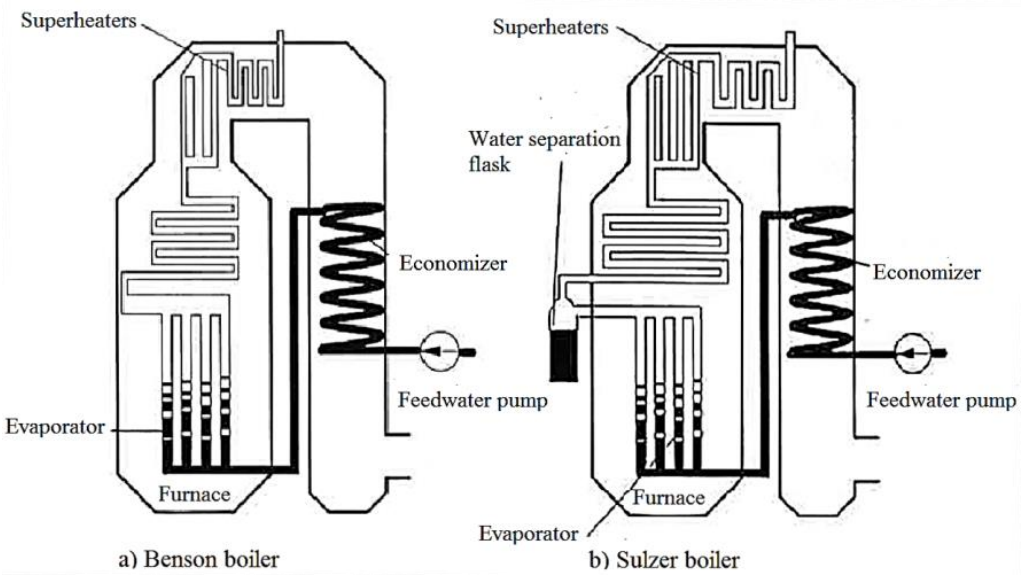

Figure 26. *Once-through boilers a) Benson and b) Sulzer boiler. Adapted from Huhtinen et al. 1994, p. 115-116.*

In Benson boiler, the end point for evaporation is transient, whereas the end point for evaporation can be fixed in Sulzer boiler due to a water separation flask. Originally, the water separation flask was used to demineralize the boiler water by blowing some of the water out, but the development of water treatment technologies has eliminated this requirement. Nowadays, the water separation flask is used in start-up and partial load situations, and it is also installed to Benson boilers to ease the operation of the boiler. (Huhtinen et al. 1994, p. 114-116) Due to smaller water volume inside the OT boilers, they are quicker in start-ups and shutdowns than steam drum boilers. However, the control of OT boilers needs to be more sophisticated than steam drum boilers, and the feedwater pump has to overcome large pressure losses of the boiler, which increases the internal consumption. (Teir et al. 2002, p.18-20) The overall advantages and disadvantages of NC, FC and OT boilers are presented in the following Table 1.

Table 1. *The advantages and disadvantages of natural circulation, forced circulation and once-through boilers (Teir et al. 2002, p.7-20; Huhtinen et al. 1994, p.112).*

Boiler	Advantages	Disadvantages
NC	- Steam drum can act as "buffer" for small load changes - Oldest of water-tube boiler techniques - Simple configuration - Greater tolerance for feedwater impurities - High reliability - Low internal consumption	- Sensitivity to pressure variations - Large circulation number (5-100) - Large circulation number makes NC slow in start-ups and shutdowns - Larger pipes increase the requirement for space and steel. Thus, boiler needs to be accurately dimensioned
FC	- Steam drum can act as "buffer" for small load changes - Low circulation ratio (3-10) - Circulation pump assures the circulation in the evaporator - Wider power range than NC boilers - Smaller tube diameters than NC boilers	- Sensitivity to pressure variations - Location of the circulation pump needs to be directly under the steam drum in order to prevent cavitation in the pump - Higher internal consumption and investment costs than NC boilers - Higher feedwater quality than in NC boilers - Control and regulation of the co-operation of feedwater pump and circulation pump - Lower reliability than NC boilers
OT	- Suitability for supercritical pressures in larger units - Evaporation is directly proportional to power load demand - Quicker in start-ups and shutdowns than NC and FC boilers	- No capacity buffer due to lack of steam drum - More sophisticated control regime is required due to small water/steam volume - High pressure losses in the boiler which causes high internal consumption of the feedwater pump

As a conclusion of the process engineering of steam boilers, the NC boilers are the most reliable of the water-tube boilers, as its configuration is the simplest. In addition, its internal consumption is the smallest. Furthermore, NC and FC boilers can also store some energy to their steam drums in order to apply it to small load changes, whereas OT boilers cannot store any energy, as the evaporation is directly proportional to the power output of the plant. In addition, control of NC boilers is simpler than in FC and OT boilers. However, NC and FC boilers are slower at start-ups and shut downs and more sensitive to pressure variations than OT boilers.

2.2.3 Process engineering of steam cycles

Three examples of process schemes of subcritical steam cycles are presented in the Appendix F, from which the one steam cycle configuration is presented in the Figure 27. The 210 MW_e subcritical unit is a regenerative and reheated unit, in which live steam parameters are 537 °C and 150 bar (Sengupta et al. 2007, p.17). The steam power plant includes two high pressure feedwater heaters (HP FWH) and three low pressure feedwater heaters (LP FWH).

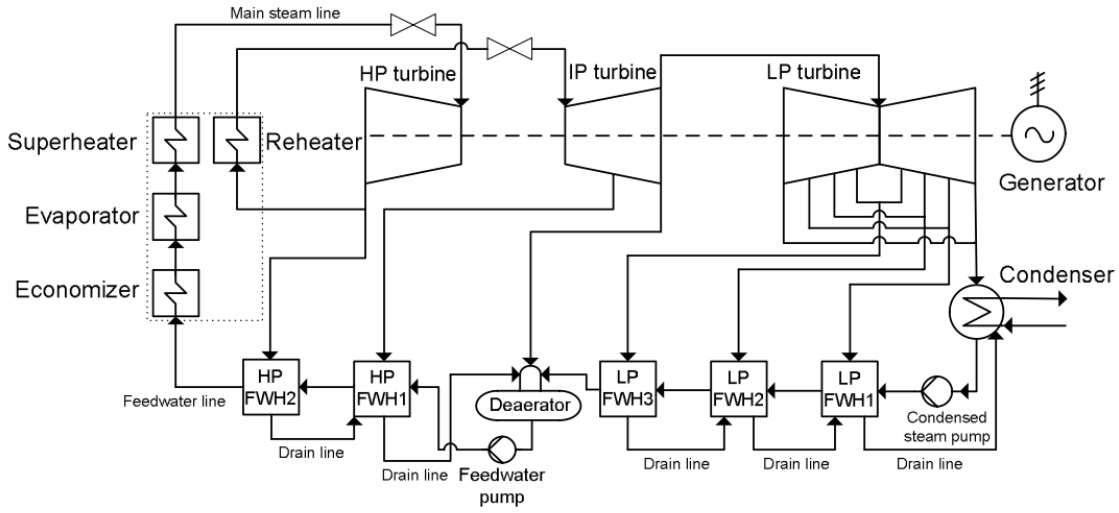

Figure 27. *Schematic process diagram of a 210 MW_e steam power plant. Adapted from Sengupta et al. 2007, p.17.*

The main sections of typical steam cycles are feedwater preheating, boiler and turbine sections. On any steam power plant the feedwater is preheated in the FWHs before it enters the boiler. This improves the net efficiency of the steam cycle, as the average heat input temperature is increased. It also allows the boiler to be used only for evaporation of the feedwater. The feedwater is preheated by extracting steam from the turbine sections, but this reduces the power output of the plant, as the steam mass flow through the turbine sections is decreased. In addition, multiple HP and LP FWHs are installed in the steam cycle, as in a single FWH system the temperature profile of extracted steam from the turbine does not match well with the temperature profile of feedwater. Thus, large amount of exergy is lost. (Hu et al. 2010, p.2883) Firstly, in the preheating the condensed feedwater from the condenser enters a condensate pump, which increases the pressure of the feedwater in order to allow its flow to deaerator, which pressure is determined by the bled off steam line entering the deaerator. Then, the feedwater flows through the LP FWHs into the deaerator. The deaerator is an open type FWH, in which steam from the turbine is mixed with the incoming feedwater to further preheat the feedwater, and oxygen and other incoaguable gases are removed from the feedwater. After the deaerator, a feedwater pump raises the pressure of the feedwater, and the feedwater is fed through the HP FWHs before it enters the boiler. (Raiko et al. 2013, p.45 & p.52)

The boiler includes economizer, evaporator and superheaters and reheaters. Preheated feedwater from the FWHs enters the economizer, which increases the feedwater temperature close to its boiling temperature before it enters the evaporator. The outlet temperature of the economizer is kept about 10 K under the boiling temperature in order to prevent boiling in the economizer. (Teir et al. 2002, p.6) Overall, the feedwater is typically preheated from 40 °C to 300 °C before it is evaporated (Hu et al. 2010, p.2883). Then the evaporator produces either water-steam mixture or saturated steam depending on the boiler type. After the evaporator, the superheaters increase the steam temperature

up to its design point in order to avoid condensation in the turbine sections. The minimum of superheating depends on the process and the turbine, but it could be, for example, 50 °C (Alguacil et al. 2014, p.23). The reheaters are used after the HP turbine section in order to further increase the net efficiency of the power plant and lower the moisture content of the final expanded steam after the intermediate (IP) and LP turbine sections.

The turbine sections include high pressure turbine section, intermediate pressure and low pressure turbine sections, and after the turbine sections the steam cycle includes a condenser. The live steam from the superheaters enters the HP turbine section, in which the steam expands, and the thermal energy of the steam is converted to kinetic energy of the turbine blades and shaft. The kinetic energy is then converted to electricity by a generator. After the HP turbine section, expanded steam is typically reheated in the boiler and fed to the IP turbine section, in which the steam is further expanded. A typical steam power plant is a condensing power plant, in which the steam is expanded to the lowest attainable pressure and only electricity is produced. The end point of the expansion is determined by the available cooling water temperature in the condenser. Finally, the expanded steam is condensated to subcooled water, which is yet again fed into the condensate pump and through the FWHs. (Raiko et al. 2013, p.18)

2.2.4 Control engineering of steam power plants

Control engineering is applied to steam power plants in order to produce desired thermal output of the boiler and desired power output of the plant. In addition, the produced live steam must have correct temperature and pressure, and the produced electricity must have correct voltage and frequency. These objectives are achieved in steam power plants by applying a coordinative control strategy between the steam boiler, turbine and generator without overloading the components. (Joronen et al. 2007, p.149) The coordinative control strategy combines the controls of the fuel power, generator power, turbine power and steam pressure (Figure 28).

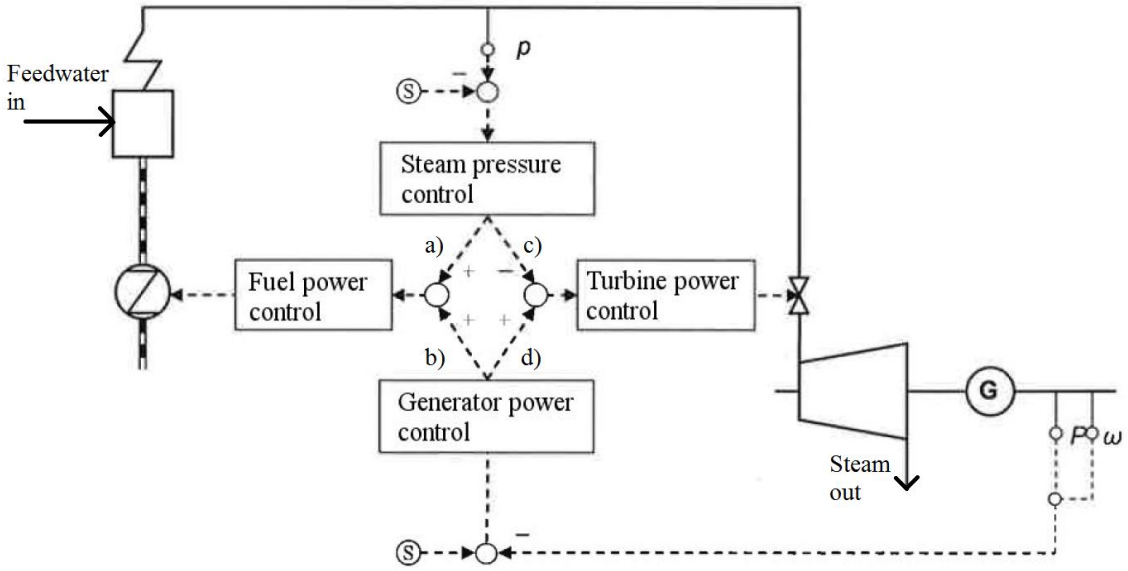

Figure 28. *Possible coordinative control strategies. Adapted from Joronen et al. 2007, p.149.*

Three modes of coordinative control strategy can be described: boiler follow mode, turbine follow mode, and coordinated control mode (Joronen et al 2007, p.149; Basu et al. 2015). In the boiler follow mode, the fuel power is controlled by live steam pressure, and generator power is controlled by adjusting the throttle of the turbine. In other words, connections a) and d) are activated in Figure 28. In the turbine follow mode, the fuel power is controlled by the generator power, and the live steam pressure in controlled by throttle of the turbine. In other words, connections b) and c) are activated in Figure 28. In the coordinated control mode, the control of the boiler and turbine are integrated with each other in order to control the power output of the plant as quickly as possible. Thus, for example, connection c) is activated with connections a) and d) in order to keep the pressure variations inside certain limits and minimize heat stress of the boiler (Joronen et al. 2007, p.151). Depending on the coordinative control system, combination of several interacting control loops has to be applied (Basu et al. 2015). In addition, the applied control loops of the steam power plant depend on the boiler type, as there is a steam drum in NC and FC boilers but not in OT boilers. The main five control loops of steam power plants are (Raiko et al. 2013, p.157-158):

1. Control of the live steam pressure.
2. Control of the live steam temperature.
3. Control of the amount of feedwater.
4. Control of the combustion.
5. Control of the furnace pressure.

The control of the live steam pressure is closely related to the control of the fuel power of the boiler and power output of the plant. It can be divided into two main categories:

fixed pressure and sliding pressure (Figure 29) (Joronen et al. 2007, p.158; Raiko et al. 2013, p.158). The fixed pressure stands for keeping the live steam pressure constant at all levels of power output. Thus, the enthalpy drop in the turbine is constant and the power output of the plant is adjusted by the live steam mass flow rate. On the other hand, in the sliding pressure mode the live steam pressure is directly proportional to the fuel feeding: the live steam pressure is at maximum, as the turbines are operated at maximum load, and the live steam pressure decreases directly proportional to the power output of the plant. (Joronen et al. 2007, p.158)

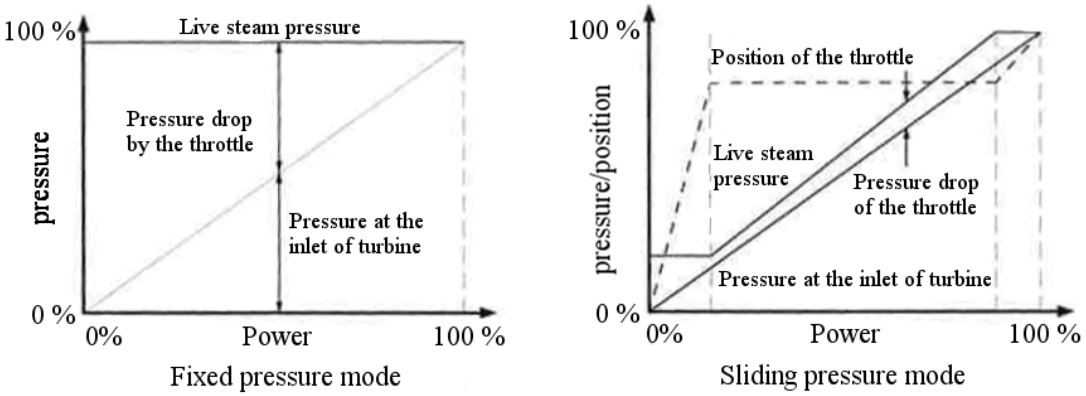

Figure 29. *Live steam pressure control modes for fixed pressure and sliding pressure. Adapted from Joronen et al. 2007, p.158.*

The fixed pressure control method is different for the boiler follow mode and turbine follow mode. In the boiler follow mode, the live steam pressure is kept constant by fuel feeding, as the power output of the plant is adjusted by the main steam valve of the steam boiler. In boiler follow mode, if the power output of the plant is increased, the main steam valve is opened, which decreases the live steam pressure. Thus, the fuel feeding is increased in order to compensate the pressure decrease accordingly. On the other hand, in the turbine follow mode the live steam pressure is kept constant by the main steam valve of steam boiler, as the power output is adjusted by fuel feeding. If the power output is increased, the fuel feeding is increased, which raises the live steam pressure. Thus, the main steam valve is opened accordingly. (Joronen et al. 2007, p.149-150)

The sliding pressure mode can be divided into pure sliding pressure and modified sliding pressure modes according to the position of the throttle of the turbine. In pure sliding pressure mode, the throttle is kept always fully open, and the steam pressure is directly proportional to the power output. On the other hand, the throttle is kept slightly choked in the modified sliding pressure mode. (Raiko et al. 2013, p.159-161) If the power output is increased in modified sliding pressure mode, the throttle is opened in order to compensate small load changes. As a consequence, the fuel power of the boiler needs to be increased accordingly. As fuel feeding of the steam boiler is adjusted to the changed power demand, the throttle of turbine is restored to its initial state. The step

response times of all four live steam pressure control methods is presented in Figure 30. The fastest change of power output can be achieved with fixed pressure and boiler follow mode, whereas the pure sliding pressure mode is the slowest control method.

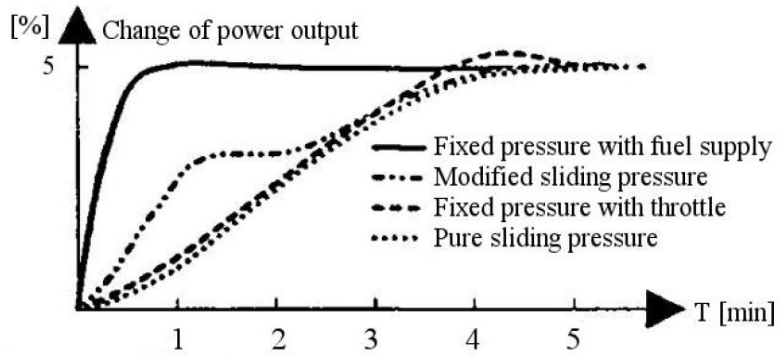

Figure 30. *The step response times for a 5 % step change in power output in different steam pressure control modes. Adapted from Raiko et al. 2013, p.162.*

Natural circulation boiler or forced circulation boilers are not usually operated on sliding pressure mode, since it would have restrictions on load changes (Spliethoff 2010, p.97). Furthermore, the end point of evaporation is fixed with steam drum in NC or FC boilers, and the ratio of superheating and evaporation heat surfaces is optimized. (Huhtinen et al. 1994, p. 114-116; Teir 2002, p.6) Thus, if NC boiler is operated with sliding pressure mode, the end point of evaporation would change and the ratio of heating surfaces is not any more optimal. On the other hand, OT boilers can be operated under fixed pressure or sliding pressure modes. (Spliethoff 2010, p.97)

Control of the live steam temperature is applied in order to keep the temperature of the steam at its design point as accurately as possible. There are three methods for temperature control: spray cooling of the steam, by-passing of the flue gases and using of additional heat exchanger. The spray cooling is the most common way in the control of steam temperature, as it is simple, inexpensive and easy to apply (Figure 31). (Joronen et al. 2007, p.166) The attemperators are opened after the steam temperature reaches its design point with a certain part load of the boiler, for example at part load of 70% (Rayaprolu 2009, p.237). The spray cooling water is taken after the feedwater pump, and its amount is controlled by the temperatures of the steam before and after the superheater surface. In addition, information about the load of the steam boiler is needed. (Joronen et al. 2007, p.152)

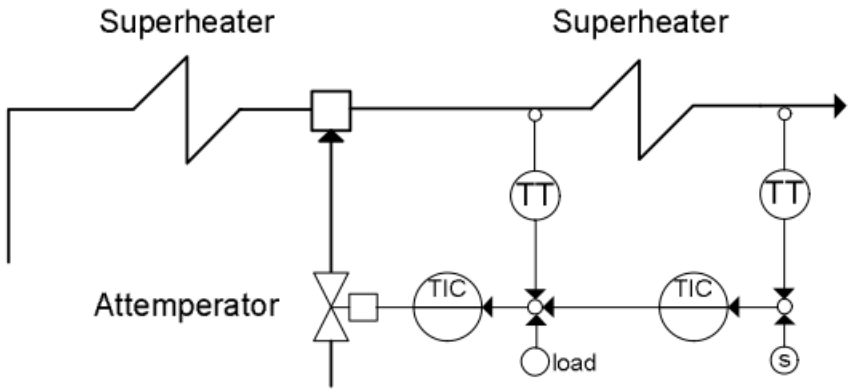

Figure 31. *Schematic of temperature control of live steam by spray cooling. TT = temperature transmitter, TIC = Temperature indication and control, s = set point. Adapted from Joronen et al. 2007, p.106 and Raiko et al. 2013, p.170.*

Attemperators can also be applied to adjust the reheated steam temperature. In addition, the reheated steam temperature can also be controlled by by-passing of the flue gases or by using an additional heat exchanger. In by-passing, the flue gases are redirected in the flue gas duct by control sheets. In addition, flue gases can be recycled in the flue gas duct by a blower, which directs some of the cooled flue gases back to furnace. As a consequence, the furnace cools down, the heat transfer based on radiation worsens, but the heat transfer based on convection improves. Furthermore, an additional heat exchanger can be installed between the superheaters and reheaters in order to transfer heat between the heat surfaces. (Raiko et al. 2013, p.172)

Control of the amount of feedwater is different for steam drum, Sulzer and Benson boilers. In the steam drum boilers, the feedwater control aims to maintain the level in the steam drum constant, whereas in Sulzer boilers the feedwater control aims to maintain the level in the water separation flask constant. On the contrary, in a Benson boiler the level of water separation flask is not suitable control variable for feedwater control. Instead, feedwater control of Benson boilers is based on the ratio between the flow rate of feedwater and the flow rate of spray cooling. The ratio is kept constant by adjusting the flow rate of feedwater. (Raiko et al. 2013, p.165-167)

The method for feedwater control in steam drum boilers is based on the three element cascade control, which measures the level of feedwater in the steam drum, the flow rate of feedwater and the flow rate of steam (Figure 32) (Raiko et al. 2013, p.165). Previously, a control valve was applied in order to control the amount of feedwater, but nowadays pumps are used for direct control of the flow due to frequency converters. (Joronen et al. 2007, p.152) The sensitivity of feedwater control is dependent on the ratio of water volume in the steam drum and the overall water volume in the boiler: the smaller the volume ratio is, the more sensitive the system is. (Raiko et al. 2013, p.165)

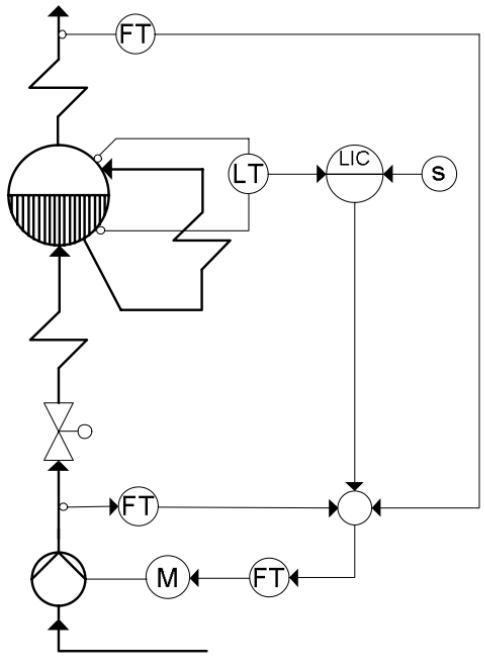

Figure 32. *Schematic of three element cascade feedwater control in steam drum boilers. FT = flow transmitter, LT = level transmitter, LIC = level indication and automatic control, s = set point, M = motor. Adapted from Joronen et al. 2007, p.156 and Raiko et al. 2013, p.166.*

In the Sulzer boiler, the control of feedwater can be arranged like in steam drum boilers, but also by throttling some of the evaporated steam. The throttling of the steam increases the temperature of the steam, and the measured temperature increase can be used as control variable for the feedwater control. If the steam is superheated a lot by the throttling, the amount of feedwater is too small and vice versa. The best result is obtained, as the feedwater control is arranged in both arrangements: by measuring the level of water separation flask and the temperature before water separation flask (Figure 33). (Raiko et al. 2013, p.167)

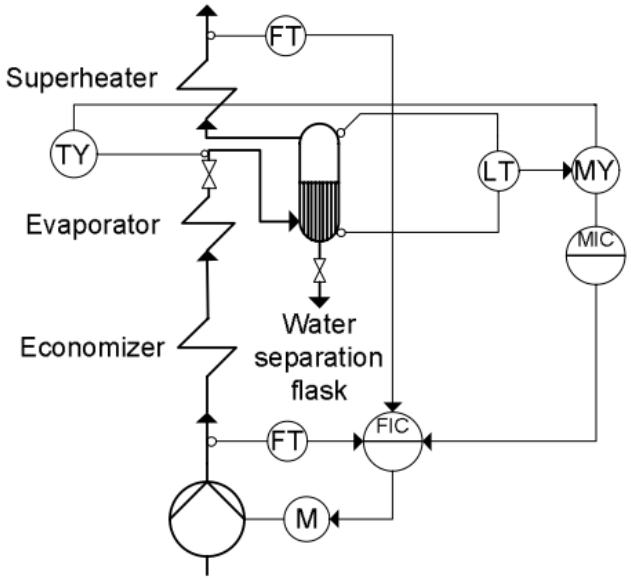

Figure 33. *Schematic of feedwater control in Sulzer boiler. FT = flow transmitter, TY = temperature calculating function, LT = level transmitter, MY = multiple variable calculating function, MIC = multiple variable indication and control, FIC = flow indication and automatic control. Adapted from Raiko et al. 2013, p.167.*

In Benson boiler, the feedwater control is based on the ratio between spray cooling flow rate and feedwater flow rate. In addition, information of the load is required. In Benson boilers, temperature difference is measured over the superheaters or the attemperators (Figure 34). (Raiko et al. 2013, p.167) As the temperature of live steam is increased, the flow rate of spray cooling is increased, which increases the ratio of spray cooling flow rate and feedwater flow rate. The ratio is returned to its design value by increasing the flow rate of feedwater, which decreases the superheating and lowers the flow rate of spray cooling.

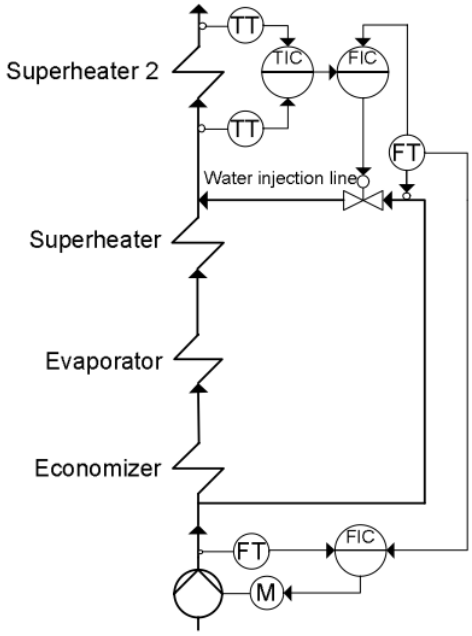

Figure 34. *Schematic of feedwater control in Benson boiler. TT= temperature transmitter function, TIC= temperature indication and controls, FT = flow rate transmitter function, FIC = flow rate indication and automatic control, M = motor. Adapted from Raiko et al. 2013, p.168.*

Control of the combustion aims to keep the correct ratio between combustion air and fuel supply, since low-level of combustion air leads to imperfect combustion, and excess combustion air decreases the net efficiency of the plant. As a result, the level of oxygen in flue gases is used as control variable for the combustion control, which aims to keep the level of excess air in flue gases to its safest minimum. In addition, the control of combustion air is typically operated parallel with fuel feeding. Thus, any disturbances in the fuel feeding or in the combustion air supply are noticed in the undisturbed variable. (Joronen et al. 2007, p.160) The amount of combustion air is controlled by adjusting the rotation speed or inlet guide vanes of fresh air blower, adjusting the dampers or adjusting the blade angle of an axial blower (Raiko et al. 2013, p.163).

Control of the furnace pressure aims to keep under pressure in the furnace in order to prevent flue gas leaks into the boiler room (Joronen et al. 2007, p.164; Raiko et al. 2013, p.164). The flue gases are induced from the furnace by a blower, which speed, inlet guide vanes or blade angles are adjusted accordingly to the desired furnace pressure (Raiko et al. 2013, p.164). Steady pressure in the furnace ensures correct conditions for combustion. On the contrary, any disturbances in the furnace pressure often result from disturbances in the combustion conditions. (Joronen et al. 2007, p.164)

2.3 Concentrated solar power and steam power plant hybrids

CSP and steam power plant hybrid consists of a solar field and conventional steam power plant, which use the joint steam cycle. The investigation of CSP hybrids is not a novel research area, since the first serious attempts in order to investigate the hybrid systems were conducted in the 1970's due to the oil crisis (Petrov et al. 2012, p.3). The integration of CSP with steam power plants is currently considered as a medium CSP hybrid, in which the solar field and the steam power plant are physically connected to each other and share the major components of steam cycle, like turbines, condenser and FWHs. However, in medium CSP hybrids the solar field does not function without the steam power plant, but the steam power plant functions without the solar field. In addition, the typical solar share of medium CSP hybrid plants is below 10% of the installed plant. Due to the typically low solar share, the possibilities to reach higher solar shares should be investigated in order to further reduce the CO_2 emission level and fuel consumption. These hybrids are considered as strong hybrids, in which the solar share is over 30% of the installed capacity, and the power plants work in parallel side by side. Examples of strong hybrid systems are CSP plants using another fuel to further superheat the solar steam, CSP plants used to raise the steam parameters of low temperature renewable energy sources, such as geothermal energy and biomass energy, and CSP plants providing superheated solar steam to the joint turbine. (Peterseim et al. 2014, p.179)

There are several benefits in the integration of CSP with steam power plants. These are, for example, lower installation costs and LCOE of CSP, greater annual generation of electricity, decreased fuel consumption and CO_2 emissions, wider suitable areas for CSP applications (Peterseim et al. 2013, p.520-521), higher first and second thermodynamic law efficiencies compared to stand-alone CSP plants and steam power plants and higher solar-to-electricity conversion (Hu et al. 2010, p.2882). The joint-use of existing infrastructure of the steam power plant can provide a significant reduction of LCOE of CSP. Building of CSP hybrids could boost the building of stand-alone CSP plants, ramp up the manufacturing capabilities for CSP plants, and relevant project implementation experience could be gained from the hybrid systems. Moreover, it reduces investment risks associated with the CSP technology. Unlike stand-alone CSP plants, CSP hybrid systems can generate dispatchable energy until cost-effective energy storage technology is available. In addition, the dispatchability avoids the problems with solar irradiation as a fluctuating energy source. (Peterseim et al. 2013, p.520-521)

CSP hybrid systems are an attractive option for power generation in countries, which are rich in solar resources, such as Australia, China, India (Suresh et al. 2010, p.267), South Africa (Pierce et al. 2013, p.657) and the United States. (Lovegrove et al. 2012, p.404) The CSP integration can be done to repower older units, or to construct new CSP hybrid plants. However, the CSP retrofit installations in older units need to be carefully considered, since the lifetime of existing power plants should not be extended, and in-

vestments in renewable energy plants should not be delayed. For example coal-fired power plants are designed to have a lifetime of approximately 40 years, whereas CSP plants can currently require up to 20 years in order to break even in investment costs. Peterseim et al. (2014) suggest that retrofits should not be done to units older than 10 to 15 years, as in older units the short operation time of the hybrid system can offset the avoided CO_2 emissions due to the typically low solar share. (Peterseim et al. 2014, p.179) Since the performance of the turbines and the boiler is possibly affected in retrofits, it may be more attractive to construct new hybrid plants, in which the size and performance of the main components are optimized according to the thermal power of the solar field while maximizing the achievable solar share. (Petrov et al. 2012, p.5)

The integration of CSP with steam power plants can be readily achieved with a DSG system, since solar steam is directly injected to the steam cycle without additional HTF and heat exchanger. In addition, there is no need for energy storage equipment, since the fuel supply of the steam boiler can be adjusted within the boiler's operating limits to compensate the intermittency of solar irradiation. (Lovegrove et al. 2012, p.421) However, the ease of the integration depends on the operation mode, the selected process arrangement, and the development of flexible control engineering for the hybrid system. In addition, the disadvantages of water as HTF should be considered (see Chapter 2.1.1). In the following chapters the operation modes of CSP hybrid systems are observed (Chapter 2.3.1) before the comprehensive study of the possible process arrangements (Chapter 2.3.2 and Chapter 2.3.3). Finally, the process requirements and restrictions of CSP hybrids are presented (Chapter 2.3.4).

2.3.1 Operation modes for the hybrid systems

The operation mode of hybrid system depends on the aim of the hybrid system. Hybrid system can be used to produce more electricity with same amount of fuel or to produce same amount of electricity with less fuel. In other words, the hybrid system can be operated on power boost mode or on fuel saving mode (Figure 35). Both operation modes are applicable in real-life conditions (Petrov et al. 2012, p.3), and both modes decrease the fuel consumption rate (g/kWh) of the host plant (Yan et al. 2011, p.916).

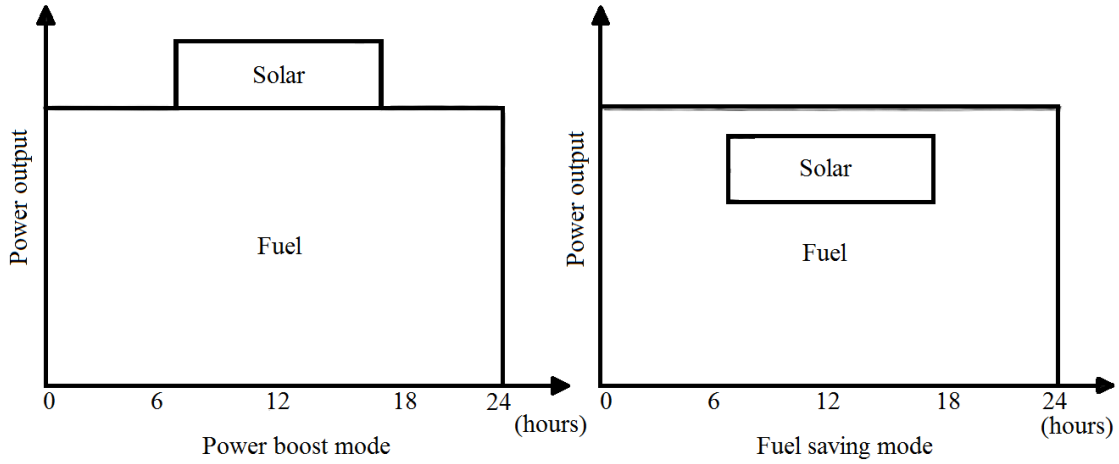

Figure 35. *The two operation modes of CSP hybrids. Adapted from Yan et al. 2011, p.911.*

In power boost mode, the operation of turbine and generator are set beyond their nominal operating points, and the boiler operates on its nominal full load. As a result, more electricity is produced with the same amount of fuel. (Lovegrove et al. 2012, p.423; Yan et al. 2011, p.911) The power boost mode is particularly suitable scenario for electricity production during peak sunshine hours in order to meet the increased energy consumption due to air conditioning (Hu et al. 2010, p.2882; Petrov et al. 2012, p.3). However, the full potential of the solar field may not be fulfilled, since the additional generated heat input of solar field may be larger than the existing turbine or generator can exploit in the power boost mode (Hu et al. 2010, p.2881-2882).

In fuel saving mode, the operation of the boiler is kept under its nominal operating point, and the turbine and generator are operated on their nominal load. As a result, the same amount of electricity is produced with less fuel. (Lovegrove et al. 2012, p.423; Yan et al. 2011, p.911) Thus, the CO_2 emission level of the power plant is reduced. Peterseim et al. (2013) propose that power boost mode should be applied in new plants, which generate low levels of CO_2 emissions, and fuel saving mode should be applied in older plants, which use expensive fuels and generate high levels of CO_2 emissions. In addition, the equipment usage should be maximized, and the spent capital should be recovered as quickly as possible. (Peterseim et al. 2013, p.527) Furthermore, Petrov et al. (2012) consider also that new power plants should be operated on power boost mode, as the solar augmentation is already a part of the power plant design, and the resulting unit has an inbuilt flexibility for utilizing the available solar energy. Moreover, it seems to be more economically feasible to produce more electricity than save fuel. (Petrov et al. 2012, p.5)

2.3.2 Possible process arrangements of the hybrid systems

There are at least seven possible process arrangements for hybrid systems considered in various references. The following seven arrangements are considered in this work and are explained in more detail:

1. Feedwater heating, in which solar field produces heated feedwater (FWHFL) (Figure 36).
2. Feedwater heating, in which superheated steam from solar field is fed into bled off steam line (FWHBOS) (Figure 37).
3. Superheated steam from solar field is fed into cold reheat line (CRH) after HP turbine (SuSCRH) (Figure 38).
4. Superheated steam from solar field is fed into the inlet of HP turbine (SuSHP) (Figure 39).
5. Superheated steam from solar field is fed into the inlet of IP turbine (SuSIP) (Figure 40).
6. Saturated steam from solar field is fed into boiler drum (SaSBD) (Figure 41).
7. Saturated steam from solar field is fed into boiler drum combined with feedwater heating (SaSBDFWH) (Figure 42).

From these process arrangements, superheated steam from solar field is fed into bled off steam line at Liddell Power Station, in which solar field replaces part of the HP FWHs (Hu et al. 2003, p.15). In addition, superheated steam from solar field is fed into cold reheat line after the HP turbine at Kogan Creek Power Station (AREVA Solar 2015c). Furthermore, in the Sundt Solar Boost Project the solar field produces superheated steam to the same steam cycle as steam booster, but the process arrangement remains unclear (Peterseim et al. 2013, p.530; Tucson Electric Power 2016). Other process arrangements are discussed at conceptual level in several publications, but the design of SuSIP process arrangement is introduced in this thesis.

In addition to several possible process arrangements, there are several possible extraction points for feedwater from the steam cycle and to the solar field. The basic four points are after the condensate pump, after the deaerator, after the feedwater pump, and before the economizer. However, the choice of extraction point depends on the chosen the process arrangement (Table 2). If the feedwater is extracted after the condensate pump, an additional boost pump is needed because of the pressure losses occurring over the solar field, and the required pressure stage of the integrated steam line needs to be met (Pierce et al. 2013, p.659). To avoid the Ledinegg instability in the solar field, an additional preheater is possibly needed before solar field. If Ledinegg instability occurs, the feedwater can vaporize instantaneously, which causes problems in the evaporator section of the solar field (Ruspini et al. 2014, p.524). If feedwater is extracted after the feedwater pump, a pressure reduction station is possibly needed, since the water pressure may not be suitable for the solar field (Yang et al. 2008, p.1213).

Table 2. *The possible extraction points for feedwater from steam cycle in different process arrangements.*

Process arrange-ment	After condensate pump	After deaerator	After feedwater pump	Before economiz-er
FWHFL	Yes	Yes	Yes	No
FWHBOS [1]	Yes	Yes	Yes	Yes
SuSCRH	Yes	Yes	Yes	Yes
SuSHP	Yes	Yes	Yes	Yes
SuSIP	Yes	Yes	Yes	Yes
SaSBD	No	No	No	Yes
SaSBDFWH	Yes	Yes	Yes	No

[1] The extraction point needs to be chosen according to the thermal parameters of the bled off steam.

For the FWHFL process arrangement, the feedwater cannot be extracted before the economizer, since otherwise the extraction point is the same as the injection point of heated feedwater. If the feedwater is extracted after the deaerator or feedwater pump, the FWHFL replaces only the HP FWHs and none of the LP FWHs. For FWHBOS, the extraction point of feedwater needs to be chosen according to the thermal parameters of the bled of steam line, in which the solar steam is fed. For SuSCRH, SuSHP, SuSIP process arrangements, the extraction of feedwater before or between the FWHs replaces also some of the FWHs. For SaSBD, the feedwater has to be extracted before economizer, since otherwise it replaces also some or all the FWHs like in SaSBDFWH. On the contrary, if the feedwater is extracted in SaSBDFWH before the economizer, it is considered as SaSBD process arrangement. In the following subtitles, the process arrangements are connected to a typical process diagram of a 200 MW_e steam power plant. For analogy, the extraction point for feedwater is the same in the Figure 36 to Figure 42, except for SaSBD in Figure 41.

In the feedwater heating (FWHFL and FWHBOS) process arrangements, the solar field is operated in parallel with the existing FWHs of the steam power plant, and the preheated feedwater or superheated steam from the solar field replaces bled off steam from the turbines. The solar field can replace all FWHs or just a single FWH, and the replacement of FWHs can be done partially or fully. (Suresh et al. 2010, p.272; Yan et al. 2010, p.3735) In the power boost mode, the mass flow through the turbines is increased, as the amount of bled off steam is decreased. On the other hand, in the fuel saving mode, the mass flow through turbine stays the same, as the amount of bled of steam is decreased. Thus, the mass flow through FWHs is decreased, as the mass flow through solar field is increased.

In the feedwater heating and heated water (FWHFL) process arrangement (Figure 36), the feedwater is extracted from the steam cycle, and the preheated feedwater from the solar field is mixed with the preheated feedwater from HP FWHs before the economizer. As a result, the solar field operates on the same inlet and outlet temperatures as the

existing FWHs. The FWHFL process arrangement is the most discussed process arrangement in publications, such as Hu et al. (2003), Hu et al. (2010), Lovegrove et al. (2012), Petrov et al. (2012), Pierce et al. (2013), Suresh et al. (2010), Yan et al. (2010) and Yinghong et al. (2007).

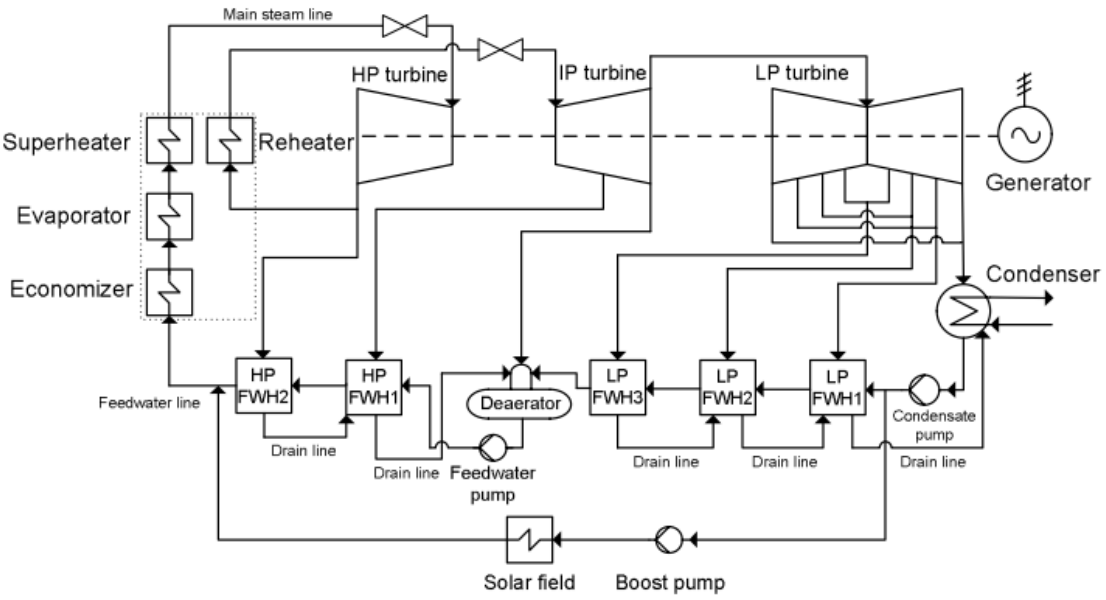

Figure 36. *Simplified schematic of FWHFL, in which all the FWHs are fully or partly replaced. Adapted from Lovegrove et al. 2012, p.405.*

In the feedwater heating and bled off steam (FWHBOS) process arrangement, superheated solar steam is fed to a bled off steam line entering a FWH. In the Figure 37, the solar steam replaces only the highest bled off steam line entering the highest HP FWH, and steam parameters in this steam line are around 340 °C and 40 bar for subcritical units (Suresh et al. 2010, p.272; Yan et al. 2010, p.3734). This process arrangement is discussed in publications, such as Lovegrove et al. (2012), Yan et al. (2010) and Yang et al. (2008). Solar steam can also be injected to other bled off steam lines if the solar field is capable of producing solar steam at multiple enthalpy levels (Hu et al. 2010, p.2884). For perspective, the lowest steam parameters entering the lowest LP FWH are approximately 65 °C and 0.26 bars. In all cases, the solar field has to attain the steam parameters of the bled off steam line (Yang et al. 2008, p.1213).

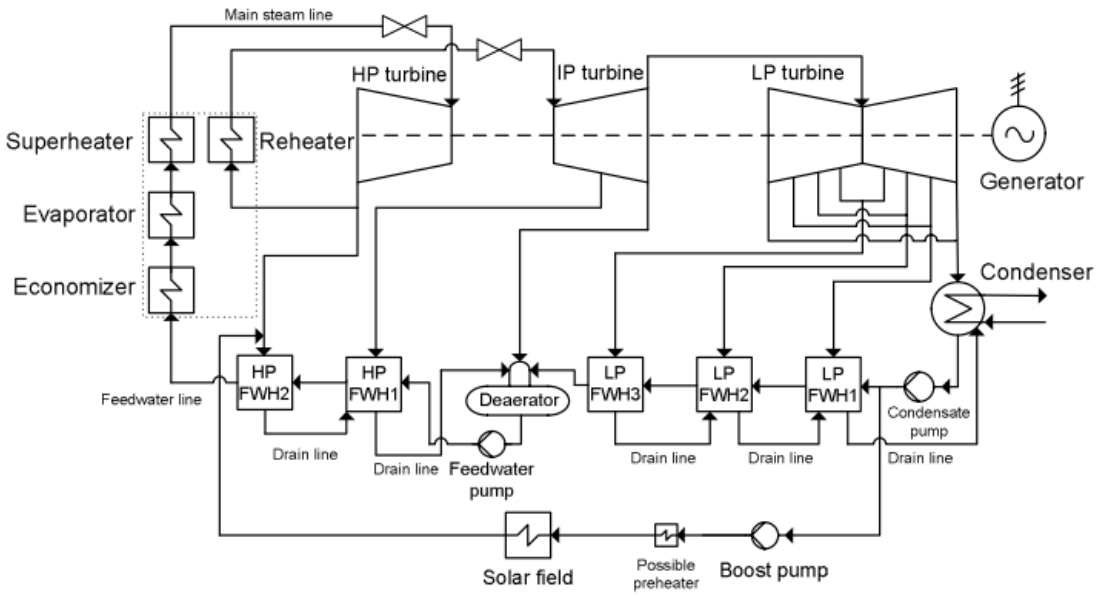

Figure 37. *Simplified schematic of FWHBOS in which single bled off steam line is replaced. Adapted from Lovegrove et al. 2012, p.422.*

In the superheated solar steam into the cold reheat line (SuSCRH) process arrangement, the superheated solar steam is injected into the exit steam flow from the HP turbine (Figure 38). In a subcritical unit, the steam parameters in this CRH line are around 340 °C and 40 bar (Hu et al. 2010, p.2883; Suresh et al. 2010, p.272), which solar steam has to attain. The SuSCRH process arrangement is discussed in publications, such as Lovegrove et al. (2012) and Yang et al. (2008). In the power boost mode, the steam mass flows through reheaters, IP and LP turbine are increased. The increased steam mass flow through reheaters could create an imbalance between the heat surfaces of the steam boiler. On the other hand, in the fuel saving mode the mass flow through the boiler and HP turbine is lowered. As a result, the IP and LP turbine have to be operated over their nominal load to compensate the partial load of HP turbine in order to keep the power output at its nominal value. Thus, an imbalance is possibly created also between the different turbine sections.

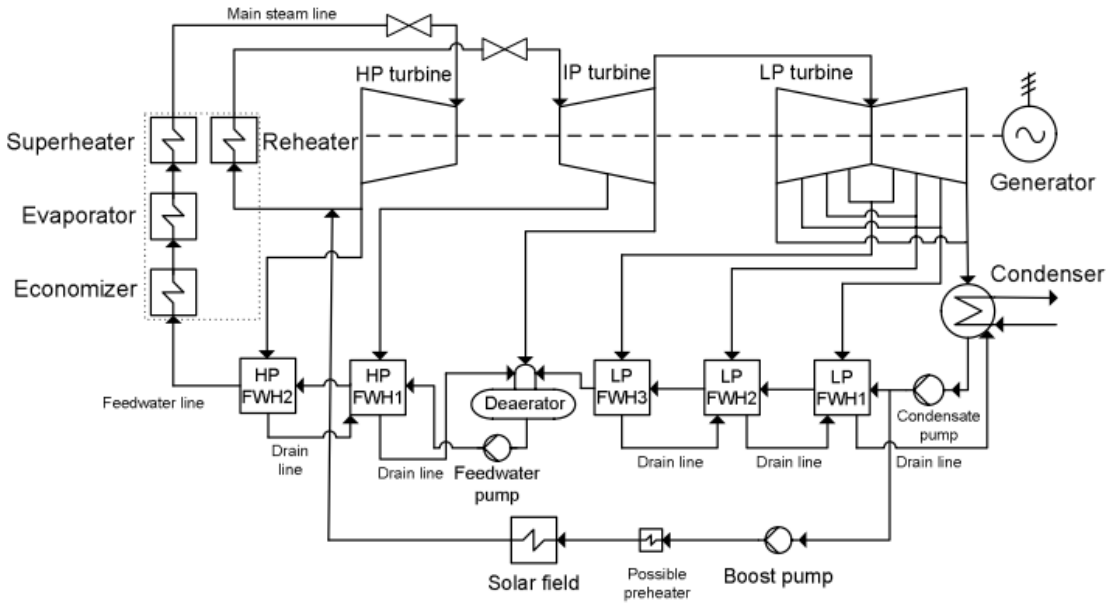

Figure 38. *Simplified schematic of SuSCRH. Adapted from Lovegrove et al. 2012, p.422.*

In the superheated solar steam into the inlet of HP turbine (SuSHP) process arrangement (Figure 39), superheated solar steam is fed into the inlet of HP turbine at live steam conditions, which are around 160 bar and 540 °C for a subcritical unit. The solar field is operated in parallel with the boiler, as it produces part of the superheated steam. This process arrangement is discussed in publications, like Lovegrove et al. (2012), Peterseim et al. (2013), and Peterseim et al. (2014). In the power boost mode, the steam mass flows through the HP, IP and LP turbine sections and reheaters are increased. The increased steam mass flow through reheaters could create an imbalance between the heat surfaces of the steam boiler. On the contrary, in the fuel saving mode the mass flow through the boiler needs to be reduced, as the steam mass flows through turbines and reheaters stay at nominal values and part of the steam is produced in the solar field.

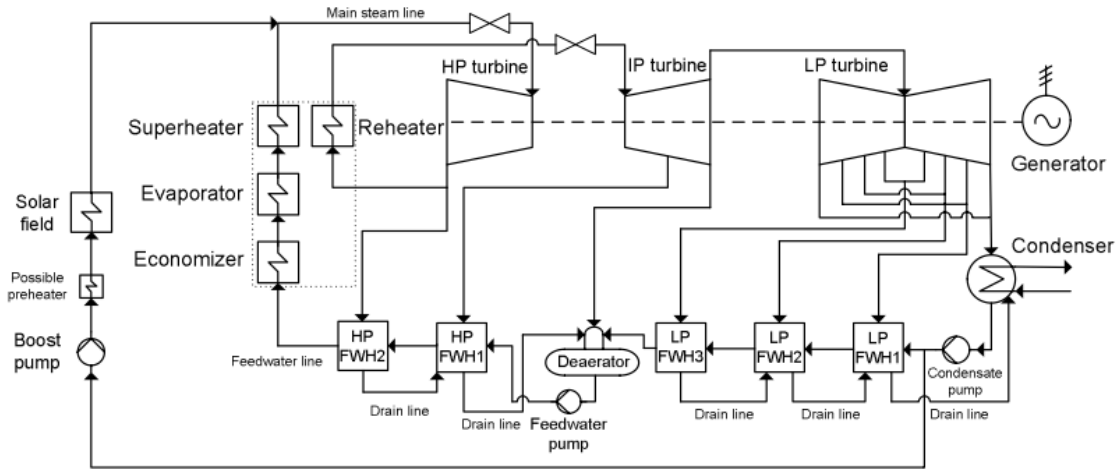

Figure 39. *Simplified schematic of SuSHP. Adapted from Lovegrove et al. 2012, p.405.*

The superheated solar steam into the inlet of IP turbine (SuSIP) is a variation of the SuSHP process arrangement. In SuSIP, the superheated solar steam is fed into the inlet of IP turbine, and the steam parameters of solar field are related to the reheated steam (Figure 40). The steam parameters in this steam line are approximately 40 bar and 540 °C in subcritical units (Suresh et al. 2010, p.272), which solar field have to attain.

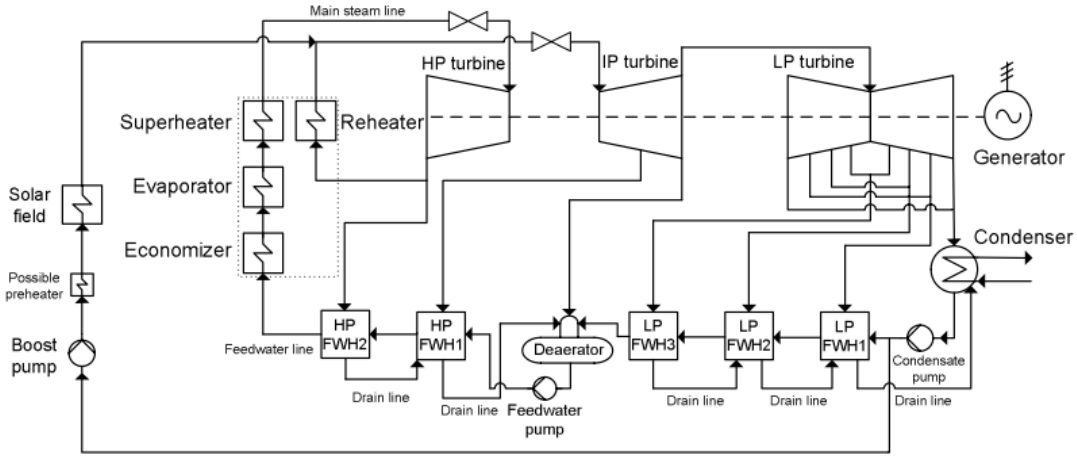

Figure 40. *Simplified schematic of SuSIP. Adapted from Lovegrove et al. 2012, p.405.*

The SuSIP is not proposed in any of the publications referred in this thesis. This process arrangement was invented based on the problems associated with the reheaters in the SuCRH and SuSHP process arrangements. Problems may occur while operating with high solar shares, as the partial load of the boiler cannot possibly guarantee the thermal performance of the reheaters. The injection of superheated solar steam after the reheaters could preserve the balance within the steam boiler. In the power boost mode the mass flow through IP and LP turbine sections is increased. On the other hand, in the

fuel saving mode the mass flow through boiler, HP turbine section and reheaters are decreased. As a result, the IP and LP turbine have to be operated over their nominal load to compensate the partial load of HP turbine in order to keep the power output at its nominal value. Thus, an imbalance is possibly created between the different turbine sections.

In the saturated solar steam into the boiler drum (SaSBD), the solar field is operated parallel with the economizer and boiler (Figure 41). The feedwater for solar field is extracted before the economizer, and saturated steam is injected into the steam drum. A possible pressure reduction stage is needed before solar field if the pressure of feedwater is inappropriate for the operation of the solar field.

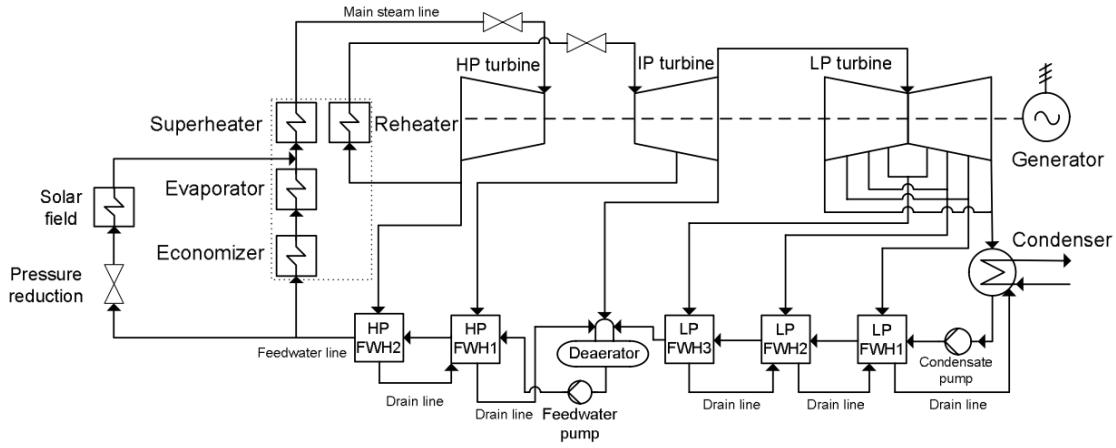

Figure 41. *Simplified schematic of process arrangement in which saturated steam from solar field is injected into the steam drum of the boiler. Adapted from Lovegrove et al. 2012, p. 405.*

This process arrangement is discussed in publications, like Lovegrove et al. (2012) and Yinghong et al. (2007). In the power boost mode the mass flow through superheaters, reheaters and turbine sections is increased. On the contrary, in the fuel saving mode, the mass flow through boiler and economizer is decreased, as the steam mass flows through superheaters, reheaters, turbine sections and FWHs stay at nominal values.

Saturated solar steam into the boiler drum and for feedwater heating (SaSBDFWH) is a variation of the SaSBD and FWHFL process arrangements (Figure 42). The solar field is connected parallel with the boiler, economizer and FWHs. The feedwater is extracted somewhere before or between the FWHs, and the solar field provides saturated steam into the steam drum of the steam boiler.

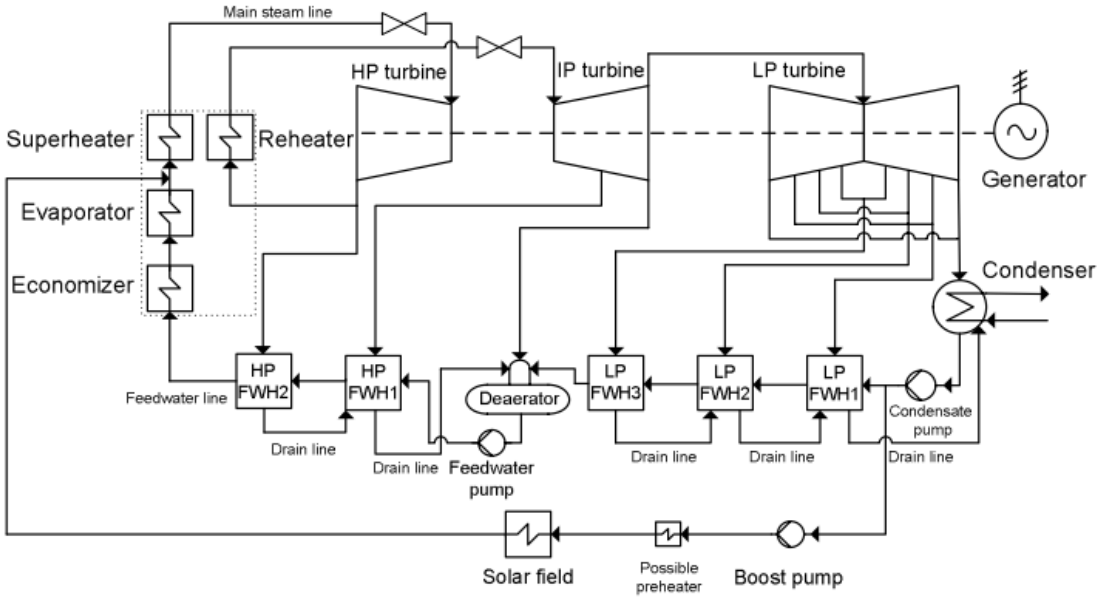

Figure 42. *Simplified schematic of evaporation and preheating process arrangement in which saturated steam from solar field is injected into the steam drum of the boiler. Adapted from Yinghong et al. 2007, p.1208.*

This process arrangement is discussed in Yinghong et al. (2007). In the power boost mode, the mass flow through the superheaters, reheaters and turbine sections is increased. On the other hand, in the fuel saving mode the mass flow through the boiler, economizer and the FWHs is decreased, as the steam mass flows through superheaters, reheaters and turbine sections stay at nominal values.

2.3.3 Advantages and disadvantages of different process arrangements

The advantages and disadvantages of different process arrangements are observed and discussed more closely in order to provide information for the selection of the process arrangement. The advantages and disadvantages of different process arrangements are presented in the Appendix G.

The feedwater preheating process arrangements allow updating the steam power plant without complex integration with the steam boiler (Lovegrove et al. 2012, p.424). In addition, the parallel operation of existing FWHs with solar field ensures the operation of the power plant at full capacity if disturbances occur in solar irradiation. However, sophisticated control strategy needs to be developed in order to assure the parallel operation. (Suresh et al. 2010, p.268) Hu et al. (2010), Petrov et al. (2012) and Suresh et al. (2010) conclude that valuable work can be obtained from both high-temperature and low-temperature applications in FWHFL, but the profit is much greater in the substitution of HP FWHs than in substitution of LP FWHs. As a result, it is more feasible to replace all the FWHs or HP FWHs instead of only the LP FWHs. Hu et al. (2010) con-

clude also that the energy efficiency of the regenerative Rankine cycle is increased, as the FWHs are replaced by the solar field. Same kind of results can be found from FWHBOS process arrangement in Yan et al. (2010) and Yang et al. (2008).

Both feedwater heating arrangements (FWHFL and FWHBOS) are realistic approaches to hybrid systems especially in retrofits, since the changes in the existing steam cycle can be considered as little invasive as possible, and the net efficiency of the steam power plant is improved. In addition, the feedwater preheating is proved to be theoretically the most efficient technical solution for hybrid especially in low-to-medium temperature solutions (Yan et al. 2011, p.920). However, only heated water can be produced in the FWHFL, and it promotes the least the steps towards affordable stand-alone CSP plants. Furthermore, the full potential of state-of-the-art line-focusing DSG collectors is neither fulfilled in the FWHBOS, since the steam parameters in the highest bled steam line are approximately 340 °C and 40 bar although steam parameters up to 550 °C and 160 bar can be possibly reached with state-of-the-art line-focusing collectors in near future. However, high pressure up to 160 bar sets challenges to the durability of absorber tubes. Moreover, in both configurations the maximum solar share in the power boost mode is limited by the maximum load of turbine sections and the capacities of FWHs. As a result, it is possible that if the maximum solar share is reached as all the FWHs are replaced, the turbines cannot operate on that load. On the contrary, in the fuel saving mode the maximum solar share is restricted by capacities of FWHs, as the FWHs cover approximately 20% of the thermal output of the steam boiler. Thus, the maximum solar share in FWH process arrangements is approximately 20% if the solar field is capable of producing steam with multiple enthalpy levels and all the FWHs are replaced (Yan et al. 2010, p.920). For example, the thermal powers and energy shares of FWHs are presented of a 150MW_e steam power plant, which thermal power is 382.1 MW_{th} (Table 3) (Farhad et al. 2008, p.6-7). The steam power plant consists of three LP FWHs and two HP FWHs, and the energy share of each FWH is calculated by dividing the thermal power of FWH with thermal power of steam boiler. The thermal powers of steam boiler and FWHs are calculated with state point data presented in Appendix H.

Table 3. *Thermal powers and energy shares of three LP FWHs and two HP FWHs in 150 MWe power plant. Adapted from Farhad et al. 2008, p.6-7.*

Component	**Thermal power [MW_{th}]**	**Energy share [%]**
LP FWH1	11.83	3.09
LP FWH2	19.01	4.98
LP FWH3	16.74	4.38
HP FWH1	21.90	5.73
HP FWH2	20.97	5.49
Total	**90.45**	**23.67**

In the SuSCRH process arrangement, the steam parameters of the cold reheat line are readily achievable with current line-focusing collectors with DSG, but the full potential of the state-of-the-art technology is not fulfilled, since higher temperature and pressure can be attained. In addition, the partial load of HP turbine in fuel saving mode reduces the net efficiency of the power plant, since the efficiency of Rankine cycle is higher for the higher inlet turbine conditions. Furthermore, the increased or decreased mass flow through part of the system can result in a disturbance in balance between the different heating surfaces and turbine sections while operating with higher solar shares. Therefore, in the SuSCRH process arrangement, the main component of the boiler to be investigated more closely is the reheater, since its heat absorption affects to the thermodynamic performances of the boiler, the IP and the LP turbine sections (Yang et al. 2008, p.1213). In the power boost mode, the maximum solar share is limited by the maximum capacities of reheater, IP and LP turbine sections. If the capacity of the reheater is not sufficient for the increased steam mass flow through the reheaters, the operation conditions for IP turbine are not reached. In the fuel saving mode, the maximum solar is limited by the minimum load of boiler, which guarantees the thermal performance of the reheater with increased steam mass flow and also by the maximum loads of the IP and LP turbines, as they need to compensate the partial load of HP turbine.

In the SuSHP process arrangement, the live steam temperature of 540 °C is achievable with current line-focusing collectors and DSG technology, but the high pressure of 160 bar sets challenges to the collector durability especially in the joints between the collectors in parabolic troughs. In addition, the fluctuating nature of solar irradiation causes changes in the thermal power of solar field, in which the boiler has to response with adequate time frame in order to keep the steam conditions before HP turbine as constant as possible. With high solar shares, the SuSHP might be technically challenging, since the quality of the solar steam need to be assured in order to avoid condensation inside the turbine, which might damage it. (Lovegrove et al. 2012, p.423) Furthermore, a sophisticated control strategy needs to be designed, and possible difficulties can be countered in the thermal performance of reheater if the boiler is operated at low partial load with high solar share. Moreover, the maximum solar share in power boost mode is restricted by the maximum capacities of the turbine sections and the capacity of reheater. On the contrary, the maximum solar share in fuel saving mode is limited by the minimum load of boiler, which guarantees the thermal performance of the reheater. However, the full potential of state-of-the-art line-focusing collectors with DSG can be fulfilled in the near future with SuSHP process arrangement, and it can be seen as a long term goal for CSP hybrids. It is also the most promoting process arrangement in the development of affordable stand-alone CSP plants.

In the SuSIP process arrangement the steam parameters of 540 °C and 40 bar are achievable with line-focusing collectors with DSG. Hence, the SuSIP process arrangement can be considered as medium term goal for CSP and steam power plant hybrids. In

the power boost mode, the maximum solar share is limited by the maximum capacities of the IP and LP turbine sections. In the fuel saving mode, the maximum solar share is limited by the minimum partial load of the boiler. In addition, the maximum solar share might also be limited by the imbalance between the HP turbine section and other turbine sections. Moreover, the net efficiency of the power plant is affected, as the solar steam is not expanded in the HP turbine. From the solar field point of view, it might also be disadvantageous to provide superheating of almost 290 °C, as the pressure is only 40 bar, but it is technically possible.

In the SaSBD process arrangement, the performances of superheaters and reheaters are affected, as the boiler operates on partial load with high solar share (Yinghong et al. 2007, p.1208). In the power boost mode, the maximum solar share is limited by the maximum capacity of turbine sections. On the other hand, in the fuel saving mode, the maximum solar share is limited by the minimum partial load of the boiler, which guarantees the thermal performances of superheaters and reheaters. Compared to previous process arrangements, only saturated steam is produced in the solar field. On the other hand, superheaters can assure the quality of live steam if the boiler is operated with adequate load. The SaSBDFWH is similar to the SaSBD process arrangement, but the feedwater for solar field is extracted before or between the FWHs instead of before the economizer.

For the current applications and for retrofits the FWHFL, FWHBOS and SuSCRH with low solar share are possibly suitable, since the integration is readily achievable without any complex integration arrangements. Furthermore, the FWHBOS and SuSCRH have been done as retrofits with small solar shares. For new hybrid power plants in the near future it might be more beneficial to apply the SuSHP or SuSIP process arrangements, since the solar share can be greater, the hybrid system can be thoroughly optimized, and these technologies promote the steps towards affordable stand-alone CSP power plants.

2.3.4 Process requirements and restrictions of the hybrid systems

Process requirements and restrictions of the hybrid systems can be observed from the steam power plant point of view and from the CSP plant point of view. From the steam power plant point of view, the main process requirements and restrictions are the operational limitations for FWHs, turbines, and boiler. For the optimum performance of FWHs, the steam extractions from turbines should be optimized in order to maintain the heating requirements for feedwater preheating (Sharma et al. 2015, p.1626). In other words, the pressures and mass flow rates of bled off steams should be kept constant. In addition, the turbine inlet conditions are designed to be kept as constant as possible, and flow instabilities should be avoided during spatially and temporally changing irradiation conditions (Eck et al. 2007b). For example, if the turbine inlet conditions vary, the mass

flow through the turbine and the pressure difference between each stage of the turbine varies (Hong-juan et al. 2013, p.713). Furthermore, the extraction of additional steam from one point of turbine affects the following extraction points. If the amount of bled off steam is increased at one point, it decreases the pressure at that stage and vice versa. As a result, the pressure is also lower in the following points, which correspond to lower quality of bled off steam to the following FWHs. Thus, the knowledge of the load behaviour is crucial for the optimum design of FWHs.

Most modern boilers and turbines are capable to handle increased loads up to 10% above the nominal continuous load (Petrov et al. 2012, p.3). However, running the boiler continuously at its peak load should be avoided, since the lifetime of the boiler is decreased due to continuously higher temperatures in the heat surfaces of the furnace. Thus, the maximum peak load duration is considered to be 4 h per day without significant reduction of boiler's lifetime. If the peak load rating or duration is higher, the boiler should be resized to adapt the increased peak rating. As a result, the turbine has to be also resized. In addition, the optimum operation of the steam power plant should be assured when solar energy is not available. Therefore, oversizing of the components should be avoided, since oversized components reduce the efficiency of the plant and increase the investment and operational costs. (Rayaprolu 2009, p.8) Another important factor is the load transients in the boiler, as the steam boiler has to be capable of compensating the transients from solar field under fluctuating solar irradiation conditions. For example, stored energy in the steam drum can be possibly applied during the small load transients. Furthermore, heat stress should be kept as minimum as possible in order to promote lifetime of the components. For heat surface of the steam boiler, the metal temperatures should be controlled. Thus, the amount of spray water is usually limited to 8% of the total flow in order to reduce thermal shock on steam pipes and to ensure the full vaporization of the water droplets before HP turbine (Rayaprolu 2009, p.240). For turbines, the absolute temperature should not be exceeded 28 K above the rated temperature, whereas the absolute pressure should not be exceeded 120% above the rated pressure. Furthermore, the rotation speed of the turbine should be kept between 98% and 101% of the rated rotating speed. As a rule of thumb, the acceptable steam temperature gradients for turbine are smaller than 5 K/min, but the allowable steam temperature transient varies between different turbine types and manufacturers. (Birnbaum et al. 2011, p.665) Currently, Siemens promotes themselves as the world market leader of CSP plant suitable steam turbines, which have been optimized to handle the intermittent power generation and periodicity of solar irradiation (Siemens 2011).

In order to accommodate the system for higher solar share without oversizing the components, the boiler needs to be run at partial load, as the turbine is operated at its maximum load. The thermal performance of the boiler is usually designed to be slightly better at lower loads than at the maximum continuous load rate (Popov 2011, p.344). This is due to the foul up of the heat surfaces, and erosion of the boiler components with ag-

ing. Therefore, the efficiency of the boiler is typically designed to be optimum at normal continuous load rate, which is 90 % of the maximum continuous load (Rayaprolu 2009, p.8). If the boiler is designed to be operated on partial loads for longer time, the part load performance data have to be obtained from the boiler manufacturer, as the part load performance varies among boilers and technologies. For example, the part load performance of BFB boilers is significantly lower than CFB and PCC boilers. (Rayaprolu 2009, p.28) In addition, partial load of the boiler affects to the performance of heat surfaces. At lower loads, the temperature of the flue gases decreases, and larger heat transfer surfaces are required to maintain live steam and reheated steam temperatures constant. Typically, the load range is 70% to 100% of the maximum continuous load, in which the steam temperatures after superheaters and reheaters are required to be held constant. (Rayaprolu 2009, p.237) Furthermore, the final temperature of the flue gases should be 140 °C to 150 °C if the flue gases contain sulphur (Raiko et al. 2013, p.105). In other words, the final temperature of flue gases should not be decreased under the dew point of the flue gases.

From the CSP plant point of view, the requirements and restrictions includes the optimum design for the operation of the CSP plant as well as the size of the solar field. The optimum operation is highly dependent on the identification of local conditions, such as DNI level, climate, topography, as well as restrictions in the use of land and water. As a result, the achieved annual solar-to-electricity efficiency is also highly dependent on the local conditions. (Peterseim et al. 2013, p.521) An accurate estimation of the daily solar irradiation needs to be determined for the optimum design and operation of the CSP plant throughout the year and also for the needed capacity of the steam power plant. (Zhang et al. 2013, p.467) In addition, the solar field has to accurately track the sun using sensors and virtual tracking systems (Kalogirou 2014, p.148). Furthermore, the ambient temperature and wind velocity affect to the heat losses occurring in the solar field (Parvareh et al. 2015, p.514).

Areas with sufficient DNI for CSP plants are usually arid and many lack water for condenser cooling. Therefore, dry-cooling has to be applied to steam turbines. The dry-cooling technology is commercially available, but it creates efficiency penalties and additional costs due to higher condensing temperature and more complex cooling systems than in wet-cooling towers. For large CSP plants, the dry-cooling could be further improved and efficiency penalty reduced or suppressed with modified “Heller System”, which uses condensing water in a closed system with a cooling tower tall enough to allow natural updraft. Thus, wet-dry hybrid cooling can significantly improve performance, but the water consumption is greater than in dry-cooling. (International Energy Agency 2014a, p.13) Another problem is cost-effective cleaning of dust from the reflector surfaces while working in desert areas. During night-time the reflectors can be cleaned by pulsating high pressure sprays, which use demineralized water. The reflectivity of the mirrors is periodically monitored to assure the quality of the process, to

optimize mirror-washing frequency and the labour costs associated with washing. (Kalogirou 2014, p.548)

The optimization of the size of the solar field should be conducted in order to avoid wasted solar heat and extra investment costs (Wu et al. 2015, p.125). Wu et al. (2015) researched the annual performance of a solar aided coal-fired power generation system with various solar field areas and thermal energy storage capacities. In addition, Hongjuan et al. (2013) investigated the performance of solar aided feedwater heating of coal-fired power generation under different operating conditions. It is concluded, that the LCOE, solar-to-electricity efficiency and fuel consumption are dependent on the available DNI: Higher DNI enables higher annual solar-to-electricity efficiencies, and lower LCOE and fuel consumption rates can be reached. However, too small or too large aperture area related to the available DNI level increases the LCOE and decreases the solar-to-electricity efficiency. Thus, minimum of LCOE and maximum of solar-to-electricity efficiencies can be found for aperture area according to the available DNI.

3. DEVELOPMENT OF CONCENTRATED SOLAR POWER AND CONVENTIONAL POWER PLANT MODEL

The development of concentrated solar power and conventional power plant model is conducted by using Advanced Process Simulator (Apros) software (Chapter 3.1), which is a dynamic simulation tool for different industrial processes (Lappalainen et al. 2012, p.62). VTT has previously developed multiple Apros models for conventional steam power plants as well as few models for solar fields with direct steam generation (Chapter 3.2). One steam power plant model and one solar field model are used as reference models for the development of the CSP hybrid model. One reference setup for the development of the hybrid model is selected and defined by conducting an energy analysis for the different process arrangements and by observing the current situation and future perspectives of line-focusing collectors as well as the possibilities to reach higher solar shares with high efficiencies in hybrid systems (Chapter 3.3). Then, the process engineering and control engineering details of the selected hybrid configuration are described as well as the modifications of the steam power plant model based on the process and control engineering of the hybrid (Chapter 3.4). For the developed Apros model, multiple test cases (Chapter 3.5) are defined in order to conduct steady state simulations with different loads of solar field and steam power plant. Furthermore, transient simulations are conducted in order to observe transients within the joint steam cycle and demonstrate the operation of the applied control strategy.

3.1 Dynamic modelling and simulation of power plants with Apros

The selected hybrid configuration is dynamically modelled and simulated with Apros software. Dynamic modelling and simulation (DMS) is needed for the development of CSP and conventional power plant hybrids, as the solar irradiation is a fluctuating energy source, which impacts to the behaviour and dynamics of the conventional steam power plant can be investigated with dynamic simulations. DMS aims to predict dynamic behaviour of power plants and provide a virtual tool, which can be operated similarly than the actual power plants. The major uses of plant scale DMS can be categorized into six groups: development of control strategies, analysis of the system operation, verification of plant design, testing of control system, training of operators and development of operation and control practises. However, before DMS is conducted, it often needs to be complemented with data from steady state simulations, various dimensioning calcula-

tions and computational fluid dynamics (CFD). These provide input data, for example, of process connections, physical dimensions and positions of process equipment and pipelines, equipment specific parameters, automation concept diagrams, control parameters and initial condition information. (Lappalainen et al. 2012, p.62-63)

One of the available DMS tools is Advanced Process Simulator (Apros) software, which is multifunctional software for the DMS of different industrial processes including their automation and electrical systems. The software has been developed since 1986 by Fortum and VTT Technical Research Centre of Finland, and it is committed to continuous development. Currently, it is used in 26 countries (Apros 2015a) for multiple applications, such as nuclear and combustion power plants, pulp and paper mills, general heating and cooling processes, smart cities and alternative power generation applications, such as fuel cells and solar power. Thus, Apros can be used for the purpose of operation and maintenance (O&M), engineering, and research and development (R&D) (Figure 43) in various industrial processes. (Apros Training Course Material 2015)

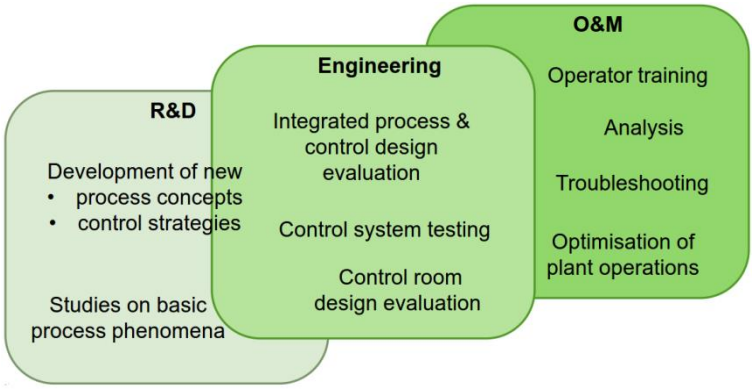

Figure 43. *Use of Apros software (Apros Training Course Material 2015).*

Apros uses a fully graphical user interface, which allows user to enter process-related input data through a dialog window to components and connections between them. The components can be dragged and dropped from comprehensive model libraries, which cover component modules, such as pipes, valves, pumps, tanks, heat exchangers, turbines, measurements, proportional-integral-derivative controllers (PID-controllers) and electric generators. The component modules are analogous with the concrete devices. As the user draws connection between the component modules and inserts input data to the model, the result is a piping and instrumentation diagram with specific additions considering the simulation, such as supervision of the calculated variables (Figure 44). Apros is an online simulator, which allows changes in the configuration during simulations. (Apros 2015b) In addition, Apros is an open simulator, which allows user to include own models and have an easy access to external models, control room equipment and automation systems (Apros Training Course Material 2015).

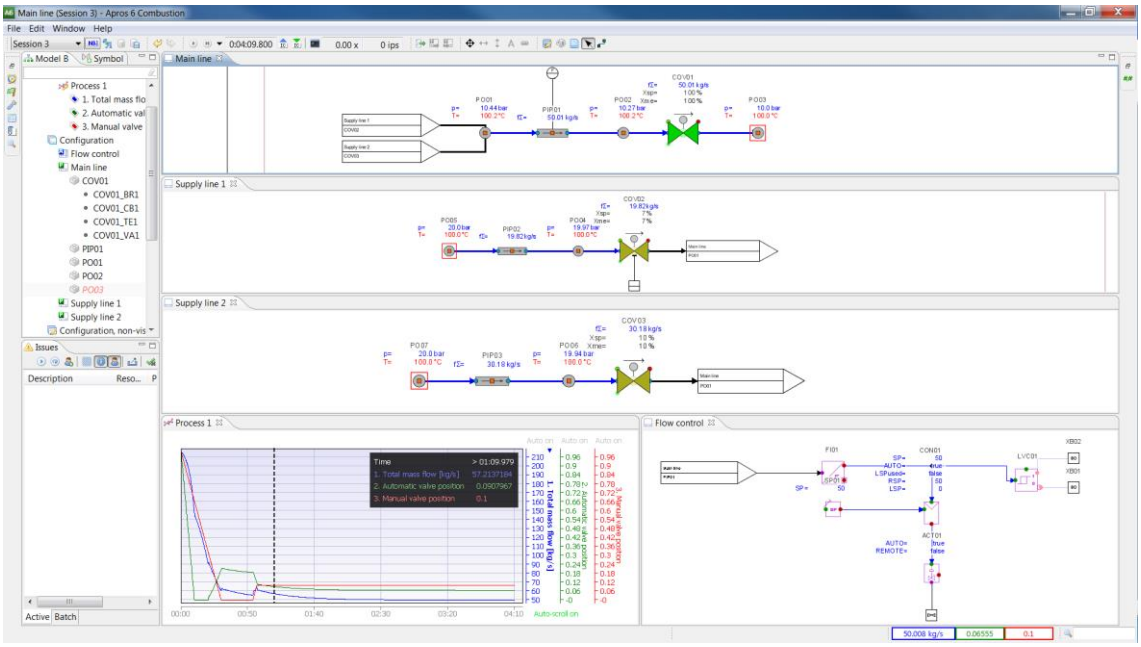

Figure 44. *Graphical user interface of Apros. Figure is taken from an exercise performed in the Apros Training course.*

Apros includes a systematic model hierarchy, which consists of diagrams, process component modules and calculation level (Figure 45). A single model consists of multiple diagrams, a single diagram consists of multiple component modules, and a single component module consists of calculation levels, such as nodes and branches. The user manages the model with diagrams, which can be either generic, process or automation type. However, the model is built with component modules. In addition, a process diagram can only include process component modules, and an automation diagram can only include automation component modules, whereas generic diagram can include both component types. A component module consists of calculation levels, which include the necessary model equations and choice of solution methods. Apros creates automatically the calculation level for component modules, and the user has to seldom change the details in the calculation level. One example of calculation level of a process with two points and a heat pipe is exposed in the Appendix I. The state variables, such as pressure and enthalpy, are calculated in the nodes and variables considering the flow are calculated in branches, which act as borders for nodes. The simulated fluid can be selected by the attribute fluid section, which determines the properties and composition of the fluid. The options are, for example, air, flue gas, water-steam and combustion fuels. Furthermore, it is possible to define own fluid in Apros. (Apros Training Course Material 2015)

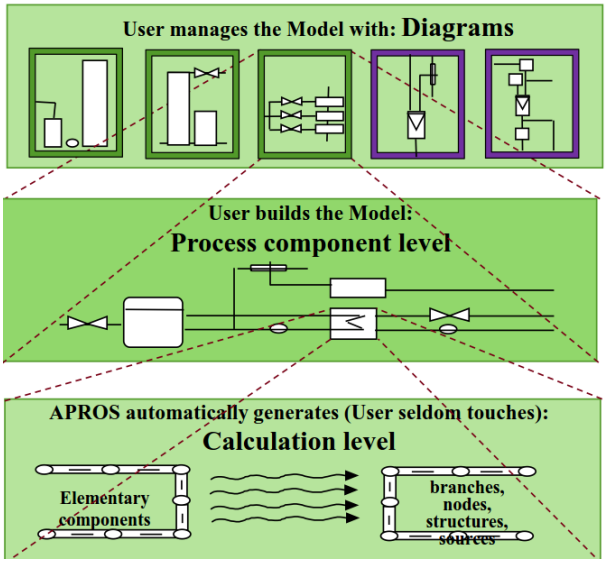

Figure 45. *The model hierarchy in Apros and example of process and calculation level (Apros Training Course Material 2015).*

In the calculation level, Apros uses flow model, which refers to the selection of thermo-hydraulic solution. In other words, it refers to the selection of accuracy level in the solutions of flows, pressures and heat transfer. Different thermohydraulic flow models can be used in different components and connection modules of a simulated system. The options for the flow model are 0, 1, 2, 5 and 6, from which the most commonly used ones are 2 and 6 models. The flow model 2 is used as default, and it is called as 3-equation model, since it resolves conservation equations for mass, momentum and energy for a homogenous fluid mixture of liquid and gas. In other words, it includes the solution of thermohydraulic node pressures, flows and enthalpies and the simulations of the heat structure temperatures and the heat transfer between the fluid and heat structures. All available fluids for simulations are compatible with the flow model 2. The flow model 6 is called 6-equation model, since it calculates the three conservation equations separately for liquid and gas phases. Compared to the flow model 2, the heat transfer is also simulated between the two phases. In addition, the only available fluid for flow model 6 is water-steam mixture. (Apros Training Course Material 2015)

The flow model 5 is a modification of the flow model 6 with a difference in calculation of momentum, as it is calculated for a homogenous mixture instead of two phases, and it uses explicit solution. It is recommended to use the flow model 6 instead of the flow model 5. The flow model 1 differs from flow model 2, as the pressures, flows and enthalpies are calculated using simplified conservation equations and less material properties with no iteration of the process. It can be used in processes, where is no need for simulation of heat transfer between the fluid and heat structures. In the flow model 0, the mass flows in the pipelines are given by user and not resolved from pressure dynamics. Instead, the dynamics of the process reside in tank modules, as the solution pro-

ceeds in order from module to module and iterations are needed in the case of recirculation. (Apros Training Course Material 2015)

3.2 Previously developed power plant models

VTT has previously developed several Apros models for conventional steam power plants and few models for line-focusing solar fields with DSG, which are used as reference models for the development of CSP and conventional power plant hybrid model. The performance of Apros code has been validated with more than 70 cases, in which different test facilities are modelled and the calculation results are compared to large set of measurements from selected transients (Apros 2015d). From the conventional steam power plant point of view, the flow networks and heat transfer of fuel, flue gas and water/steam lines can be modelled and simulated together with automation and electrical systems. In addition, different kinds of boilers can be modelled and simulated with Apros, such as PCC, grate and both BFB and CFB boilers. In addition, the steam cycle can be designed to be either subcritical or supercritical. Furthermore, fuel properties can be adjusted according to the used fuel type, such as coal, peat, gas or oil. (Apros 2015c) From the solar field point of view, VTT has developed Apros models for PTC field with DSG and for LFR field with DSG. The PTC field model is based on EuroTrough collector design developed by the European Commission's EuroTrough projects, and the LFR field model is based on NOVA-1 and Supernova LFR design developed by Novatec Solar.

3.2.1 Conventional steam power plant model

The chosen conventional steam power plant model in this thesis is based on a developed subcritical FBC power plant model, which is used as host plant for the solar field. The steam boiler of the model is designed to be a natural circulation boiler, which fuel power is approximately 400 MW, and the power output of the turbines is approximately 134 MW. The model consists of six diagrams, which include the modelled flue gas side of the steam boiler, water-side of the steam boiler, turbine island, main control loops of the steam boiler and two miscellaneous diagrams for calculation of the energy and mass flow equations of the steam boiler.

The flue gas side of the boiler island consists of the developed FBC boiler module and the modelled fuel supply, combustion air supply, superheaters, reheaters, economizer, and air preheating (Figure 46). Fuel is combusted in the FBC module with excess preheated combustion air, from which 70% is modelled to be primary air and 30% is modelled to be secondary air. The set point for oxygen level of flue gas is designed to be 3.5% at 100% load, as the pressure at the furnace is designed to be 1.01 bar. Superheaters include primary (SH 1), secondary (SH 2) and tertiary heat surfaces (SH 3), whereas reheaters include primary and secondary heat surfaces (RH 1 and RH 2). The economiz-

er consists of two heat surfaces, and the air preheating consists of two parallel heat transfer surfaces: one for primary air and one for secondary air.

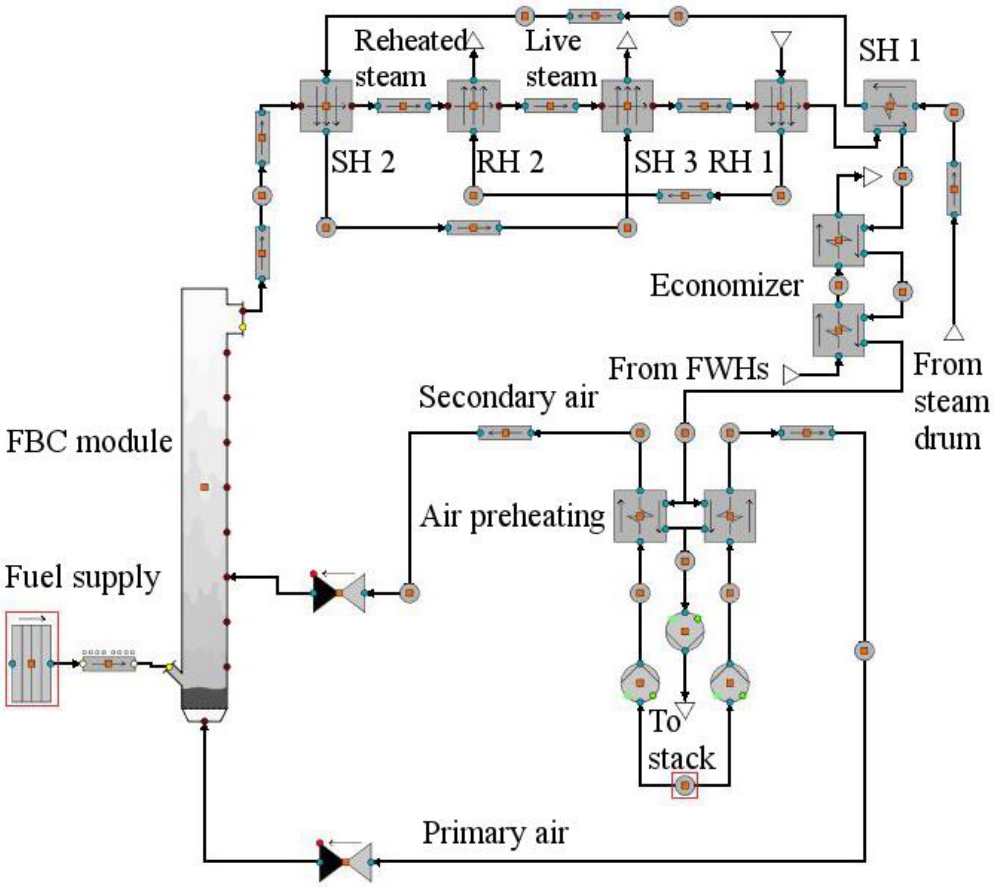

Figure 46. *Schematic of the flue gas side of the steam boiler modelled in Apros.*

Water-side of the steam boiler consists of the steam drum of the boiler and the heat structures of the water tubes in the furnace wall (Figure 47). The water wall of the furnace is modelled with multiple water tubes. One water tube is divided to 10 heat pipe sections, in which heat is transferred from the FBC module. Different heat transfer coefficients can be given to the different heat pipe sections, as the heat transfer is not uniform across the furnace wall.

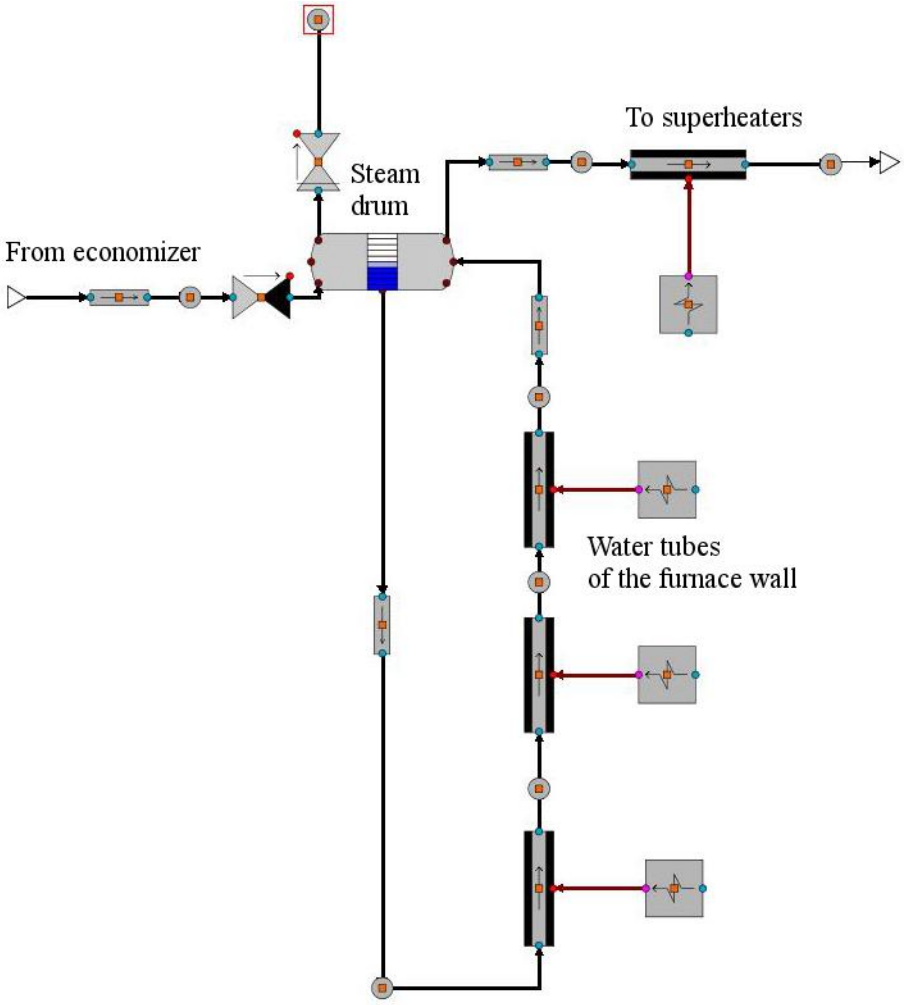

Figure 47. *Schematic of the modelled water side of the steam boiler in Apros.*

The turbine island consists of turbine sections, a condenser, LP FWHs, a deaerator and HP FWHs (Figure 48). In the model, there are seven turbine sections, two HP FWHs and three LP FWHs. Thus, six bled off steam lines and reheating section are modelled by dividing the turbines into seven sections. The isentropic efficiency (η_{st}) of turbine can be calculated with Equation 1 (Raiko et al. 2013, p.27):

$$\eta_{st} = \frac{\Delta h}{\Delta h_{st}} \tag{1}$$

in which

Δh is real enthalpy drop of the expansion of steam in the turbine [J/kg]

Δh_{st} is the isentropic or theoretical enthalpy drop of the expansion of steam [J/kg]

The isentropic efficiency is defined in the model to be different for each turbine sections, as the isentropic efficiency of HP turbine (section 1) is modelled to be the highest, and the efficiency drops in the IP (sections 2 and 3) and LP turbine sections (4 to 7) due to pressure reductions of reheaters and bled off steams (Table 4).

Table 4. *Isentropic efficiencies of modelled turbine sections.*

Turbine section	**1**	**2**	**3**	**4**	**5**	**6**	**7**
η_{st} (%)	85	84	84	83	83	83	81

In the HP FWHs, the superheated bled off steam is firstly cooled to saturated steam. The saturated steam is then condensed and subcooled before it is fed to the drain line entering the deaerator. On the other hand, in the LP FWHs the superheated steam is either cooled to saturated steam and condensed or just condensed before it is fed to the drain line entering the condenser. The amount of bled off steam is controlled by keeping the level in the condensing heat transfer surface constant. Thus, as the feedwater mass flow is increased through the FWHs, more steam is condensed in the heating surface. Therefore, the level in the condensing heat transfer surface is increased, and the valve after the condensing heat transfer surface is opened in order to restore the level of the FWH.

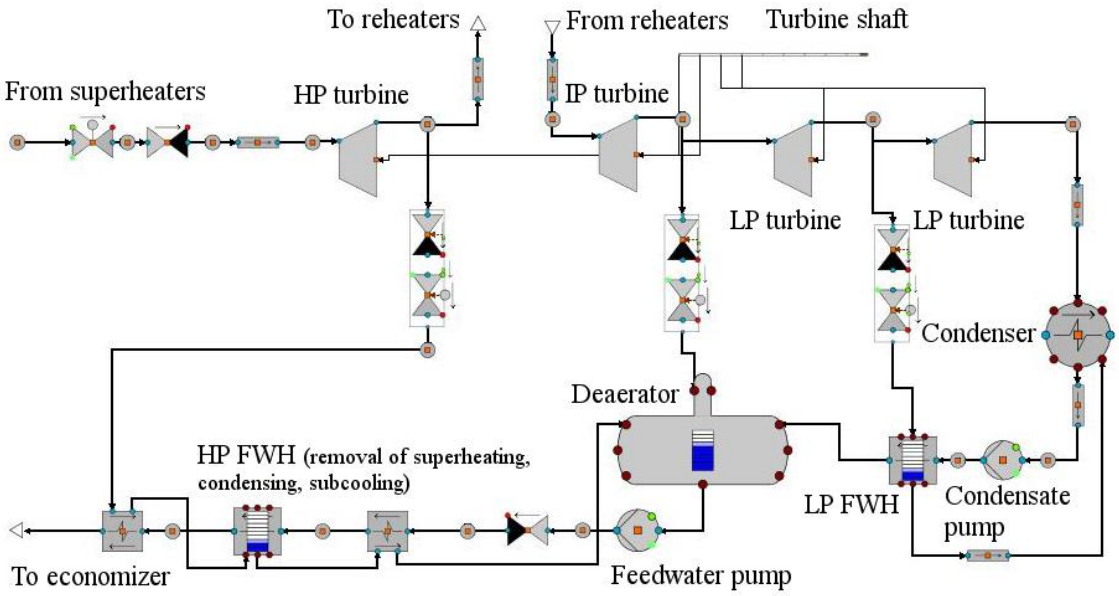

Figure 48. *Simplified schematic of the modelled turbine island in Apros.*

Master control loops include control loops for fuel and combustion air feeding, amount of feedwater, steam temperatures, and furnace pressure. The control loops consists of PID, PI, cascade and feedforward control loops. The fuel supply and combustion air supply control loops are connected in series. As fuel supply is adjusted by the live steam pressure or by the power output of the turbines, the fuel supply control sends a set point for the combustion air feeding. The amount of feedwater is controlled by three element cascade system, which measures the level of the steam drum, the mass flow of produced

steam and the mass flow of feedwater entering the HP FWHs. Thus, it controls the rotation speed of the feedwater pump in order to keep the constant level in the steam drum. The steam temperature control loops uses also cascade control loops for enthalpy control. Thus, the steam temperature control loops measure the final temperature of the steam and the spray water mass flow through the attemperator, and controls the spray water mass flow accordingly to the steam temperature. In addition, furnace pressure control loop measures the pressure at furnace and adjusts the rotation speed of the flue gas blower accordingly.

Two miscellaneous diagrams for calculation of the energy and mass flow equations are modelled in order to calculate the fuel power of the steam boiler and the thermal power of all the components related to the steam cycle. In addition, the thermal powers of flue gases leaving from furnace and entering the stack are calculated. Thus, it can be observed the quantity of energy transferred into the steam cycle and the quantity of energy, which is lost with the flue gases. Furthermore, the wall masses of heat transfer surfaces are calculated in order to observe the quantity of energy, which is stored in the wall masses of the heat surfaces.

3.2.2 Solar field model

The solar field model used in this thesis is the LFR model, as DSG is more common in LFRs than in PTCs. In addition, the LFRs require simpler connections than PTCs, which favours operation at higher pressures up to 160 bar. The LFR solar field model for producing superheated steam consists of two generic diagrams: process model diagram and automation diagram. The process diagram consists of one modelled collector row, which includes different collector components for the evaporation and superheating sections of the collector row and auxiliary components, such as phase separator tank, pumps, pipes and valves (Figure 49). The collector modules are different, as the evaporation module has a non-vacuumed absorber tube, whereas the superheating collector module has a vacuumed absorber tube. The calculations inside the developed collector components are based on Novatec Solar's NOVA-1 and SuperNova collector technologies. These calculations include a reflector receiving solar irradiation from the sun and reflecting it onto the absorber tube. Thus, one of the results is the thermal power of the collector module. The calculations also include the losses related to collector optics and incidence angle, heat transfer from the reflected sun onto the absorber tube and heat loss from the absorber tube to the atmosphere. Thus, another result of the calculations is the energy loss.

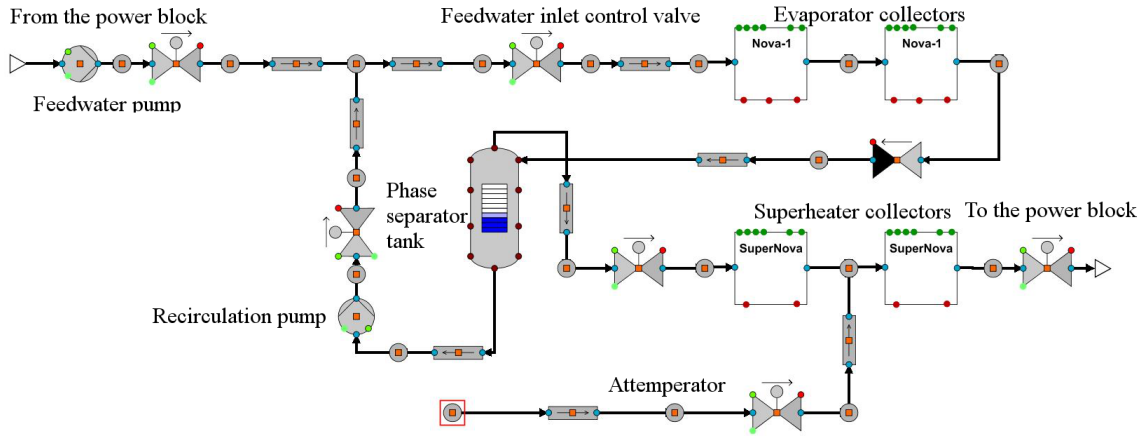

Figure 49. *Schematic of the simplified LFR model in Apros.*

A reference collector row of the LFR model consists of 14 evaporation modules and 7 superheating modules, but the amount of these modules can be changed according to the desired process. Typically, the evaporation section presents about 70% of the total amount of collectors, and the superheating section presents about 30%, as the design point for live steam temperature is close to 500 °C (Selig et al. 2010, p.6). The process arrangement in the model is the recirculation mode with centralized separator tank, and its reference design values are:

1. Inlet pressure and temperature are 170 bar and 180 °C.
2. Outlet pressure and temperature are 160 bar and 550 °C.
3. In the separator tank pressure and temperature are 165 bar and 350 °C.

The applied control loops in the LFR model consists of PI-controls and cascade controls, and the control strategy of the solar field is different during normal operation and during start-up and shut down procedures. In this thesis, only the control strategy during normal operation is described, as the start-up and shutdown procedures are excluded from this thesis. During normal operation, the model is designed to produce saturated water-steam mixture at the desired temperature, pressure and steam mass fraction, and further produce superheated steam at desired temperature and pressure. The amount of recirculation flow is set fixed. Thus, the recirculation flow can be adjusted according to the steam generation of the solar field in order to keep the level of the separator tank constant. The two main control loops used during normal operation are:

1. The steam mass fraction at the outlet of the evaporation section is controlled by controlling inlet feedwater mass flow to the collector row.
2. The outlet temperature of the superheating section is controlled with one attemperator before the last superheater collector.

The inlet feedwater mass flow is determined by the effective DNI level on collectors in order to keep the steam mass fraction at the end of the evaporator close to 0.75. During normal operation, the evaporation section determines the amount of produced steam, whereas the outlet temperature is determined by the superheating section. The super-

heating section is slightly over-dimensioned, and the outlet temperature is controlled by utilizing one attemperator. The control of outlet temperature is conducted by enthalpy control, which measures the steam temperature after the last superheating module and the spray water mass flow, and controls the spray water mass flow accordingly to the outlet temperature.

The solar field model is configured to be either flexibly connected to different parts of conventional power plant or to be used as stand-alone power plant for steam generation. However, some of the details of the solar field have to be remodelled according to need of the user. The user can flexibly change the amount of collectors and capacities of pumps depending on the design inlet pressure and temperature and the design outlet pressure and temperature of the simulated case.

3.3 Selection of the reference setup

Live steam parameters of subcritical steam power plants are almost attainable with state-of-the-art line-focusing collectors with DSG. Therefore, the variety of possible process arrangements for CSP hybrid systems is large. In order to select one reference setup for the hybrid system, a preliminary energy analysis is conducted to possible process arrangements (see Chapter 2.3.2) in order to calculate the amounts of solar heat, which could be add to the joint steam cycle. In order to conduct the energy analysis, state point data from the conventional steam power plant modelled in Apros is collected.

Energy analysis is based on the first law of thermodynamics, which is related to the conservation of energy. For an open system with a steady flow process, the first law of thermodynamics can be calculated with Equation 2 (Gupta et al. 2010, p.1229):

$$\sum E_i + \sum_{j=1}^{n} Q_j = \sum E_o + W_{net} \tag{2}$$

in which

E_i is energy of mass flow entering the system [W]

E_o is energy of mass flow leaving the system [W]

Q_j is heat transfer to system from source at T_j [W]

W_{net} is the net work done by the system [W]

The kinetic and potential energy changes are neglected in the Equation 2. The performance of thermal power plants can be evaluated with the first law efficiency η_I (Equation 3), which is defined as the ratio of estimated energy output to the supplied energy input of the system (Gupta et al. 2015, p.569):

$$\eta_I = \frac{Estimated\ energy\ output}{Supplied\ energy\ input} \quad (3)$$

First law efficiency is often related to the net efficiency of the plant, which includes the calculation of thermal efficiency, the efficiency of the generator and needed reactive power. As generator efficiency and reactive power of the hybrid are not calculated in the energy analysis, the efficiency of the hybrid plant is evaluated through thermal efficiency η_{th} (Equation 4), which is defined as the ratio of mechanical work of steam turbine divided by the total heat input (Schenk et al. 2012, p.57):

$$\eta_{th} = \frac{Mechanical\ work\ of\ steam\ turbine}{Total\ heat\ input} \quad (4)$$

Furthermore, the total heat input can be calculated for the hybrid system with Equation 5 (Popov et al. 2011, p.348):

$$Total\ heat\ input = Q_{th,solar} + Q_{boiler} \quad (5)$$

in which

$Q_{th,solar}$ is the thermal power of solar field [W_{th}]

Q_{boiler} is the fuel power of the steam boiler [W]

For the selection and definition of the reference setup, an energy analysis is conducted with two different thermal powers of the solar field in a reference case and five comparison cases. In addition, the extraction point for feedwater is selected from three different options: after the condensate pump, after the deaerator and before the economizer. The cases for energy analysis are:

1. Feedwater heating process arrangement, in which superheated solar steam is fed into bled off steam lines and the two HP FWHs are fully replaced (FWHBOS). This is selected as reference case, since it is achievable for current state-of-the-art line-focusing collectors with DSG.
2. First comparison case is feedwater heating process arrangement, in which heated water from solar field is fed into feedwater line (FWHFL).
3. Second comparison case is the cold reheating line process arrangement, in which superheated solar steam is injected before the reheaters (SuSCRH).
4. Third comparison case is the injection of superheated solar steam at the inlet of HP turbine (SuSHP).
5. Fourth comparison case is the injection of superheated solar steam into inlet of the IP turbine (SuSIP).
6. Last comparison case is the injection of saturated solar steam into steam boiler drum (SaSBD).

For all the cases, thermal solar shares (x_{solar}) are calculated (Equation 6). x_{solar} is defined as the ratio of thermal power of the solar field ($Q_{th,solar}$) divided by the thermal power of the solar field and the fuel power of the steam boiler (Q_{boiler}):

$$x_{solar} = \frac{Q_{th,solar}}{Total\ heat\ input} * 100\% = \frac{Q_{th,solar}}{Q_{th,solar} + Q_{boiler}} * 100\% \qquad (6)$$

By using x_{solar}, the reactive power and generator efficiency can be neglected. The thermal solar shares are comparable only if the power output of the power plant is assumed constant in all the cases. Thus, the power output of the turbines is kept constant in the energy analysis, and the fuel power of steam boiler is decreased directly proportional to the thermal power of the solar field. In order to conduct the energy analysis, a steady state mass flow diagram of host steam cycle is presented in Figure 50. The power output of the turbines is 134.2 MW, and the fuel power of the steam boiler is 402.8 MW without solar field. Thus, the reference thermal efficiency of the plant is approximately 33%, which is calculated with Equations 4 and 5.

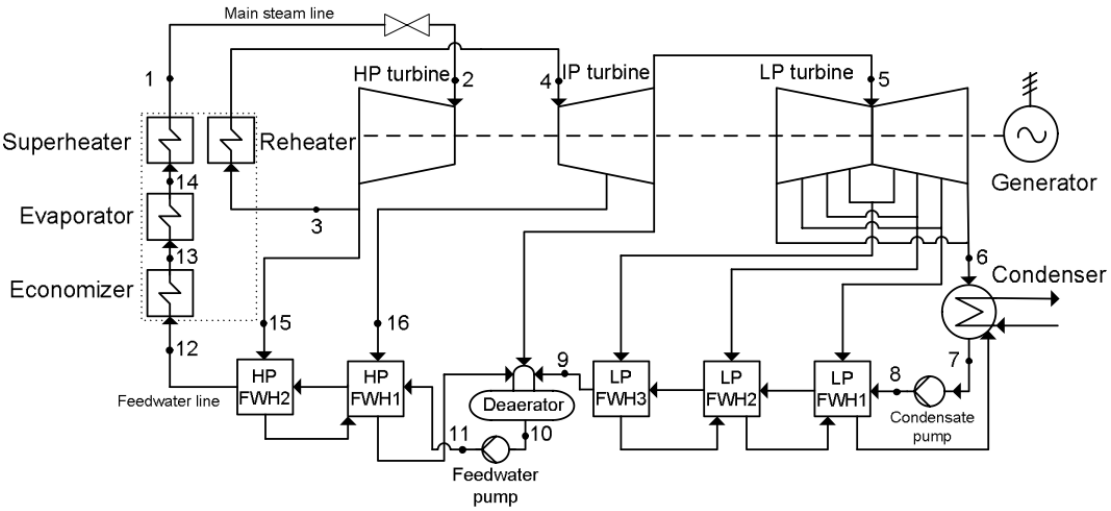

Figure 50. *A diagram of the developed steam cycle in Apros. Adapted from Sengupta et al. 2007, p.17.*

Furthermore, the information of state points related to Figure 50 are presented in Table 5, which includes the values of pressure, temperature, enthalpy and mass flow related to the state points in the Figure 50. The state point data for the points 1 to 16 are observed in order to calculate the different cases of energy analysis.

Table 5. *State point data of the steam power plant used for energy analysis.*

State point	Pressure (bar)	Temperature (°C)	Enthalpy (kJ/kg)	Mass flow (kg/s)
1	145.12	550.00	3455.62	109.24
2	137.83	547.12	3455.59	109.24
3	38.79	359.67	3119.94	103.92
4	36.93	549.70	3562.42	112.78
5	11.64	387.67	3235.40	100.06
6	0.15	53.90	225.64	85.36
7	0.44	45.10	188.89	101.05
8	12.85	44.78	188.63	101.05
9	10.65	136.21	573.44	101.05
10	10.25	144.96	610.91	118.10
11	168.57	147.82	633.24	101.94
12	163.92	242.65	1051.71	101.94
13	153.86	319.64	1450.89	101.94
14	153.64	347.20	2638.68	101.94
15	40.40	363.80	3126.57	5.32
16	21.30	466.70	3393.13	12.80

Energy analysis for the different cases is based on values in the Table 5 and on Equations 5 and 6. In addition, the solar field is assumed to be operated with same input and output temperatures and pressures, as in the state points of the steam cycle. Thus, the thermal power of solar field is calculated with Equation 6 (Gupta et al. 2009, p.600):

$$\dot{Q}_{th,solar} = \dot{m}_{solar} \times (h_{out} - h_{in}) \tag{6}$$

in which

$Q_{th,solar}$	is the thermal power of the solar field	[W_{th}]
$\dot{m}_{solar}$	is the mass flow through solar field	[kg/s]
h_{out}	is the enthalpy of solar steam or heated feedwater	[J/kg]
h_{in}	is the enthalpy at the extraction point of the feedwater	[J/kg]

The results of the first calculation are presented in Table 6, as the solar field produces 18.12 kg/s of superheated steam. This is the equal amount of bled off steam entering the two HP FWHs. Thus, the two HP FWHs are fully replaced in the first calculations. The results include the thermal power of solar field as well as the fuel power of the steam boiler. It is estimated that the fuel power of steam boiler is decreased relative to the thermal power of the solar field. In addition, the thermal solar shares are calculated in all cases by using Equation 6, and the power output of turbines is kept at 134.2 MW for all cases.

Table 6. *Results of the first energy analysis calculations.*

Extraction point for feedwater	**Case**	**FWHBOS**	**FWHFL**	**SuSCRH**	**SuSHP**	**SuSIP**	**SaSBD**
After condensate pump	Thermal power of the solar field (MW_{th})	56.65	15.64	53.12	59.20	61.13	44.39
	Fuel power of boiler (MW)	346.15	387.16	349.68	343.60	341.67	358.41
	x_{solar} (%)	14.06	3.88	13.19	14.70	15.18	11.02
After deaerator	Thermal power of the solar field (MW_{th})	49.00	7.99	45.46	51.55	53.48	36.74
	Fuel power of boiler (MW)	353.80	394.81	357.34	351.25	349.32	366.06
	x_{solar} (%)	12.16	1.98	11.29	12.80	13.28	9.12
Before the economizer	Thermal power of the solar field (MW_{th})	41.01	-	37.48	43.56	45.49	28.76
	Fuel power of boiler (MW)	361.79	-	365.32	359.24	357.31	374.04
	x_{solar} (%)	10.18	-	9.30	10.81	11.29	7.14

The thermal solar shares are lower than 30% in all the cases in Table 6. In order to increase the solar share, more feedwater have to flow through the solar field. In FWHBOS process arrangement, the maximum thermal solar share is 14.06%, when the both HP FWHs are fully replaced, and the feedwater is extracted after the condensate pump. Thus, this process arrangement is excluded from the following calculations, in which higher solar shares are investigated. In addition, the FWHFL process arrangement is excluded, as the achieved thermal solar shares in FWHFL are much lower than in other process arrangements. Next calculations are conducted with an overall mass flow of 40 kg/s through the solar field in order to achieve thermal solar shares close to 30%, as in the previous calculations the maximum solar share is approximately 15 % with 18.12 kg/s steam mass flow from solar field. The thermal power of solar field, the fuel power of boiler, the thermal solar shares are calculated for the 40 kg/s mass flow (Table 7).

Table 7. *The results of the calculation of a hybrid in which the overall mass flow through the solar field is 40 kg/s.*

Extraction point for feedwater	**Case**	**SuSCRH**	**SuSHP**	**SuSIP**	**SaSBDFWH**
After condensate pump	Thermal power of the solar field (MW_{th})	117.25	130.68	134.95	98.00
	Fuel power of boiler (MW)	285.55	272.12	267.85	304.80
	x_{solar} (%)	**29.11**	**32.44**	**33.50**	24.33
After deaerator	Thermal power of the solar field (MW_{th})	100.36	113.79	118.06	81.11
	Fuel power of boiler (MW)	302.44	289.01	284.74	321.69
	x_{solar} (%)	24.92	**28.25**	**29.31**	20.14
Before the econo-mizer	Thermal power of the solar field (MW_{th})	82.73	96.16	100.43	63.48
	Fuel power of boiler (MW_{th})	320.07	306.64	302.37	339.32
	x_{solar} (%)	20.54	23.87	24.93	15.76

The thermal solar share of over 30% can be reached with the mass flow of 40 kg/s if feedwater is extracted after the condensate pump, and solar steam is injected into the inlet of HP turbine or IP turbine. In addition, thermal solar share of 29.11% is reached if the feedwater is extracted after the condensate pump and solar steam is injected into the cold reheat line entering the reheaters. Furthermore, thermal solar share of 29.31% is reached if the feedwater is extracted after the feedwater pump and solar steam is injected into the inlet of IP turbine. Moreover, thermal solar share of 28.25% is reached as feedwater is extracted to solar field after the deaerator and solar steam is fed into the inlet of HP turbine. As a conclusion, the thermal solar share over 30% or close to 30% is reached with mass flow of 40 kg/s if feedwater is extracted after the condensate pump or after the deaerator and solar steam is fed into joint turbine or cold reheat line of steam boiler. The calculated thermal solar shares of all cases are collected in the Figure 51 for comparison.

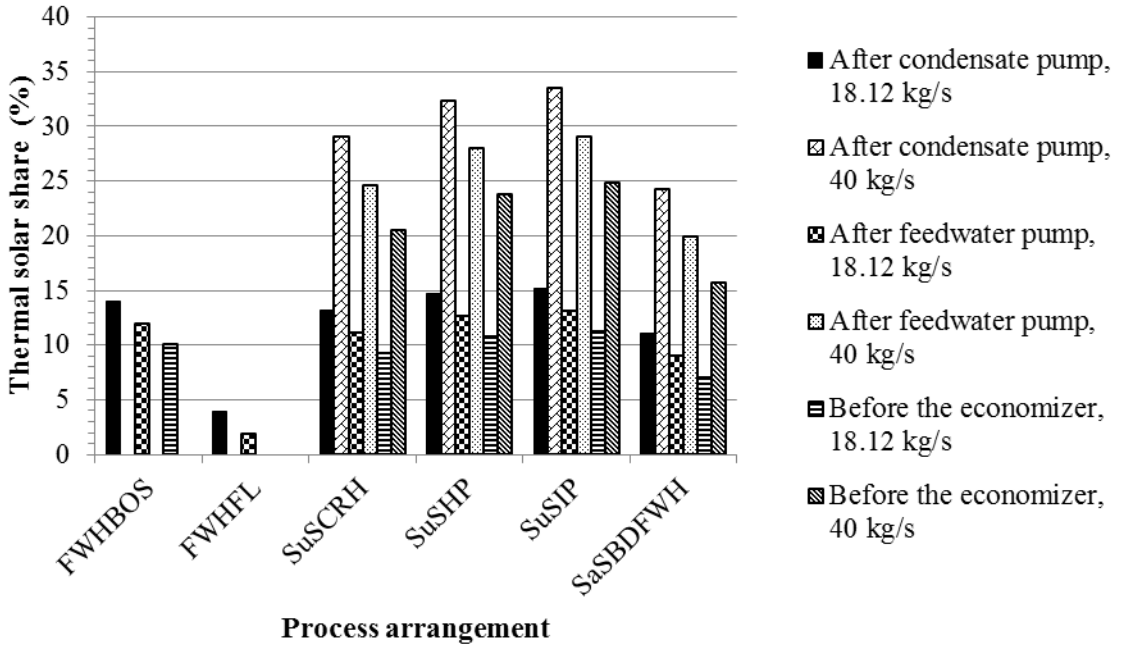

Figure 51. *The calculated thermal solar shares in six cases with two different overall mass flows through the solar field.*

For conclusion, the extraction point for feedwater affects to the reached thermal solar share. If feedwater is extracted after the condensate pump, the thermal solar share is greater than if feedwater is extracted after the feedwater pump or before economizer. This is due to the preheating of feedwater in solar field and not in the existing FWHs. On the other hand, the overall size and the size of preheating section of the solar field are greater if the feedwater is extracted after condensate pump than before the economizer. Furthermore, as the one of the objectives of this thesis is to investigate the possibilities to reach higher solar shares up to 30%, the selection of the reference case is between the process arrangements, in which higher thermal solar shares can be achieved. In other words, the selection is between the SuSCRH, SuSHP and SuSIP process arrangements, as the solar shares are higher in these arrangements compared to other arrangements (Figure 51).

The selected reference setup for the CSP and conventional steam power plant hybrid model is the SuSHP process arrangement, as the full potential of line-focusing solar fields with DSG can be likely achieved with the SuSHP process arrangement in the near future. Furthermore, the efficiency of the hybrid can be greater in SuSHP than in SuSCRH or SuSIP process arrangements, as the solar steam does not by-pass the HP turbine. However, for later work, the selected process arrangement should be compared also against the complexity of the process arrangement as well as the economic feasibility of the process arrangement.

3.4 Description of the hybrid model

The developed hybrid model consists of ten generic diagrams, from which two are related to the solar field model presented in Chapter 3.2.2. Thus, one diagram includes the modelled collector row of the solar field and the other one includes calculation and controls for the modelled collector row. Two other diagrams are related to the interface of the two power plants. One includes the piping between the two power plants and the other one includes the controls of the interface as well as the calculation of the overall solar field with coefficients (Chapter 3.4.1). The last six of the generic diagrams are related to the conventional steam power plant model. Based on the designed process and control engineering of the hybrid (Chapter 3.4.1 and Chapter 3.4.2), the steam power plant model is modified in order to match the steam power plant model with the solar field model (Chapter 3.4.3).

3.4.1 Process engineering of the hybrid plant

The process engineering of the hybrid plant includes connections between the solar field and the steam cycle, modifications of the solar field model based on the connection points of the two power plant models, and modelling of the overall solar field. The connection points of the solar field and the steam cycle are after the deaerator and before the HP turbine (Figure 52). The feedwater for the solar field is taken after the deaerator in order to maximize the solar share and minimize the preheating section of the solar field. Thus, the solar field includes its own feedwater pump, which increases the pressure of feedwater approximately from 10 bar to 170 bar. The other connection point for the two steam streams is between the main steam valve of steam boiler and the HP turbine, but the actual technical solution for combining the two steam lines before HP turbine should be investigated more thoroughly. Currently, the connection arrangement of two steam lines is based on Birnbaum et al. (2010), in which main steam line of solar field and main steam line of thermal storage are connected before HP turbine and both steam lines has own main steam valves (Birnbaum et al. 2010, p.2). However, Birnbaum et al. (2010) presents also an additional third valve between the two main steam valves and the HP turbine. In addition, the operation purpose of the three valves is not explained. Thus, it remains unclear whether all the three valves are control valves or some are only check valves.

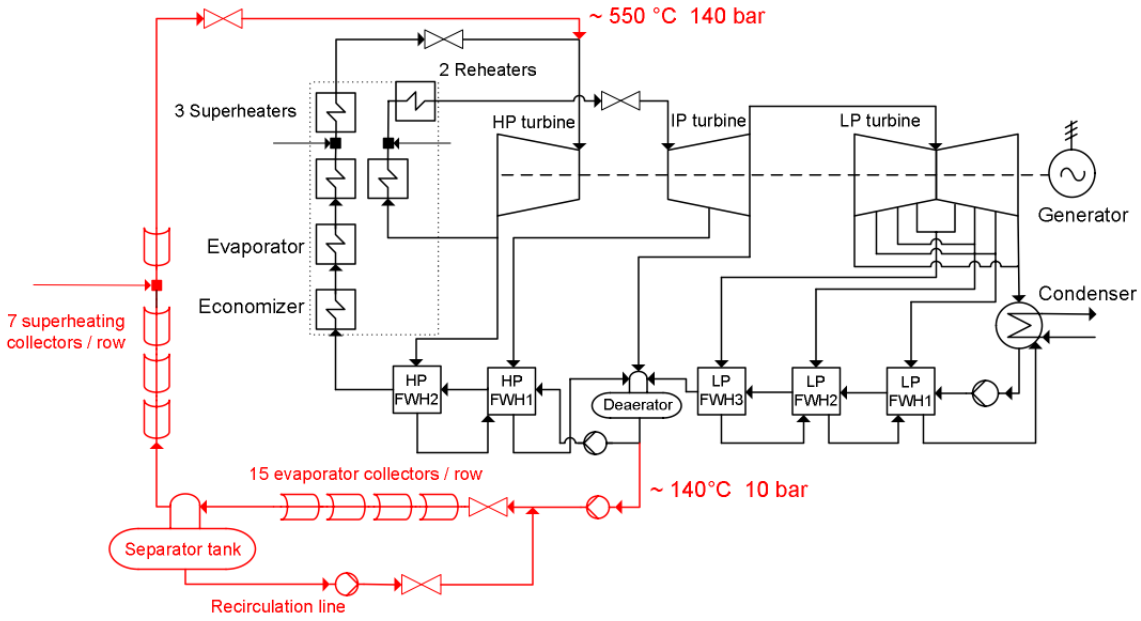

Figure 52. *Schematic of the hybrid process arrangement modelled in Apros.*

In the reference solar field model, the inlet pressure and temperature of the solar field model are 170 bar and 180 °C, but now the inlet conditions are approximately 10 bar and 140 °C after the deaerator of the steam cycle (Figure 52). Thus, one evaporator collector is added into the collector row, as the inlet temperature is 140 °C instead of 180 °C. In addition, the feedwater pump of solar field is adjusted to provide the appropriate pressure increase, as the inlet pressure is 10 bar instead of 170 bar. On the other hand, the reference outlet pressure and temperature of the solar field are 160 bar and 550 °C, whereas the connection point is approximately at 140 bar and 550 °C. Thus, the solar field is producing steam at higher pressure than in the connection point, as pressure losses occurs at the connection piping between the two power plants. However, at the connection point the pressure difference should be kept at its minimum. Thus, the solar steam with a higher pressure is throttled before mixing (Birnbaum et al. 2010, p.2).

The overall solar field is modelled by using multiplication coefficients at the inlet and outlet of the solar field model, which includes only one collector row. The coefficients multiply the mass flow through one collector row accordingly to the number of collector rows at the solar field. Thus, the right amount of feedwater is extracted from the steam cycle, and the right amount of solar steam is injected back to the steam cycle. In addition, multiplication coefficients are used to calculate the overall thermal power of the solar field, as the thermal power of one collector row is multiplied by the number of collector rows. As a result, the size and the thermal power of solar field can be easily changed by changing the coefficient values. On the contrary, all the fluctuations of the thermal power and outlet steam mass flow of the solar field are multiplied by the coefficients.

3.4.2 Control engineering of the hybrid plant

The control engineering of the hybrid plant includes the control of the steam boiler, solar field and the joint turbines. In the coordinative control system of the hybrid plant, the main variables to be controlled are fuel power of the steam boiler, live steam pressures of steam boiler and solar field, and the power output of the joint turbines. From the solar field point of view, the solar field is operated on fixed pressure with turbine follow mode, in which the outlet pressure of solar field is kept fixed by the main steam valve of solar field, and the steam mass flow from solar field varies according to the solar irradiation conditions.

From the steam boiler point of view, the steam boiler is operated also on fixed pressure mode, as the steam boiler is designed to be a natural circulation boiler. Thus, the steam boiler can be either controlled by boiler follow mode or by turbine follow mode depending on the control of the main steam valve before HP turbine. In boiler follow mode, the main steam valve is used to control the steam mass flow through the turbines, and the live steam pressure of steam boiler is kept constant by adjusting the fuel power of the steam boiler. Thus, as the solar steam is injected to the inlet of HP turbine, the main steam valve of steam boiler adjusts the live steam mass flow from steam boiler, which affects to the live steam pressure and to the fuel supply of the steam boiler. On the other hand, in turbine follow mode the main steam valve is used to keep the live steam pressure constant, and the live steam mass flow and the power output of the turbines are controlled by fuel supply. Thus, as the solar steam is injected to the inlet of the HP turbine, the main steam valve of steam boiler adjusts the live steam pressure of the steam boiler, and the live steam mass flow from steam boiler is adjusted by fuel power of the steam boiler accordingly.

The hybrid plant is designed to be a new power plant, in which power boost mode is preferred over the fuel saving mode as operation mode. Thus, the control engineering of the hybrid plant is designed in order to achieve the following operation strategy, which can be divided into two parts related to the load of the solar field:

1. As the steam generation starts from the solar field, the hybrid plant is operated first on the power boost mode up to 110% load of the turbines, as the load of the solar field is approximately 10% of the nominal load of the steam boiler.
2. As more steam is generated at the solar field, power boost mode is switched to fuel saving mode without the need of oversizing the joint equipment, like turbines, condenser and the LP FWHs.

In the first part, the hybrid operates only on power boost mode, and the power output of the turbines is increased approximately from 134.2 MW to 147.6 MW (Figure 53), as turbines is assumed to stand 10% of extra load. Thus, electricity production is increased 10% from the nominal load, as load of the solar field is 10% of the nominal load of steam boiler. In the second part, as the solar field generates more steam, the power boost

mode is combined with fuel saving mode. Thus, the power output of the turbines is kept at 147.6 MW, whereas the load of the steam boiler is decreased accordingly to the load of the solar field (Figure 53) in order to prevent overload of turbines.

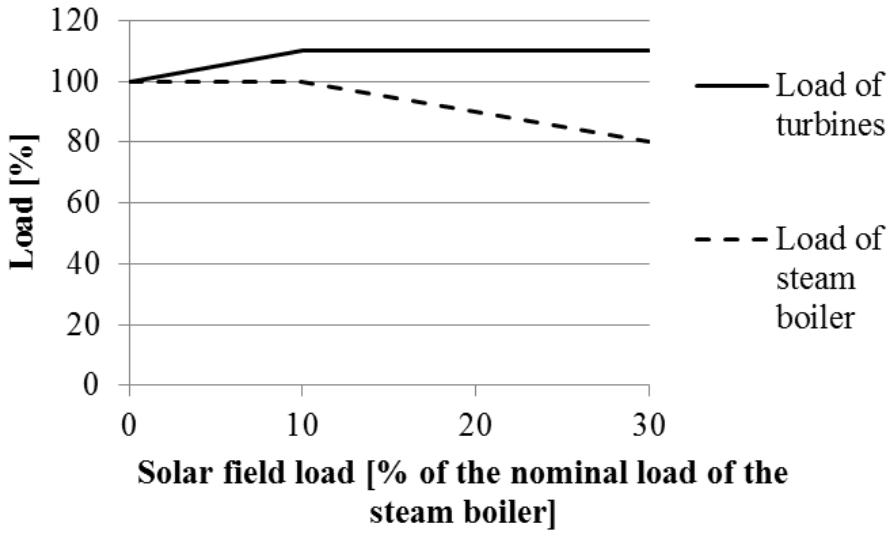

Figure 53. *The applied operation strategy of the hybrid system.*

However, disadvantage of the applied operation strategy is related to the increased mass flow through turbines in power boost mode. As the steam power plant is designed to be a condensing power plant, in which the back pressure is kept constant at the condenser, the increase of mass flow through turbines causes a pressure increase at the inlet of the turbines related to the Elliptic rule (Equation 8) invented by Stodola (Raiko et al. 2013 p.66):

$$\frac{\dot{m}}{\dot{m}_0} = \frac{p_i}{p_{i,0}} \sqrt{\frac{1-(p_o/p_i)^2}{1-(p_{o,0}/p_{i,0})^2}} \tag{8}$$

in which

$\dot{m}$	is the mass flow through turbine	[kg/s]
p_i	is the inlet pressure	[bar]
p_o	is the outlet pressure	[bar]
$\dot{m}_0$	is the design mass flow through turbine	[kg/s]
$p_{i,0}$	is the design inlet pressure	[bar]
$p_{o,0}$	is the design outlet pressure	[bar]

By keeping the outlet pressure and the design values constant, the Equation 8 can be presented as a hyperbola function of mass flow through turbine and inlet pressure (Figure 54).

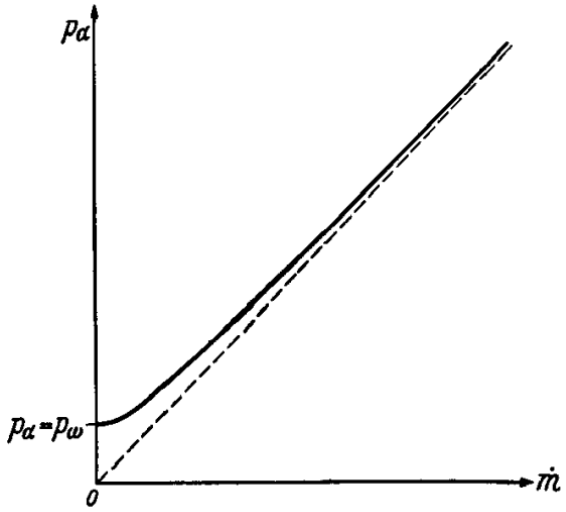

Figure 54. *Hyperbola of Elliptic rule, as outlet pressure is kept constant in Equation 8. Asymptote of the hyperbola is also presented with dash line. Adapted from Raiko et al. 2013, p.67.*

The increase of steam mass flow increases the inlet pressure of HP turbine, which increases also to the live steam pressures of steam boiler and solar field if the turbines are overloaded. Furthermore, as fluctuating solar irradiation conditions are going to cause variations to the outlet steam mass flow from solar field and to the power output of the joint turbines, it is going to cause fluctuations also to the inlet pressure of the HP turbine. Thus, the control of the steam boiler should adjust its load as quickly as possible while preventing pressure variations, as the steam boiler is designed to be a natural circulation boiler with steam drum and the operation of steam drum is sensitive to pressure variations.

The selected control method for the steam boiler is the turbine follow mode, in which the live steam pressure is controlled by the turbine, and the power output of the joint turbines is controlled by fuel supply (Figure 55). The turbine follow mode is selected as control method for steam boiler, as the control method of the solar field is also turbine follow mode. The first part of operation strategy, the power boost mode, is conducted by changing the set point for power output of the turbines directly proportional to the thermal power of the solar field. In other words, the main controller of the fuel supply of steam boiler is designed in order to allow the increase of power output of the turbines without increasing the fuel supply of steam boiler, as steam generation starts from the solar field. In the second part of the operation strategy, as more steam is generated in the solar field and the turbines are operated on 110% load, the set point for power output of the turbines is kept at 147.6 MW, and the main controller of fuel supply decreases au-

tomatically fuel feeding. Thus, the power boost mode is combined with fuel saving mode.

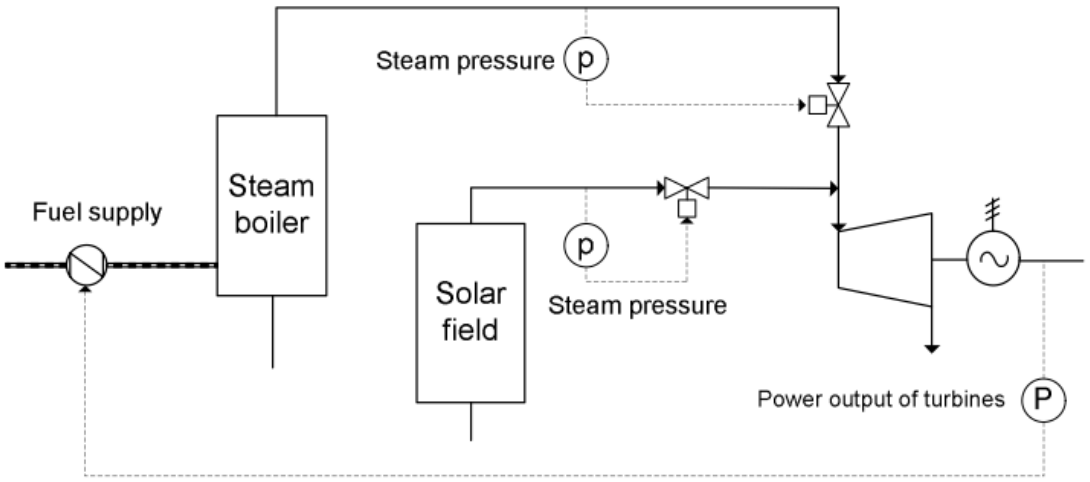

Figure 55. *Schematic of the control engineering of the hybrid system.*

The disadvantages of the fixed pressure mode are large throttling losses at partial load operation compared to sliding pressure mode. Furthermore, in turbine follow mode slower load changes of the steam boiler are achieved than in boiler follow mode (Figure 29). However, quick load changes are needed during start-ups and shutdowns of the solar field as well as under fluctuating solar irradiation conditions if the fuel supply of the steam boiler is adjusted accordingly to the thermal power of the solar field. Thus, it is predicted that more sophisticated and coordinative control method needs to be developed for the co-operation of steam boiler, solar field and the joint turbines.

Furthermore, the turbines need to be dimensioned accordingly to the chosen operation method. In power boost mode, the turbines has to be dimensioned to the highest inlet steam mass flow, which causes additional throttling of the main steam valve of the steam boiler, as the steam boiler is operated without solar field and on partial loads. Thus, it causes also more losses and lowers the efficiency of the plant compared to the fuel saving mode. In just fuel saving mode, the steam mass flow through turbines is not increased, and the throttling losses are smaller while operating without solar field and on partial loads. For that reason, the difference between the previously described operation strategy and operation strategy with just fuel saving mode should be investigated.

3.4.3 Modifications of the conventional steam power plant model

The conventional steam power plant model is modified accordingly to the process and control engineering of the hybrid plant. The modifications include changes to the heat surfaces of the steam boiler, as the sizes of the superheater and reheater surfaces are increased in order to achieve steam temperatures up to 550 °C with higher solar shares.

In addition, modifications are done to the turbines, as the nominal inlet steam mass flow of turbines is increased by 10% due to power boost mode. Thus, two steam cycles are modelled: one for applying the power boost mode and one for applying only fuel saving mode. The sizing of heat surfaces is the same for the two cycles.

The state point data of the conventional steam power plant model is presented at reference situation without the solar field, as the steam power plant is operated on 100% load. As the steam cycle is slightly different for power boost mode and just fuel saving mode, the data is presented for both cycles. The nominal power output of the turbines is 134.2 MW in both cases (Table 8).

Table 8. *Power output of turbines, fuel power and thermal efficiency of the reference steam cycles at 100% load modelled in Apros.*

Steam cycle design	**Power boost**	**Fuel saving**
Power output of turbines [MW]	134.2	134.2
Fuel power of steam boiler [MW]	406.7	403.5
Thermal efficiency [%]	33.0	33.3

In power boost cycle, the reference fuel power of the steam boiler is 406.7 MW and thermal efficiency is 33.0%, which is calculated by using Equations 4 and 5 in Chapter 3.3. On the contrary, in fuel saving cycle the fuel power of the steam boiler is 403.5 MW, and thermal efficiency is 33.3%. Thus, the efficiency of the host plant without solar field is greater in just fuel saving cycle than in power boost cycle, as the only difference between the steam cycles is the design value for inlet steam mass flow through turbines. The difference of the efficiencies is due to the additional throttling losses in power boost cycle compared to just fuel saving cycle.

As the efficiencies of the steam cycles is slightly different, the amount of combusted fuel, combustion air, initial temperature of flue gases after furnace and final temperature of flue gases before the stack are different in the two cycles (Table 9). The initial temperature of flue gas is designed to be approximately 900 °C and final temperature of flue gas after air preheating is designed to be approximately 170 °C.

Table 9. *Main details of the combustion process modelled in Apros at 100% load.*

Steam cycle design	Power boost	Fuel saving
Fuel mass flow [kg/s]	29.6	29.4
Primary air mass flow [kg/s]	196.8	195.3
Secondary air mass flow [kg/s]	67.9	67.4
Flue gas mass flow [kg/s]	294.3	292.0
Flue gas initial temperature at furnace [°C]	900.1	897.8
Flue gas final temperature before entering the stack [°C]	173.2	173.1

As the power boost has slightly lower efficiency than fuel saving due to larger throttling losses, it needs to combust more fuel in order to have the same power output of the turbines. Thus, the amount of needed combustion air is higher as well as the amount of produced emissions is higher in power boost cycle than in fuel saving cycle. As a result, the initial and final temperatures of flue gases are slightly higher in power boost cycle than in fuel saving cycle.

The superheaters and reheaters are redimensioned in order to achieve the design temperature of 550 °C, which is the same as the design live steam temperature in the solar field (Table 10). In addition, the live steam temperature and reheated steam temperature are also achieved with 70% steam boiler load without the solar field. Furthermore, the live steam pressure is designed to be 145 bar and the reheated pressure is designed to be approximately 35 bar. The lower reheated steam pressure in power boost cycle is due to larger dimensioning of the turbines compared to fuel saving cycle. Moreover, the economizer increases the temperature of the feedwater close to its boiling point. The approach temperature difference between the steam drum and the outlet of the economizer is approximately 25 K even though the ideal approach temperature difference is approximately 10 K (Teir et al. 2002, p.6). The greater approach temperature difference is due to the larger superheating and reheating surfaces, which affect to the operation of latter heating surfaces, such as economizer and air preheating.

Table 10. *State point data of the operation of superheaters, reheaters and economizer modelled in Apros at 100% load.*

Steam cycle design	Power saving	Fuel saving
Live steam temperature [°C]	550.0	550.0
Live steam pressure [bar]	145.0	145.0
Reheated steam temperature [°C]	550.0	550.0
Reheated steam pressure [bar]	35.1	37.0
Approach temperature difference after economizer [K]	25	25

The evaporator sections are the same for power boost and fuel saving cycles (Table 11). The steam boiler is designed to be a natural circulation boiler, in which the circulation

number of the boiler is designed to be close to 5. As the circulation number is defined as the ratio of the amount of water evaporating within the steam boiler and the total amount of water-steam mixture circulating in the evaporator, the mass fraction of steam at the end of the evaporator is close to 0.2, which is the maximum for natural circulation boilers.

Table 11. *State point data of the evaporator modelled in Apros at 100% load.*

Operation method	**Power boost**	**Fuel saving**
Pressure at steam drum [bar]	154.2	154.2
Temperature at steam drum [°C]	347.5	347.5
Circulation number [-]	5	5
Mass fraction of steam at the end of the evaporator [-]	0.2	0.2

The main difference of the power boost cycle and fuel saving cycle can be seen in the temperature and pressure of the steam before HP turbine. As the main steam valve before HP turbine is more throttled in power boost cycle than in fuel saving cycle due to dimensioning of the turbines, the steam temperature and pressure are lower before the HP turbine in power boost cycle than in fuel saving cycle (Table 12). In power boost cycle, the steam pressure and temperature before HP turbine are 125.5 bar and 542.2 °C, whereas they are 137.3 bar and 546.9 °C in fuel saving cycle at 100% load.

Table 12. *Main design details of the steam cycle at 100 % load modelled in Apros.*

Steam cycle design	**Pressure [bar]**		**Temperature [°C]**		**Mass flow [kg/s]**	
	Power boost	**Fuel saving**	**Power boost**	**Fuel saving**	**Power boost**	**Fuel saving**
Live steam	145.0	145.0	550.0	550.0	109.2	108.8
Before HP turbine	125.5	137.3	542.2	546.9	109.2	108.8
Before reheaters	37.1	38.9	362.8	360.2	104.9	103.7
Before IP turbine	35.1	37.0	549.7	549.7	114.6	113.1
Before condenser	0.15	0.15	54.0	54.0	87.3	85.7
Before LP FWHs	12.9	12.9	44.7	44.8	101.8	100.9
Before deaerator	10.7	10.7	129.7	133.2	101.8	100.9
Before HP FWHs	169.3	169.3	141.5	142.3	102.7	102.6
Before economizer	164.6	164.6	241.4	243.1	102.7	102.6
After economizer	154.4	154.2	321.8	321.8	102.7	102.6

The throttle losses lower the efficiency of the plant, the reheated steam pressure as well as reached feedwater temperatures of FWHs. Furthermore, the steam mass flows to turbines and in the rest of the cycle are greater in power boost cycle than in fuel saving cycle due to throttling losses. After the last LP turbine section, the steam fraction of the expanded steam is designed to be 96.5% with final pressure of 0.15 bar and temperature

of 54.0 °C. Furthermore, the pressure in the deaerator is designed to be 10 bar and the final temperature of feedwater after HP FWHs is designed to be close to 240 °C.

3.5 Definition of steady state and transient simulation cases

The hybrid model is simulated under several steady state and transient conditions in order to research the behaviour of the hybrid plant under different loads of steam boiler and solar field and under fluctuating solar irradiation conditions. Steady state cases are modelled in order to observe the transients and challenges within the joint steam cycle with different loads of the steam boiler and the solar field (Chapter 3.5.1). On the other hand, transient simulation cases (Chapter 3.5.2) are conducted for one hybrid configuration, in which the load of the solar field is changed either by changing the DNI level or the number of collector rows. Thus, transients within the joint steam cycle are observed as well as the operation of the applied control strategy.

3.5.1 Steady state simulation cases

In the steady state simulation cases, the location of the hybrid plant, date and time are kept constant. The hybrid plant is located on southern Spain, and the simulations are conducted on June 21st at 12.00 a.m. (Table 13).

Table 13. *Initial conditions for steady state simulations.*

Parameter	**Value**
Date	21.6.
Time	12.00 a.m.
Latitude	38.2784111
Local longitude	1.6002806
Turbidity Linke factor	3
Peak DNI level [W/m^2]	957.14
Peak effective DNI on collectors [W/m^2]	886.13

The peak DNI at the location is 957.14 W/m^2 on June 21st at 12.00 a.m. whereas, the peak effective DNI on collectors is 886.13 W/m^2. The effective DNI is defined as the amount of DNI collected on the surface of the absorber tube, as the sun is tracked throughout its daily course. The turbidity Linke factor is an attribute, which models the optical thickness of the atmosphere due to absorption and scattering of the solar irradiation under clear sky (CRA-CIN 2009). The value of turbidity Linke factor depends on the moisture and aerosol content of the air (Table 14).

Table 14. *Turbidity Linke factor and air features (CRA-CIN 2009).*

Turbidity Linke Factor	Air features
2	Very clean cold air
3	Clean warm air
4-6	Moist warm or stagnating air
> 6	Polluted air

As the value of turbidity Linke factor is 3, the hybrid plant is operated in a clean and warm atmosphere. Furthermore, the operation of hybrid plant is tested under peak DNI level without defocusing the solar field collectors. In other words, the operation of the hybrid is tested under the peak solar irradiation conditions, in which the hybrid plant must be capable of operating without dumping any energy at solar field.

Overall, four steady state cases are simulated with Apros, from which the first two are simulated in order to demonstrate the operation strategy described in Chapter 3.4.2:

1. Firstly, the hybrid is simulated only on power boost mode, in which the power output of the turbines is increased from 134.2 MW to 147.6 MW, and the thermal power of solar field is approximately 40 MW_{th}, which is approximately 10% of the nominal load of the steam boiler (Figure 56).
2. Secondly, the hybrid is simulated in order to keep the power output of the turbines at 147.6 MW, but the thermal power of the solar field is increased from 40 MW_{th} by increasing the number of collector rows (Figure 56). As the steam generation from solar field is increased, the power boost mode is combined with fuel saving mode, as the fuel supply of the steam boiler is decreased until the steam temperatures of live steam and reheated steam at the steam boiler drop below 550 °C.

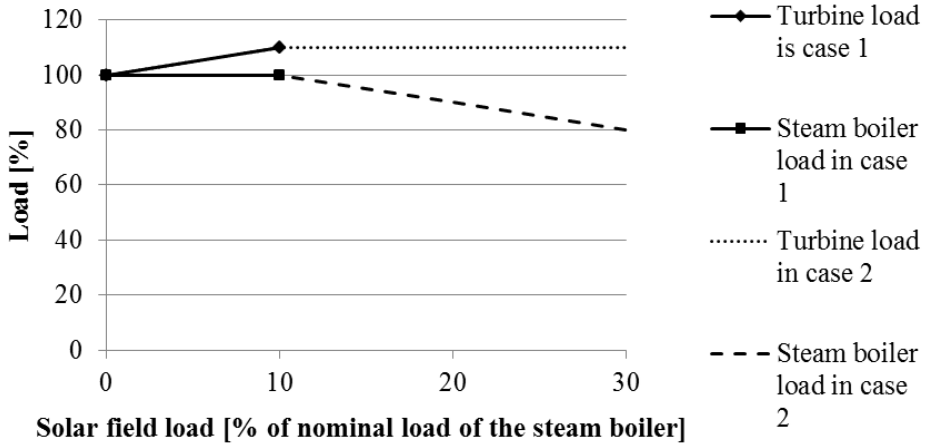

Figure 56. *Steady state cases 1 and 2.*

Third steady state case is simulated in order to determine the load range, in which only power boost hybrid can be operated without overloading the turbines or decreasing the

live steam and reheated steam temperatures of the steam boiler. Thus, in case 3 the solar field is same sized as in case 1, but the load of the steam boiler is decreased (Figure 57):

3. The thermal power of solar field is approximately 40 MW_{th} in case 1 and 3, but in case 3 the load of the steam boiler is decreased in order to observe the steam boiler load, in which the design temperatures of 550 °C are reached for live steam and reheated steam of the steam boiler.

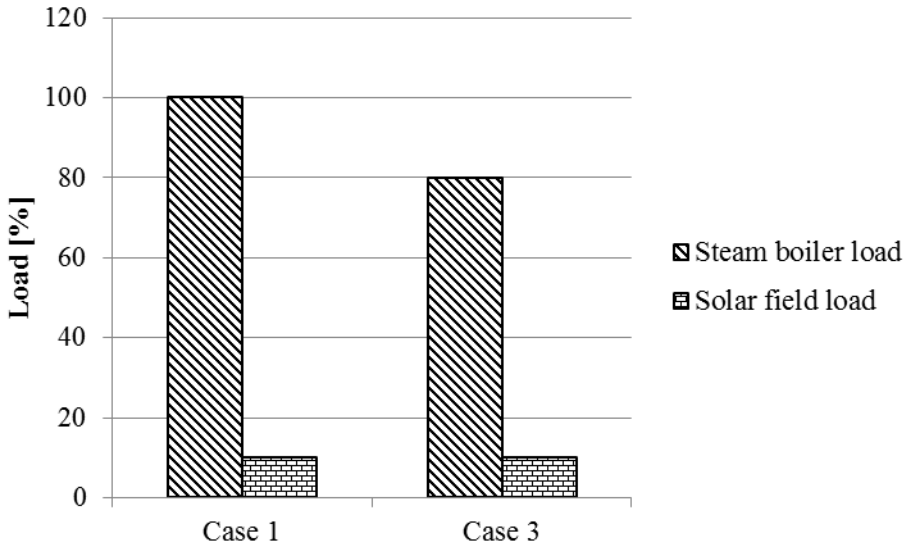

Figure 57. *Difference between steady state cases 1 and 3.*

The final fourth steady state case is conducted in order to observe the difference between two operation strategies of the hybrid plant: power boost mode and fuel saving mode. For the power boost mode, the hybrid configuration is the same as in case 2. For the fuel saving mode, the steam cycle designed only for fuel saving mode is applied. By applying only fuel saving mode, the load of the steam boiler is immediately decreased, as steam generation starts at the solar field. On both cases, the hybrid operates on solar share, in which the design temperature of 550 °C is reached for live steam and reheated steam:

4. The results from the case number 2 are compared to results while operating only on fuel saving mode, in which the turbines are operated at 100% load and the steam boiler operates on a load, in which the design temperature of 550 °C is reached for live steam and reheated steam.

Results from the four steady state simulation cases include the overall operation of the hybrid plant, operation of the combustion process, operation of different heat surfaces of the steam boiler, turbines and the rest of the steam cycle. The main results are presented from Apros simulations, as the hybrid model is simulated on steady state. However, the thermal solar shares and thermal efficiencies for the hybrid system are calculated by using Equations 4, 5 and 6 in Chapter 3.3.

3.5.2 Transient simulation cases

The initial conditions for transient simulation cases are the same as in steady state analysis (Table 13). On June 21st, the steam generation starts in the solar field approximately from 6.30 a.m. and ends at 19.00 p.m. (Figure 58).

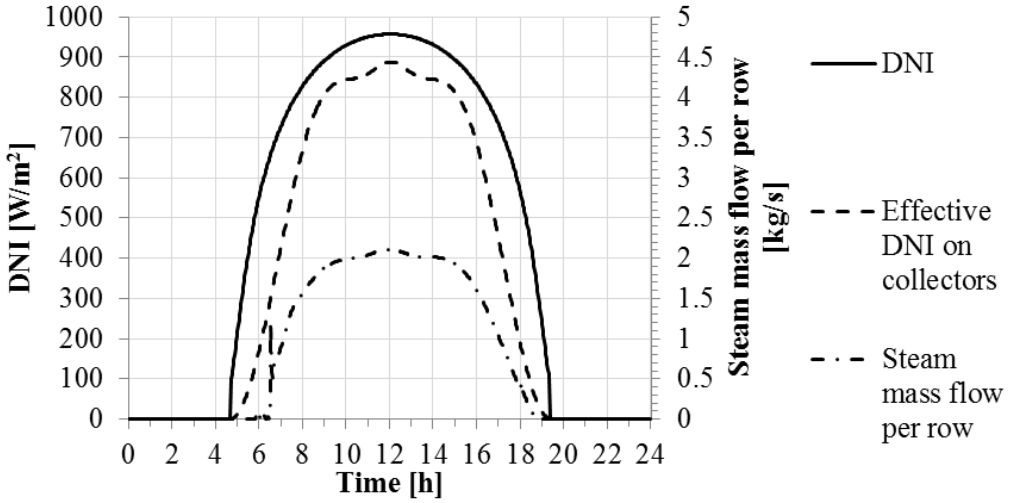

Figure 58. *Steam generation from one collector row on June 21st.*

The steam generation starts from the solar field rapidly, as the effective DNI on collectors exceeds 200 W/m^2. On the other hand, thermal inertia of the solar field can be seen from the shutdown of the solar field, as the steam generation ends less rapidly than during the start-up. On June 21st and on a clear day, one collector row produces at 7.00 a.m. approximately 0.9 kg/s of superheated steam, and at noon it produces approximately 2.2 kg/s of steam per collector row. The steam generation in solar field follows curve of the effective DNI on collectors throughout the day. As the start-up and shutdown procedures are not elaborated in this thesis, the operation of the hybrid can be observed, as the solar field produces steam on its design values after the start-up and before shutdown procedures. Thus, on June 21st the collector row produces steam steadily at 550 °C and 160 bar approximately from 7.00 a.m. to 18.30 p.m. on a clear day (Figure 59).

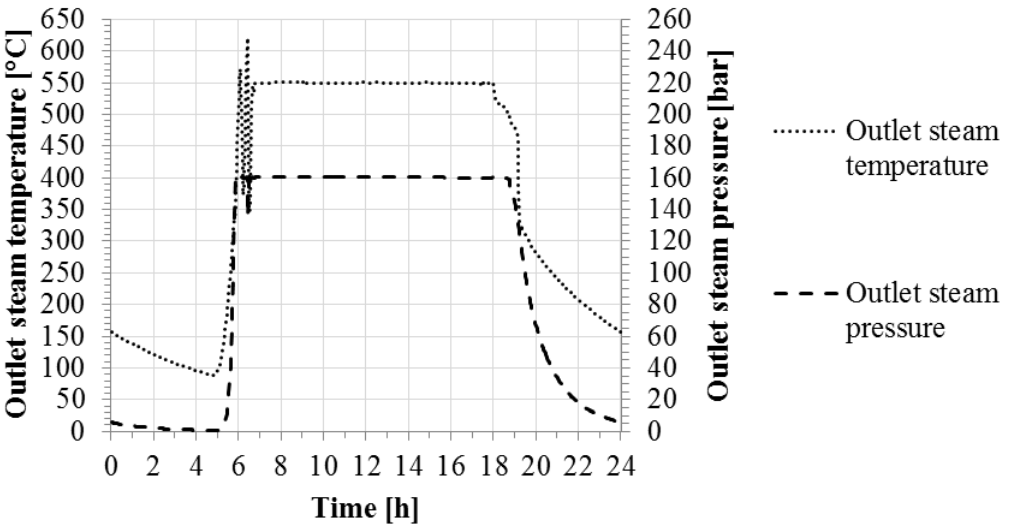

Figure 59. *Outlet steam temperature and pressure of solar field on June 21st.*

The transient simulations are conducted in a power boost hybrid with full load of the steam boiler. Thus, the hybrid plant is designed in order to produce approximately 10% more electricity on a summer day, as the steam boiler is operated on full load (Table 15). In other words, the amount of combusted fuel is kept constant regardless of the load of the turbines. The transients within the joint steam cycle are observed, and the timeframe for steam boiler can be studied, in which the steam boiler has to response to variations from the solar field if the steam boiler is used to compensate the fluctuations.

Table 15. *Hybrid configuration for transient simulations.*

Design detail	**Value**
Fuel power of steam boiler without solar field [MW]	406.7
Power output of turbines without solar field [MW]	134.2
Number of collector rows	5
Peak thermal power of solar field [MW_{th}]	30.9
Peak power output of the turbines [MW]	147.5

The transient simulations can be conducted either by changing the DNI level or the size of the solar field in order to simulate the hybrid system under different solar irradiation conditions. The changes of the DNI level affects to the whole solar field. Thus, it affects primarily to the outlet steam mass flow, which decreases due to smaller effective DNI level on collectors. In addition, it affects secondarily to the outlet steam temperature and pressure especially with larger transients. On the other hand, if the size of the solar field is changed by altering the multiplication coefficients, the outlet steam mass flow from solar field can be changed. However, the change of coefficients does not include variations to the outlet pressure and temperature, which may happen especially with larger transients.

Two different sized step changes are conducted to the hybrid system (Table 16). Initially, the hybrid is operated at steady state on June 21st at noon, in which the effective DNI on collectors is 886.13 W/m^2. First step change is a smaller one, in which the effective DNI on collectors is decreased by 10%, and second step change is a larger one, in which the effective DNI on collectors is decreased by 50%. These transients can be considered as a small and medium sized transients, as it is also possible that the effective DNI on collectors is decreased by 100% (Khenessi et al. 2015, p.1609).

Table 16. *Transient simulation cases.*

Case	Effective DNI on collectors [W/m^2]	Change of DNI [%]
Reference	886.13	0
1	797.68	-10
2	443.15	-50

The hybrid is firstly operated at steady state for 4 minutes (Figure 60). After the four minutes, a step change is conducted to the DNI level, and the simulations are carried out 30 minutes after the step change.

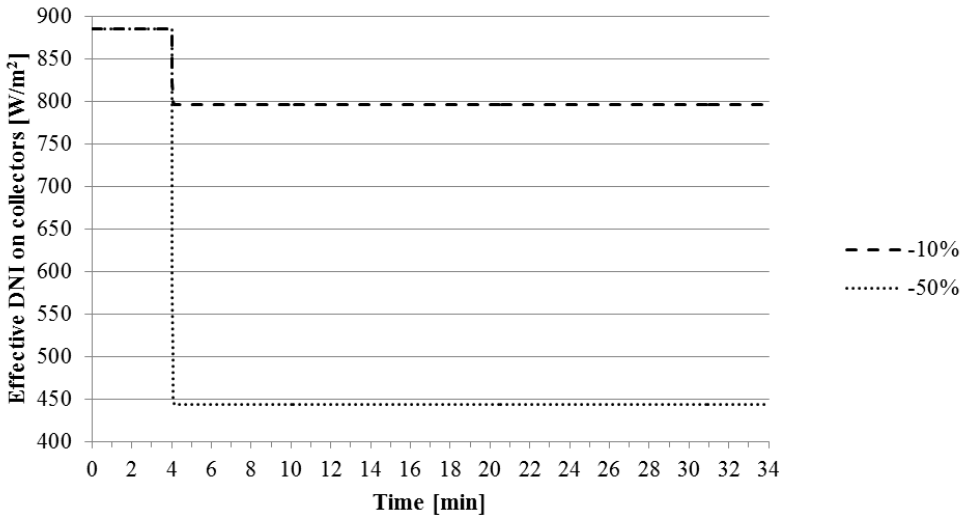

Figure 60. *Conducted step changes for transient simulations.*

The focus of the transient simulations is on the gradients of steam mass flows, steam pressures, power output of the turbines and steam temperatures, which occur right after the step change in the DNI level. However, the hybrid system may not be at steady state after 30 minutes of simulation especially with the larger transient case. Furthermore, in real transient situations, the hybrid system is constantly exposed to fluctuations of the DNI level. Therefore, in future the hybrid system should be tested with more sophisticated transient cases over longer time periods.

4. RESULTS

The hybrid model used in the simulation cases is described in the previous Chapter 3.4, whereas the simulation cases are described in the previous Chapter 3.5. The results of the thesis include results from the different steady state and transient simulations cases conducted with the developed CSP and conventional steam power plant hybrid model. Thus, the results from four steady state cases (Chapter 4.1) and two transient simulation cases (Chapter 4.2) are described.

4.1 Steady state simulations

Steady state simulations are conducted with four steady state cases in order to simulate the hybrid under different loads of solar field and steam boiler. All the results from the steady state simulations in Apros are presented in Appendix J. In addition, the Appendix J includes thermal solar shares and thermal efficiencies, which are calculated by using Equations 4, 5 and 6 in Chapter 3.3. However, only the main results are presented in the following chapters. In the four steady state cases, following solar fields are integrated with the steam cycle (Table 17).

Table 17. *Overall results from the four steady state cases.*

Steady state case	**1**	**2**	**3**	**4**
Applied operation mode, steam cycle and strategy	Power boost	Power boost and attainable solar share	Power boost and attainable load range	Fuel saving and attainable solar share
Number of collector rows in the solar field	7	15	7	10
Thermal power of solar field [MW_{th}]	41.3	88.5	41.3	59.0

In cases 1 and 3, the solar field includes 7 collector rows and the thermal power of the solar field is 41.3 MW_{th}, which is approximately 10% of the nominal fuel power of the steam boiler. However, in case 3, the load of the steam boiler is decreased from 100% load in order to observe the load, in which live steam and reheated steam temperatures are still achieved in steam boiler. Thus, the cases 1 and 3 defines the load range, in which only a power boost hybrid could be operated without overloading the turbines and decreasing the steam temperatures. In case 2, the solar field includes 15 collector rows, and the thermal power of the solar field is 88.5 MW_{th}. Thus, the case 2 defines the size and peak load of the solar field, which could be integrated with power boost cycle

without overloading the turbines or decreasing the steam temperatures. In case 4, the solar field includes 10 collector rows, and the thermal power of the solar field is 59.0 MW_{th}. Thus, the case 4 defines the size and peak load of the solar field, which could be integrated with fuel saving cycle, as the turbines are operated on their nominal load and the steam temperatures of steam boiler are not decreased. In addition, the results of case 4 are compared to case 2 in order to observe the difference between power boost mode and fuel saving mode. The first results are represented from cases 1 and 2 (Chapter 4.1.1), second results are from cases 1 and 3 (Chapter 4.1.2) and third results are from cases 2 and 4 (Chapter 4.1.3).

4.1.1 Power boost mode and attainable thermal solar share

Power boost mode is simulated with cases 1 and 2, in which the power output of the turbines is increased by 10% from 134.2 MW to 147.6 MW (Table 18). For both cases, the reference case is the power boost steam cycle on 100% steam boiler load without solar field. In case 1, solar field of 41.3 MW_{th} is integrated with the steam boiler, as it is approximately 10% of the nominal fuel power of steam boiler. The load of the steam boiler is decreased by 3.4% from 406.7 MW to 392.9 MW, and the total heat input to the system is increased by 6.8% from 406.7 MW to 434.3 MW. In other words, by increasing the total heat input to the hybrid system by 6.8%, the power output of the turbines is increased by 10%. In addition, the thermal efficiency is increased by 1.0%-point from 33.0% to 34.0%.

Table 18. *Overall operation of the hybrid plant in cases 1 and 2.*

Component	Detail	Reference case	Case 1	Case 2
Solar field	Number of collector rows [-]	0	7	15
	Thermal power of solar field [MW_{th}]	0.0	41.3	88.5
Turbines	Power output of the turbines [MW]	134.2	147.6	147.6
	Turbine load [%]	100.0	110.0	110.0
Steam boiler	Steam boiler load [%]	100.0	96.6	80.9
	Fuel power [MW]	406.7	392.9	328.8
Overall	Total heat input to hybrid plant [MW]	406.7	434.3	417.3
	Thermal solar share [%]	0.0	9.5	21.2
	Thermal efficiency [%]	33.0	34.0	35.4

In case 2, solar field with thermal power of 88.5 MW_{th} is integrated with the steam boiler and the attainable thermal solar share is 21.2%, in which live steam and reheated steam temperatures of steam boiler are kept at design value of 550 °C. The load of the steam boiler is decreased by 19.1% from 406.7 MW to 328.8 MW, and the total heat input to the system is increased by 2.6% from 406.7 MW to 417.3 MW. Thus, the total

heat input to the system is increased less than in case 1 even though the power output of the turbines is the same in case 1 and case 2. This indicates that the thermal efficiency is increased in case 2 compared to case 1 and reference case. In case 2, the thermal efficiency is increased from 33.0% to 35.4%, which is 2.4%-point greater than in the reference case without solar field. As a conclusion from the efficiency increase, higher thermal solar share indicates higher thermal efficiency of the plant. The increased thermal efficiency is possibly due to the ratio between the load of the steam boiler and load of the turbines. With higher solar shares the load of the steam boiler is decreased, which results to smaller exergy losses of boiler and HP FWHs (Gupta et al. 2009, p.597). In addition, the turbines are operated at higher load compared to reference case, which results to smaller throttling losses and higher steam parameters. The higher steam parameters increase the efficiency of the plant. However, exergy analysis should be conducted in order to observe the exact reasons for the increased thermal efficiency.

As the load of the steam boiler is decreased in cases 1 and 2, less fuel is combusted in the FBC module (Table 19). In case 1, the amount of combusted fuel is reduced by 4.1% from 29.6 kg/s to 28.4 kg/s, while the amount of produced electricity is increased by 10%. As less fuel is combusted, the amount of produced flue gases is reduced as well. Thus, the amount of greenhouse gas emissions is also decreased by 4.1% in case 1.

Table 19. *Steady state results of the combustion process in cases 1 and 2.*

Case number	**Reference**	**1**	**2**
Fuel supply [kg/s]	29.6	28.4	23.9
Primary air flow [kg/s]	196.8	190.2	159.2
Secondary air flow [kg/s]	67.9	65.6	54.9
Flue gases mass flow [kg/s]	294.3	284.4	238.1
Flue gases initial temperature [°C]	900.1	889.7	834.8
Flue gases final temperature [°C]	173.2	171.9	164.6

On the contrary, in case 2 the amount of combusted fuel is decreased by 19.3% from 29.6 kg/s to 23.9 kg/s while the amount of produced electricity is increased 10%. Thus, the amount of greenhouse gases is also decreased by 19.3% in case 2. Furthermore, in both cases the initial temperature and final temperature of the flue gases decreases, as the thermal solar share is increased and the load of the steam boiler is decreased. However, the final temperature of the flue gases should not be decreased under the dew point of flue gases, which is approximately 150 °C for flue gases (Raiko et al. 2013, p.105).

The live steam temperature and pressure of steam boiler are kept constant at 550 °C and 145 bar in cases 1 and 2 even though the load of the steam boiler is decreased and the thermal solar share is increased (Table 20). In addition, in both cases the overall steam mass flow to HP turbine is increased due to power boost mode.

Table 20. *Steady state results from the operation of superheaters in cases 1 and 2.*

Case number	**Reference**	**1**	**2**
Live steam temperature of steam boiler [°C]	550.0	550.0	550.0
Live steam pressure of steam boiler [bar]	145.1	145.1	145.1
Live steam temperature of solar field [°C]	-	550.0	550.0
Live steam pressure of solar field [bar]	-	160.0	160.0
Steam temperature after outlet throttle of solar field [°C]	-	541.3	542.4
Steam pressure after outlet throttle of solar field [bar]	-	138.9	141.8
Steam temperature at connection point before HP turbine [°C]	542.2	546.6	546.9
Steam pressure at connection point before HP turbine [bar]	125.5	138.8	141.8
Steam mass flow from steam drum [kg/s]	102.7	101.4	92.8
Superheater spray water mass flow [kg/s]	6.5	5.1	0.1
Steam mass flow from solar field	-	14.7	31.4
Overall steam mass flow to HP turbine [kg/s]	109.2	121.3	124.3
Change of steam mass flow to HP turbine [kg/s]	-	+12.0	+ 15.1

However, in case 1 the steam mass flow is increased less than in case 2, in which the maximum steam mass flow of 124.3 kg/s enters the HP turbine. This indicates that the steam mass flow through other turbine sections has to be less in case 2 than in case 1 in order to keep the power output of the turbines at 147.6 MW. As the HP turbine is operated on maximum load in case 2 due to largest steam mass flow through the HP turbine, the main steam valves of solar field and steam boiler before HP turbine are less throttled. Thus, the steam temperature and steam pressure before HP turbine are greater in case 2 compared to the case 1 and to the reference case. The steam temperature is increased by 4.7 °C from 542.2 °C to 546.9 °C, whereas the steam pressure is increased by 16.3 bar from 125.5 bar to 141.8 bar. This is also probably one of the reasons for the increased thermal efficiency, as higher steam parameters increase the efficiency of the plant. However, the steam temperature of solar field after the outlet throttle of solar field is approximately 4.5 °C less than in the connection point, which indicates that the solar steam actually decreases the steam temperature before HP turbine. This is due to the throttling losses of the main steam valve of solar field, as the pressure difference between the outlet of the solar field and the connection point is approximately 18 bar in case 2. As a result, the steam parameters in solar field and in steam boiler should be redesigned close to each other in order to minimize throttling losses and impacts on the steam temperature before HP turbine. Furthermore, the impact of the technical solution for the main steam valves should be investigated, as in the model solar field and steam boiler have their own main steam valves, and the steam lines are connected after the valves before HP turbine.

As the steam mass flow to HP turbine is increased more in case 2 than case 1, the operation of the reheater and IP turbine is also investigated. The reheated steam temperature

is kept constant at 550 °C in cases 1 and 2 (Table 21), but the reheated steam pressure is changed accordingly to the steam mass flow through IP turbine.

Table 21. *Results from the operations of reheaters and IP turbine in cases 1 and 2.*

Case number	**Reference**	**1**	**2**
Reheated steam temperature [°C]	549.7	549.7	549.7
Reheated steam pressure [bar]	35.1	37.9	37.1
Steam mass flow from HP turbine to reheaters [kg/s]	104.9	116.7	120.6
Reheater spray water mass flow [kg/s]	9.7	7.1	0.4
Reheated steam mass flow to IP turbine [kg/s]	114.6	123.8	121.0
Change of steam mass flow to IP turbine [kg/s]	-	+9.2	+6.4

In case 1, the steam mass flow to IP turbine is 123.8 kg/s and the reheated steam pressure is 37.9 bar, whereas in case 2 the steam mass flow to IP turbine is 121.0 kg/s and the reheated steam pressure is 37.1 bar. Thus, the steam mass flow through other turbine sections is lower in case 2 than in case 1, as the steam mass flow through HP turbine is greater in case 2 than in case 1. In other words, the addition of solar steam through part of the steam cycle creates an imbalance between the turbine sections, as it is predicted in the observation of advantages and disadvantages of different process arrangements. However, the imbalance between the turbine sections possibly increases the efficiency of the plant, as the isentropic efficiency of HP turbine is greater than the other turbine sections, and the steam mass flow through HP turbine is increased relatively more than through other turbine sections.

In order to observe the imbalance between the turbine sections more closely, the changes of steam mass flows and spray water mass flows to turbines should be investigated. For HP turbine, the overall steam mass flow consists of steam mass flows from the steam drum, solar field and spray water mass flow from the superheater attemperator. On the other hand, for IP turbine the overall steam mass flow consists of steam mass flow from HP turbine and spray water mass flow from the reheater attemperator. In case 1, the steam mass flow from solar field is 14.7 kg/s, whereas in case 2 the steam mass flow from solar field is 31.5 kg/s (Table 22). As the load of the steam boiler is decreased in both cases, the steam mass flow from steam drum and spray water mass flow from superheater attemperator are decreased as well. From the previous results, the overall steam mass flow to HP turbine is increased more in case 2 than in case 1.

Table 22. *Changes of mass flows entering the HP and IP turbines in cases 1 and 2.*

Component	Change of steam mass flow	Case 1	Case 2
HP turbine (isentropic efficiency = 85%)	Change of steam mass flow from solar field [kg/s]	+14.7	+31.4
	Change of steam mass flow from steam drum [kg/s]	-1.3	-9.9
	Change of superheater spray water mass flow [kg/s]	-1.4	-6.4
	Overall change of mass flow to HP turbine [kg/s]	+12.0	+15.1
IP turbine (isentropic efficiency = 84%)	Change of steam mass flow from HP turbine [kg/s]	+11.8	+15.7
	Change of reheater spray water mass flow [kg/s]	-2.6	-9.3
	Overall change of steam mass flow to IP turbine [kg/s]	+9.2	+6.4

As the overall steam mass flow is increased to HP turbine, it indicates that the steam mass flow from HP turbine to reheaters is increased as well. Thus, the steam mass flow through reheaters is increased more in case 2 than in case 1. However, as the increased steam mass flow through reheaters is combined with the partial load of steam boiler especially in case 2, the reheater spray water mass flow is decreased. For that reason, the steam mass flow to IP turbine is less in case 2 than in case 1. As a result, the imbalance between the turbines is related to the imbalance between heat surfaces and its impacts on spray water mass flows.

For the rest of the steam cycle, the impacts of the addition of solar steam are also observed especially for the operation of steam drum, economizer, and HP FWHs. The operation of these components is affected, as the steam boiler is operated on partial load and feedwater for solar field is extracted from the deaerator (Table 23).

Table 23. *Results from the operation of steam drum, economizer and HP FWHs in cases 1 and 2.*

Case	Reference	1	2
Steam temperature at steam drum [°C]	347.5	347.3	346.5
Steam pressure at steam drum [bar]	154.2	153.9	152.2
Steam fraction at the end of the evaporator [-]	0.20	0.195	0.18
Feedwater temperature after economizer [°C]	321.8	320.7	312.2
Feedwater pressure after economizer [bar]	154.4	154.1	152.4
Approach temperature difference [K]	25.7	26.6	34.3
Feedwater temperature before economizer [°C]	241.4	245.4	245.6
Feedwater pressure before economizer [bar]	164.6	164.1	160.9
Feedwater temperature before HP FWHs [°C]	141.5	141.6	140.9
Feedwater pressure before HP FWHs [bar]	169.3	168.7	164.9

As the load of the steam boiler is decreased, less steam is generated at steam drum, in which steam pressure, steam temperature and mass fraction of steam at the end of the

evaporator are decreased in case 1 and in case 2. Same kind of results can be seen in the feedwater pressure and temperature after economizer and before HP FWHs. However, the feedwater temperature is increased before economizer. This is possibly due to the operation of HP FWHs, as less feedwater flows through the HP FWHs and the load of turbines is not decreased. As a result, the HP FWHs are operated more efficiently. In case of economizer, the approach temperature difference between the steam drum and the outlet of the economizer is increased, as thermal solar share is increased and the load of the steam boiler is decreased. This is possibly due to the increased steam mass flow through reheaters, which absorbs more heat from the flue gases and less is left for the latter heat surfaces. Thus, more fuel power is used at the evaporator in order to increase the feedwater temperature to its boiling point, as the thermal solar share is increased.

For the rest of the steam cycle the changes are small, as can be seen from Appendix J. The feedwater pressure increases before LP FWHs, before and after deaerator, as feedwater mass flow is increased through the components due to power boost mode. For the condenser, the pressure and temperature before condenser are kept constant in all cases. In addition, the steam fraction before condenser is kept almost constant even though mass flow through condenser is increased.

4.1.2 Power boost mode and attainable load range

Case 3 is conducted in order to determine the load range, in which only a power boost hybrid could be operated, as the turbines are not overloaded and the design values of live steam and reheated steam temperatures are still achieved in the steam boiler. Thus, in case 3 the size and thermal power of the solar field are the same as in case 1, but the steam boiler is operated at partial load, in which the steam temperatures of 550 °C are still achievable (Table 24).

Table 24. *Results from the operation of power boost hybrid and attainable load range in cases 1 and 3.*

Component	Detail	Case 1	Case 3
Solar field	Number of collector rows	7	7
	Thermal power of solar field [MW_{th}]	41.3	41.3
Turbines	Power output of the turbines [MW]	147.6	124.6
	Turbine load [%]	110.0	92.9
Steam boiler	Steam boiler load [%]	96.6	79.4
	Fuel power [MW]	392.9	322.7
	Fuel supply [kg/s]	28.4	23.5
Overall	Total heat input to hybrid plant [MW]	434.3	364.1
	Thermal solar share [%]	9.5	11.3
	Thermal efficiency [%]	34.0	34.2

The thermal solar share is greater, as the load of the steam boiler is decreased, and the thermal power of the solar field is kept constant. As concluded in the cases 1 and 2, higher thermal solar share possibly indicates higher efficiency. Thus, in case 3 the thermal efficiency is greater than in case 1, even though normally the efficiency is lower as the steam boiler load is decreased. This is possibly due to the fact that load of the turbines is relatively higher than the load of the steam boiler, as the solar steam is added to the joint turbine.

In case 3, the steam boiler could be operated on 79.4% partial load, in which the steam temperatures of 550 °C are still reachable. Thus, the steam boiler of power boost hybrid can be operated between 96.6% and 79.4% load without overloading the turbines and decreasing the live steam and reheated steam temperatures of steam boiler, as the thermal power of solar field is 41.3 $MW_{th.}$ This is due to the sizing and capacities of the heat transfer surfaces. However, without solar field the steam boiler could be operated on 70% partial load, in which the steam temperatures are still reachable. On the other hand, in case 2 the steam boiler could be operated only on 80.9% load, if the turbines are not overloaded or the steam temperatures are not decreased. Thus, larger solar field decreases the possibility of the hybrid plant to be operated as load following power plant if the steam temperatures are kept constant for live steam and reheated steam of the steam boiler and the turbines are not overloaded.

4.1.3 Comparison of power boost mode and fuel saving mode

The power boost mode causes additional losses in the main steam valve of steam boiler before HP turbine, as the steam boiler is operated on 100% load without the solar field or on partial load. The throttling losses are smaller if the hybrid plant is designed to be only a fuel saving hybrid, in which the load of the turbines are not increased 10% like in power boost mode. Thus, a comparison of power boost mode and the fuel saving mode is conducted in order to observe the difference between these two modes (Table 25). In both modes, the amount of solar steam is fed to the joint steam cycle, in which the design value of 550 °C are reached for live steam and reheated steam of the steam boiler.

Table 25. *Steady state results from the operation condition of HP turbine in power boost mode and fuel saving mode.*

Steam cycle and operation mode	**Power boost**	**Fuel saving**
Steam temperature after outlet throttle of solar field [°C]	542.4	542.5
Steam pressure after outlet throttle of solar field [bar]	141.8	141.9
Steam temperature at connection point before HP turbine [°C]	546.9	547.4
Steam pressure at connection point before HP turbine [bar]	141.8	141.8
Overall steam mass flow to HP turbine [kg/s]	124.3	112.7
Steam mass flow from solar field [kg/s]	31.4	21.0
Steam mass flow from steam drum [kg/s]	92.8	91.7
Superheater spray water mass flow of steam boiler [kg/s]	0.1	0.0

In fuel saving mode, the steam temperatures after the outlet throttle of the solar field and at connection point before HP turbine are greater than in power boost mode. This is due to smaller throttling losses in fuel saving cycle than in power boost cycle. However, the steam pressures at the connection point before HP turbine are the same for power boost and fuel saving modes and cycles. On the other hand, the overall steam mass flow to HP turbine is smaller in fuel saving than in power boost, as the power output of the turbines is kept at its nominal value of 134.2 MW in fuel saving mode, whereas the power output of the turbines is 147.6 MW in power boost mode (Table 26).

Table 26. *Steady state results from the comparison of the overall operation in power boost mode and in fuel saving mode.*

Component		Power boost	Fuel saving
Solar field	Number of collector rows	15	10
	Thermal power of solar field [MW_{th}]	88.5	59.0
Turbines	Power output of the turbines [MW]	147.6	134.2
	Turbine load [%]	110.0	100.0
Steam boiler	Steam boiler load [%]	80.7	79.6
	Fuel power [MW]	328.5	323.6
	Fuel supply [kg/s]	23.9	23.6
Overall	Total heat input to hybrid plant [MW]	417.0	382.6
	Thermal solar share [%]	21.2	15.4
	Thermal efficiency [%]	35.4	35.1

If the live steam and reheated steam temperatures are reached and the hybrid system is operated on power boost mode, the solar field can consists of 15 collector rows. On the other hand, if the live steam and reheated steam temperatures of steam boiler are reached and the hybrid plant is operated only on fuel saving mode, the solar field can consist of 10 collector rows. Thus, the solar field can be 33% larger if the hybrid is operated on power boost mode instead of applying only fuel saving mode. For that reason, the thermal solar share is higher if the hybrid is operated on power boost mode than only on fuel saving mode. However, the decrease of the load of the steam boiler is almost the same as well as the increase of thermal efficiency is almost the same in both cases.

4.2 Transient simulations

One hybrid configuration is simulated under transient conditions in order to observe the dynamic behaviour of the joint steam cycle under fluctuating solar irradiation conditions and to demonstrate the operation of the applied control strategy. Two different step changes are conducted to a steady state situation, in which the hybrid operates on peak load of the turbines with peak load of solar field. The fuel supply of the steam boiler is kept constant, as the hybrid is operated only on power boost mode. Thus, the fuel supply of the steam boiler is not used in order to compensate fluctuations, as the boiler is operated on 100% load.

The first step change is a 10% decrease from the peak effective DNI level on collectors (Chapter 4.2.1) and the second is a 50% decrease from the peak effective DNI level on collectors (Chapter 4.2.2). Primarily, the steam mass flow from the solar field is expected to decrease, as the DNI level is decreased. Secondarily, the step changes are ex-

pected to affect also to the outlet steam pressure and temperature of the solar field, especially in the case of larger step change.

4.2.1 Small change of DNI level

Small change of DNI level is conducted by a 10% step change on the effective DNI level collected on the surface of absorber tube. The 10% step change can be considered as small change of DNI, since the effective DNI on collectors can vary between 0% and 100%. Thus, the DNI level is decreased from 886.31 W/m^2 to 797.67 W/m^2 after the hybrid is simulated for 4 minutes at steady state. Immediately after the step change, the steam generation at the solar field starts to decrease (Figure 61). It decreases from 11.0 kg/s to 9.8 kg/s within the next four minutes after the step change. Thus, the steam generation is decreased by 1.2 kg/s, which is 10.9% of the steam mass flow before the step change.

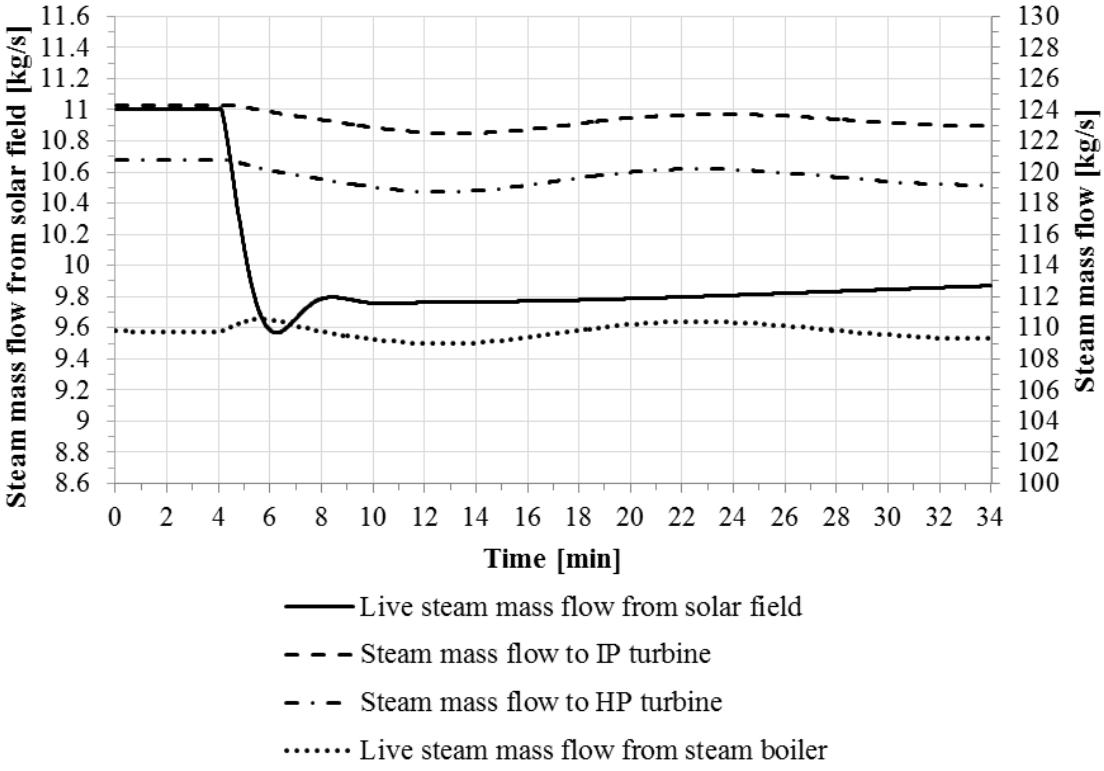

Figure 61. *-10% step change and transients of steam mass flows.*

As less steam is generated at the solar field, the steam mass flows to HP turbine and IP turbine are decreased as well. The steam mass flow to HP turbine is decreased by 2 kg/s from 121 kg/s to 119 kg/s within 8 minutes after the step change. In addition, the steam mass flow to IP turbine is decreased by 1.7 kg/s from 124.2 kg/s to 122.5 kg/s within 9 minutes after the step change. Thus, the steam mass flows to HP and IP turbines are decreased more than the steam mass flow from solar field. This is due to the operation of the steam drum, as its steam generation is affected due to pressure variations.

Due to the pressure variations, the steam mass flow from the steam drum first increases, as less steam is generated at solar field. This is due to the pressure decrease at the inlet of the HP turbine (Figure 62), as the steam mass flow through HP turbine is decreased. The pressure decrease at the inlet of HP turbine decreases also the pressure at steam drum. As the pressure decreases at the steam drum, energy is released from the steam drum and steam generation is slightly increased for short time period. However, the variations of the steam pressure affects to the operation of the steam drum, and the steam mass flow from steam drum starts to fluctuate. The outlet pressure of solar field is slightly decreased after the disturbance of DNI level, but it stabilizes quickly after the step change due to the main steam valve at the outlet of solar field, which keeps the live steam pressure of solar field constant.

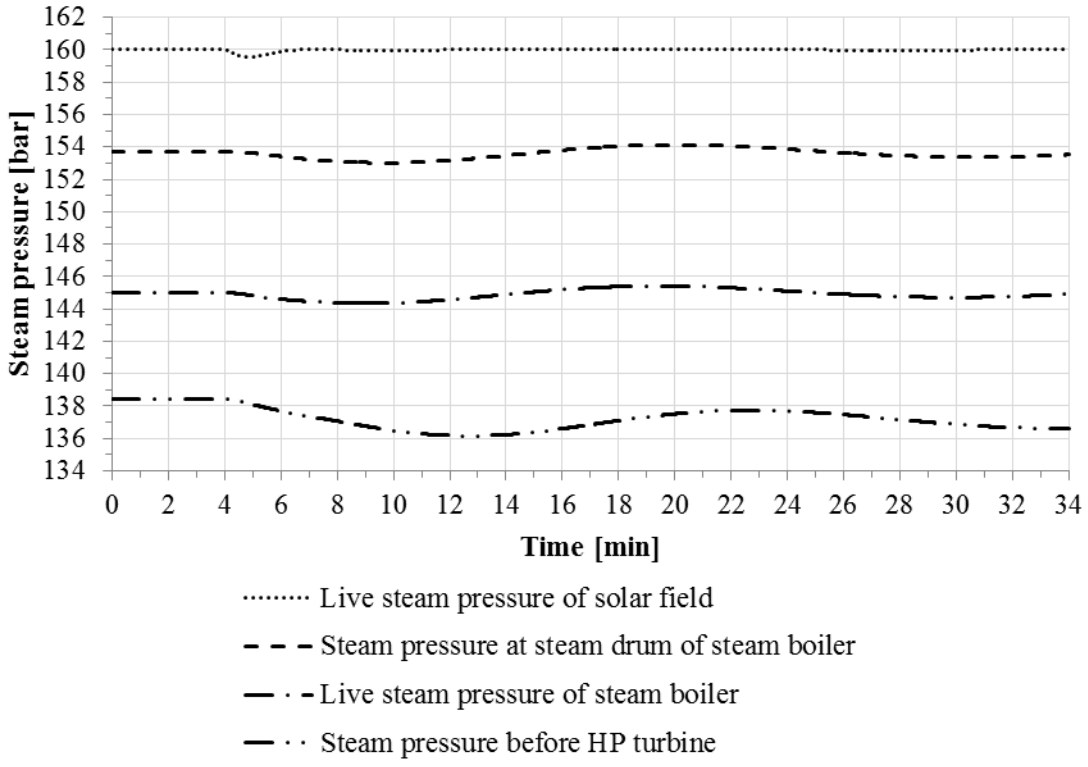

Figure 62. *-10% step change and transients of steam pressures.*

As the steam generation of solar field is decreased, the power output of the turbines is decreased. Furthermore, as the steam generation from steam drum starts to fluctuate, the power output of the turbines fluctuates as well (Figure 63). After the step change, the power output of the turbines is decreased from 147.5 MW to 145.3 MW within 8 minutes. Thus, the change of the load of the turbines is 0.18%/min, which can be compensated with the steam boiler if the steam boiler is used to compensate the fluctuations.

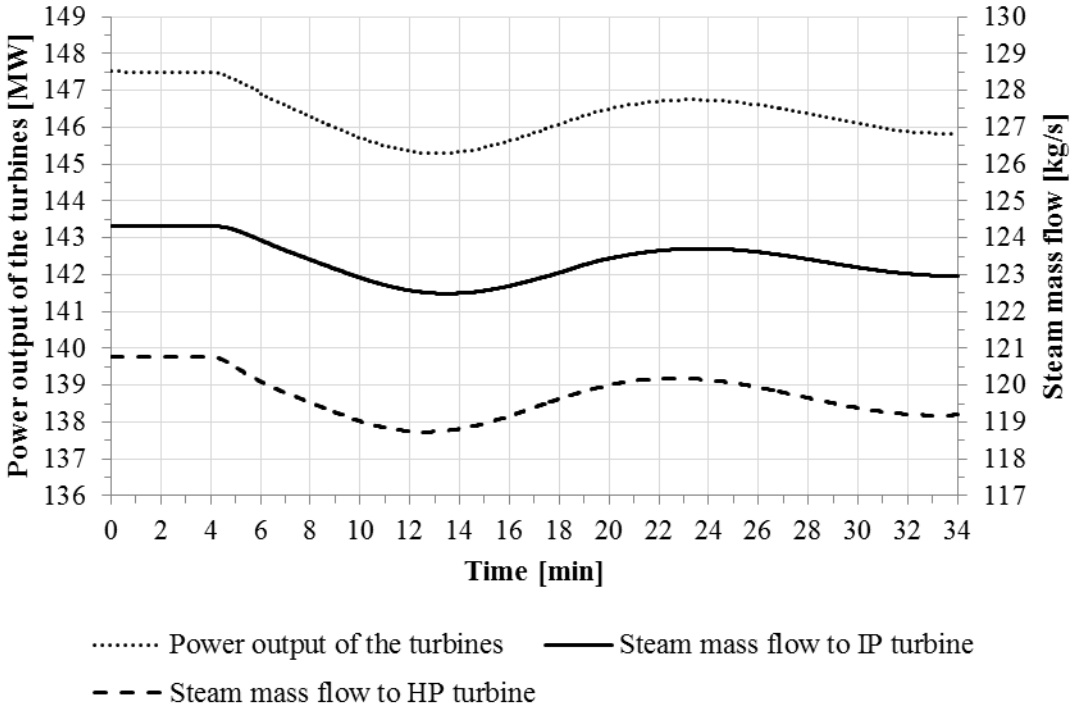

Figure 63. *-10% step change and transients in the steam mass flows to turbines and the power output of the turbines.*

In addition to steam mass flows, steam pressures and the power output of the turbines, the outlet steam temperature of the solar field is also affected right after the step change in the DNI level (Figure 64). The outlet steam temperature of solar field is decreased from 550 °C to 546.5 °C within a minute after the step change. Thus, the outlet steam temperature of solar field is decreased by 3.5 K. After the temperature drop the outlet steam temperature of solar field overshoots by 2.5 K before it stabilizes to its initial value of 550 °C.

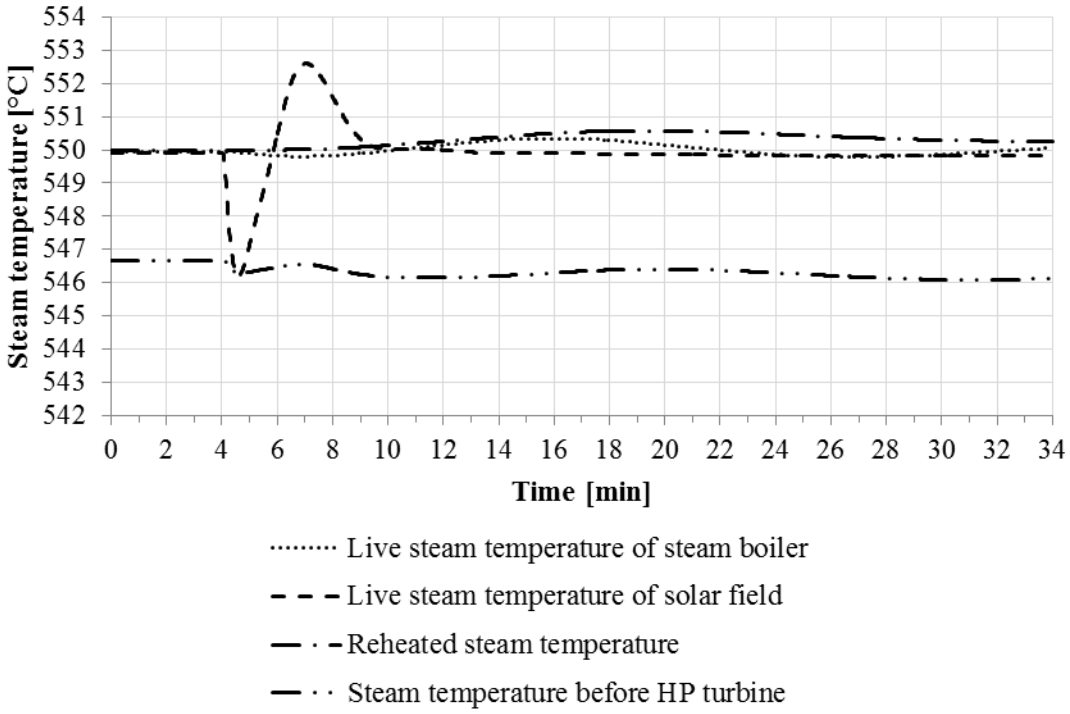

Figure 64. *-10% step change and transients in steam temperatures.*

Despite of the outlet steam temperature variations of the solar field, the impacts are small to the live steam temperature of steam boiler, the reheated steam temperature and the steam temperature before HP turbine due to small share of solar field. The live steam temperature and reheated steam temperature are slightly increased from 550 °C, as steam mass flow through reheater section is decreased. Thus, more heat is available in order to achieve the live steam and reheated steam temperatures of 550 °C in the steam boiler. In addition, the decrease of the steam temperature before HP turbine is less than 1 K/min after the step change in the DNI level, which is acceptable for the turbines.

4.2.2 Larger change of DNI level

Larger change of DNI level is conducted by a -50% step change on the effective DNI level collected on the surface of absorber tube. This is considered as medium sized change of DNI level. Thus, the effective DNI level is decreased from 886.31 W/m^2 to 443.15 W/m^2 after the hybrid is simulated for 4 minutes on steady state. Immediately after the step change, steam generation at the solar starts to decrease (Figure 65). It decreases from 11.0 kg/s to 4.9 kg/s within the next four minutes after the step change. Thus, the steam generation of solar field is decreased by 6.1 kg/s, which is approximately 55% of the steam generation before step change.

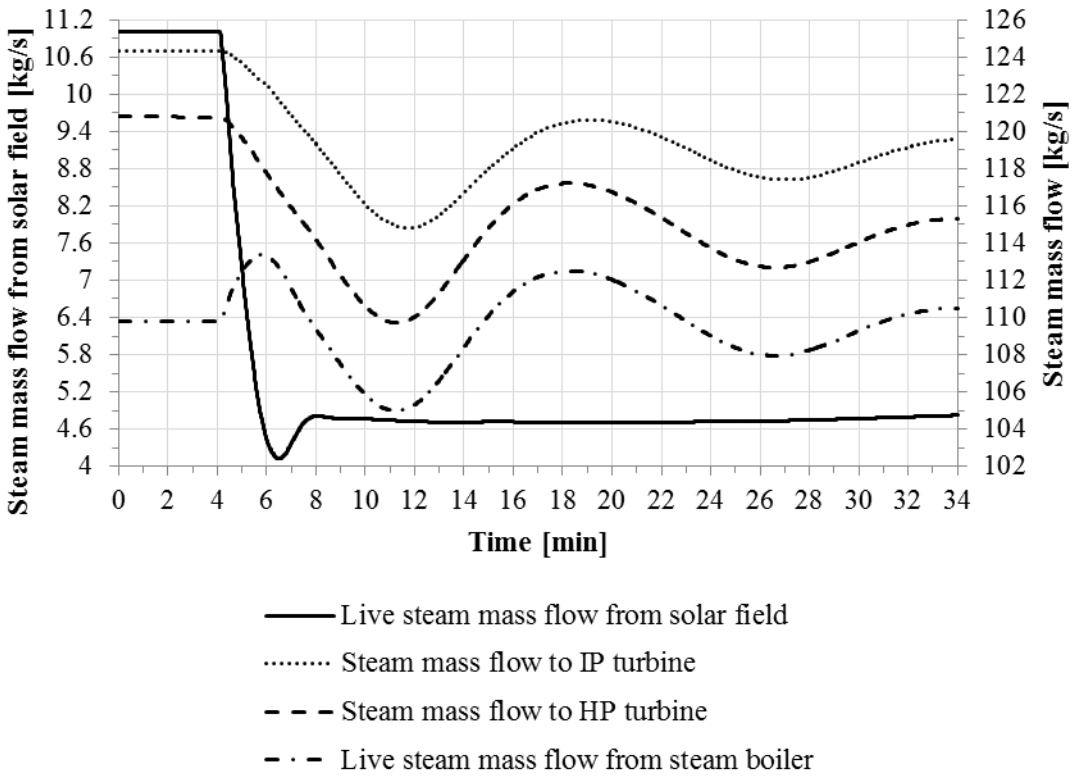

Figure 65. *-50% step change and transients of steam mass flows.*

As less steam is generated in the solar field, the steam mass flows to HP turbine and IP turbine are decreased as well. The steam mass flow to HP turbine is decreased 11.5 kg/s within 7 minutes, and the steam mass flow to IP turbine is decreased approximately 9.2 kg/s within 8 minutes after the step change. Thus, the steam mass flows to HP and IP turbines are decreased more than the steam generation from solar field, as the steam generation in the steam drum of the steam boiler is also affected like in the case of small change of DNI level.

Due to a larger step change, the steam generation at the steam boiler is more effected. The steam mass flow from steam boiler is increased more with larger step change than smaller step change. This is due to the larger pressure decrease at the inlet of the HP turbine, and the steam pressure at steam drum is more affected (Figure 66). The steam pressure before HP turbine decreases approximately 12 bar within 7 minutes after the step change, whereas with the smaller change it decreases 2 bar within 9 minutes after the step change. The outlet pressure of solar field is also more decreased with larger step change but it stabilizes quickly after the step change like in the case of small change in the DNI level.

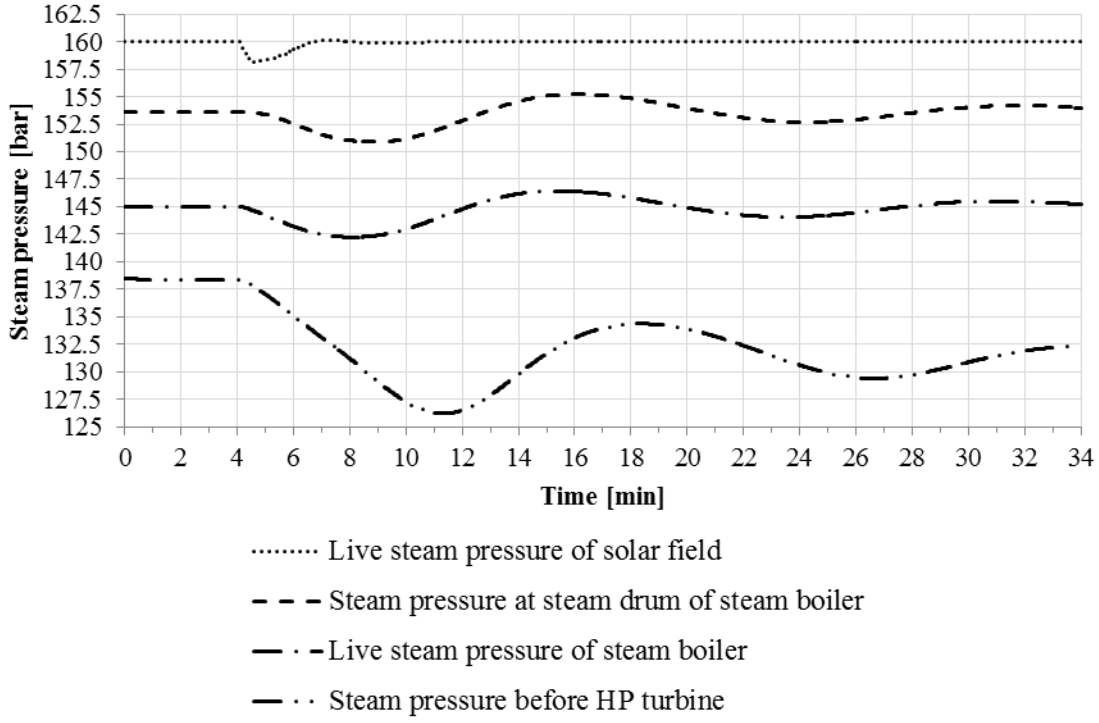

Figure 66. *-50% step change and transients of steam pressures.*

As the steam mass flow transients are greater, the steam pressure transients are greater, and the changes in the power output of the turbines are greater (Figure 67). The power output of the turbines is decreased from 147.5 MW to 136 MW within 8 minutes after the step change. Thus, the load of the turbines is changed approximately 1 %/min. However, the steam boiler is capable of compensating the power output gradient of 1 %/min, as the steam boilers are capable of changing the load 1 %/min regardless of the control strategy of the steam boiler, as described in Chapter 2.2.4. Like in the case of small change of DNI level, the power output of the turbines starts to fluctuate, as the steam mass flows to HP and IP turbines starts to fluctuate due to the pressure and steam mass flow gradients and the operation of the steam drum.

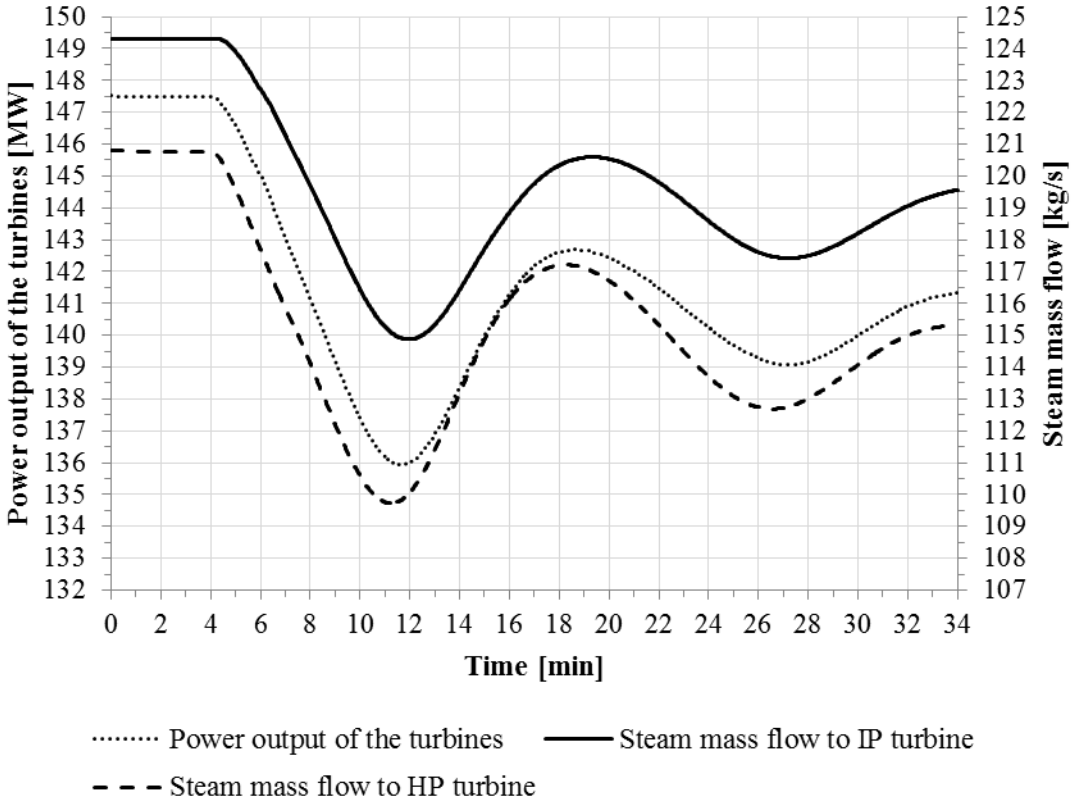

Figure 67. *-50% step change and transients in the steam mass flows to turbines and in the power output of the turbines.*

In addition to steam mass flows, steam pressures and the power output of the turbines, the outlet steam temperature of the solar field is also affected right after the step change in DNI level (Figure 68). With a larger step change the outlet steam temperature of solar field is more affected, as it is decreased from 550 °C to 521 °C within 2 minutes after the step change. Thus, the outlet steam temperature of solar field is decreased by 29 K compared to the decrease of 3.5 K in the smaller DNI step change. Thus, the steam temperature gradient at the outlet of the solar field is approximately 14 K/min. After the temperature drop, the outlet steam temperature of solar field overshoots by 4 K before it stabilizes to its initial value of 550 °C. On the other hand, in the case of small change of DNI level the outlet steam temperature overshoots by 2.5 K. Thus, the temperature overshoots slightly more with larger step change than with smaller step change.

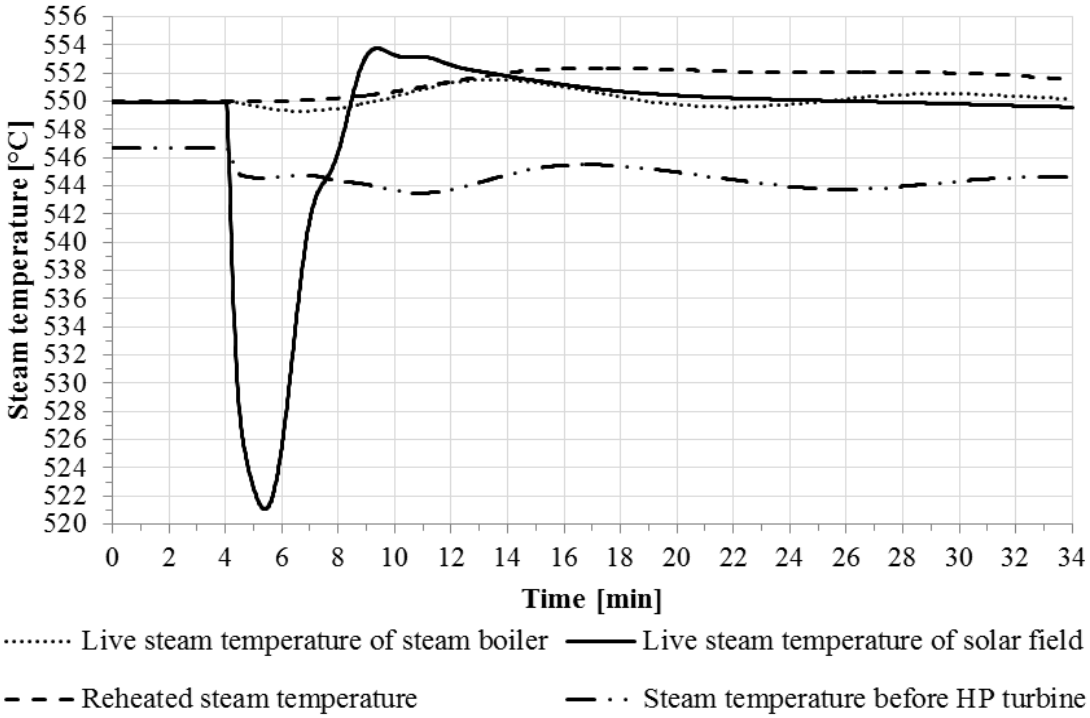

Figure 68. *-50% step change and transients of steam temperatures.*

Despite of the larger variation of the outlet steam temperature in the solar field, the impacts are still small to the live steam temperature of steam boiler, the reheated steam temperature and the steam temperature before HP turbine. The live steam temperature and reheated steam temperature are slightly increased, as steam mass flow through reheater section is decreased. In addition, the decrease of the steam temperature before HP turbine is approximately 2.5 K/min after the step change in the DNI level. The temperature gradient of 2.5K/min is still acceptable for turbines, as 5 K/min is the rule of thumb for acceptable temperature gradients in turbines. However, the temperature gradient at the outlet of the solar field is 14 K/min, and the acceptable temperature gradients at the outlet of the solar field should also be considered.

5. DISCUSSION AND ANALYSIS

The conducted simulation cases provide a lot of information about the behaviour of the hybrid system under different loads of solar field and steam boiler as well as under fluctuating solar irradiation conditions. As the steam from the solar field is fed into the joint steam cycle, it changes the thermal balance of the joint steam cycle. In other words, as the steam mass flow, steam temperature or steam pressure is changed at one point of the steam cycle, it affects to the operation of the rest of the steam cycle. The change of steam pressure and temperature are related to the changed steam mass flow, which causes, for example, increase of the steam pressure before turbine and changes in the spray water mass flows. In this chapter, the main results of the simulations are discussed and analysed. The five main results from the simulation cases are increased thermal efficiency, reduction of greenhouse gas emissions, attainable solar shares, impacts of the increased steam mass flows through reheaters and turbines in power boost mode, and main transients within the joint steam cycle during fluctuating solar irradiation conditions. As a conclusion of the discussion and analysis, the main challenges and future development requirements of the hybrid system are defined at the end of this chapter.

For a conclusion of the steady state simulations, the main results from the overall operation of the hybrid system are presented from the four different steady state cases (Table 27). The results include the thermal power of solar field, power output of the turbines, turbine load, steam boiler load, fuel power and supply, decrease of fuel combustion, total heat input to the hybrid plant, thermal solar share and thermal efficiency in each case.

Table 27. *Results from the overall operation of hybrid system in the four steady state cases.*

Steady state case	**1**	**2**	**3**	**4**
Applied operation mode, steam cycle and strategy	Power boost	Power boost and attainable solar share	Power boost and attaina-ble load range	Fuel saving and attaina-ble solar share
Number of collector rows in the solar field	7	15	7	10
Thermal power of solar field [MW_{th}]	41.3	88.5	41.3	59.0
Power output of the turbines [MW]	147.6	147.6	124.6	134.2
Turbine load [%]	110.0	110.0	92.9	100.0
Steam boiler load [%]	96.6	79.4	80.9	79.6
Fuel power [MW]	392.9	328.8	364.1	323.6
Fuel supply [kg/s]	28.4	23.9	23.5	23.6
Decrease of fuel combustion [%]	4.1	19.3	20.6	19.8
Total heat input to hybrid plant (MW)	434.3	417.3	364.1	382.6
Thermal solar share [%]	9.5	21.2	11.3	15.4
Thermal efficiency [%]	34.0	35.4	34.2	35.1

The first main result is the increased thermal efficiency of the hybrid system, which results that less heat input is needed in order to produce same amount of electricity. As the thermal solar share is approximately 10%, the thermal efficiency is increased by 1.0%-point. In addition, the higher the thermal solar share is, the higher the thermal efficiency of the plant is even though the load of the steam boiler is decreased. The increase of efficiency and the calculation of the efficiency in hybrid systems are already discussed in the previous studies, like Hu et al. (2010), Popov et al. (2011) and Suresh et al. (2010). However, the efficiency of the hybrid system is calculated differently in Hu et al. (2010), Popov et al. (2011) and Suresh et al. (2010). Hu et al. (2010) calculates the efficiency by using mechanical power output of turbines and thermal powers of solar field and steam boiler (Hu et al. 2010, p.2882), whereas Suresh et al. (2010) applies the electric power and fuel powers of solar field and steam boiler (Suresh et al. 2010, p.270). On the other hand, Popov et al. (2011) applies the almost the same method than this thesis, in which the mechanical power of the turbines is divided by total heat input, which is a sum of fuel power and solar thermal power. However, Popov et al. (2011) uses the net electric power output of the plant, which includes the generator efficiency and reactive power (Popov et al. 2011, p.348). Thus, the method to calculate the efficiency of hybrid plant is not standardized, and it is difficult to compare the results achieved in this thesis to the results in the literature. Furthermore, the reasons for the

increased thermal efficiency are not thoroughly discussed in the literature. In this thesis, it is discussed, that the thermal efficiency is possibly increased due to:

- Lower load of steam boiler compared to higher load of turbines due to steam generation in solar field. The lower load of steam boiler decreases the exergy losses of boiler and HP FWHs (Gupta et al. 2009, p.597).
- Higher load of turbines in power boost mode lowers throttling losses and increases steam parameters before turbine.
- Higher isentropic efficiency of HP turbine compared to other turbines, as the steam mass flow through HP turbine is increased relatively more through the HP turbine than the other turbine sections.

In order to define the exact reasons for increased efficiency, an exergy analysis could be conducted in order to locate and quantify the irreversibilities within the hybrid system (Gupta et al. 2015, p.568). However, the exergy of process depends on its potential difference with its environment. Thus, exergy analysis requires the definition of the site specific process restrictions and requirements. (Hu et al. 2010, p.2884) In addition, the increased efficiency should be evaluated against the increased complexity of the hybrid system, as the operation with higher solar shares requires more sophisticated control system, and the complexity of technical solutions is different for different process arrangements. Furthermore, the increased efficiency should be considered in the design phase of the hybrid, as it effects to the size of solar field required for certain electricity production especially with higher solar shares. As exergy analysis is conducted, an economic analysis should also be conducted, as the hybrid systems are proven to be technically feasible, but their economic feasibility has not been widely studied (Gupta et al. 2015, p.579).

The second main result is lower greenhouse gas emission levels, as the steam boiler combusts less fuel due to higher thermal solar share and higher thermal efficiency. However, the modelled thermal solar shares are not enough in order to achieve the objectives of CO_2 reductions, as the fuel combustion is decreased less than 20% with peak load of solar field in cases 2 and 4 compared to the annual 33% objective of CO_2 emission level reductions (Figure 5). As the solar field is operated on peak load for short period of the annual production, the annual CO_2 reductions are even less than 20%. Thus, the annual operation time of solar field as well as the average annual thermal solar share should be investigated in order to observe the annual reductions on the fuel consumption and CO_2 emission levels. In addition, the possibilities to reach higher solar shares should be investigated in order to reach lower greenhouse gas emission levels. This includes, for example, investigation of different process arrangements for CSP hybrids, as only one process arrangement is analysed in this thesis. In addition, the attainable solar share may not be enough compared to the required greenhouse gas emission level reductions due to multiple process requirements and restrictions. Therefore, it

may be required to combine the CSP with another method, such as combustion of biomass, in order to achieve the required CO_2 emission reductions.

The third main result is related to the attainable solar shares in hybrid systems. Based on simulations, if the hybrid is operated on power boost mode, the attainable solar share is higher than operating only on fuel saving mode, if the design live steam and reheated steam temperatures of steam boiler are still reached in both modes. The attainable solar share on power boost hybrid is 21.2%, whereas the attainable solar share of only fuel saving hybrid is 15.4% on nominal conditions (Table 27). The difference between the attainable solar shares is possibly due to the increased power output of the turbines in power boost mode, as the only difference of the two modes and models in this thesis is the sizing of the turbines. In power boost mode and model, the turbines are resized in order to allow 10% increase of electricity production without increase of live steam pressure. As the attainable solar shares of 15.4% and 21.2% are achieved in hybrid, the load of the steam boiler cannot be changed without decreasing the steam temperatures of steam boiler or increasing the load of the turbines. However, turbines are capable of operating with lower steam temperatures than design values as long as the steam is superheated, for example, by 50 K. Lower temperature of steam would decrease the efficiency of turbines and increase the moisture content of the expanded steam. However, in this thesis it is discussed that higher solar share increases the efficiency of the hybrid system. Thus, the lower efficiency of turbines could be possibly compensated by increased efficiency of the overall system, as the solar share is increased. Therefore, the operation of the hybrid system should be investigated with higher solar shares even though the steam temperatures would be decreased from their design values. In addition to minimum superheating of steam, other limiting factors for maximum solar share can be, for example, moisture content of the expanded steam, dew point of flue gases, maximum amount of spray water and maximum load of turbines. In addition to attainable solar shares, there are multiple other details, which should be considered as the hybrid system is designed. The details are:

- Operation of the hybrid system without solar field, as throttling losses are greater in power boost mode than in fuel saving mode due to dimensioning of the turbines. This results in lower thermal efficiency in power boost mode than in fuel saving mode without solar field.
- Need of peak electricity production, which is related to power boost mode and to the local electricity consumption curve.
- Age of the hybrid plant, as new hybrid plants are recommended to be operated on power boost mode.
- Expenses of the fuel, as fuel saving mode reduces the amount of combusted fuel.
- Possibility of the hybrid system to be operated as load following power plant, as larger solar field decreases the load range, in which hybrid system could be operated.

The fourth main result is related to power boost mode, increased steam mass flows through turbines and reheaters and to the combination of the two steam lines before HP turbine. In power boost mode, the mass flows through HP turbine, reheaters and rest of the steam cycle up to the deaerator are increased from the nominal values, as the feedwater for solar field is extracted after the deaerator. Due to increased steam mass flow, the steam pressures at the inlet of the HP turbine and in the rest of the steam cycle up to the deaerator are increased. Thus, the turbines and main steam valves are dimensioned in order to allow power boost mode without increasing the live steam pressures of steam boiler and solar field. However, as the turbines are re-dimensioned for increased steam mass flow, the throttling losses of main steam valve of steam boiler are greater without solar field and partial load of the boiler. In addition, as the solar field produces steam with higher pressure than in the connection point, throttling losses occur also in the main steam valve of solar field.

In order to avoid unnecessary throttling losses, the steam parameters of steam boiler and solar field should be designed close to each other and the connection of the steam lines before HP turbine should be investigated more thoroughly. However, temperature and pressure losses occur in the connection piping between the solar field and steam cycle, which should be considered in the design of the steam parameters of solar field. In addition, the actual technical solution for the connection of two steam lines before HP turbine should be investigated more thoroughly in order to determine its impact on steam parameters and throttling losses with different loads of steam boiler and solar field. Currently, the model applies two main steam valves: one for steam boiler and one for solar field, and the steam lines are connected after the valves. Thus, the turbine probably has to have an additional third valve before the turbine, if this kind of process arrangement is constructed. In addition, both applied main steam valves in the model are control valves. Therefore, the purpose of the steam valves should be investigated whether all valves are control valves or some are only check valves.

As the steam mass flow is increased through HP turbine, the steam mass flow is also increased through reheaters. This affects to the operation of the heat surfaces after reheaters, such as primary and tertiary superheater surfaces, economizer and air preheating. The latter heat surfaces are affected, as the increased steam mass flow through reheaters creates an imbalance between the heat surfaces. The imbalance is even greater with higher solar shares and partial load of the steam boiler. Thus, for example, the approach temperature difference between the economizer and steam drum is increased, as the thermal solar share is increased and load of the steam boiler is decreased (Table 28).

Table 28. *The effect of increased mass flow through reheaters in power boost mode.*

Case number	**Reference**	**1**	**2**
Thermal solar share [%]	0.0	9.5	21.2
Steam boiler load [%]	100.0	96.6	80.9
Approach temperature difference [K]	25.7	26.6	34.3
Change of superheater spray water mass flow [kg/s]	-	-1.4 (-21.5%)	-6.4 (-98.5%)
Change of reheating spray water mass flow [kg/s]	-	-2.6 (-26.8%)	-9.3 (-95.9%)
Change of steam mass flow from steam drum [kg/s]	-	-1.3 (-1.3%)	-9.9 (-9.6%)
Change of steam mass flow from HP turbine to reheaters [kg/s]	-	+11.8 (+11.2%)	+15.7 (+15.0%)
Change of steam mass flow to HP turbine [kg/s]	-	+12.0 (+11.0%)	+15.1 (+13.8%)
Change of steam mass flow to IP turbine [kg/s]	-	+9.2 (+8.0%)	+6.4 (+5.6%)

The increased steam mass flow through reheaters creates also an imbalance between different turbine sections especially with case 2, in which the steam mass flow through HP turbine is increased relatively more than through IP turbine (Table 28). This is due to the operation of reheaters, as the reheater spray water mass flow is especially decreased due to increased steam mass flow through reheaters and lower load of steam boiler. The imbalance between heat surfaces and turbine sections is discussed, as the advantages and disadvantages of different process arrangements are observed in Chapter 2.3.3. However, similar results cannot be found about the imbalances from the literature referred in this thesis. In addition, as the results are based on the Apros model, the operation of the model should be validated in order to validate also the simulation results even though the components and calculation of Apros are validated with several cases. Thus, the reasons as well as the impacts of the imbalance between different heat surfaces and turbine sections should be calculated and investigated more thoroughly in future work.

The increased steam mass flow through reheaters with larger solar shares sets challenges to the optimization of the heat surfaces in the steam boiler for different loads of steam boiler and solar field. Furthermore, even larger heat surfaces are needed with higher solar share and partial load of the steam boiler in order to achieve design values for live steam and reheated steam temperatures. The larger heat surfaces of superheaters and reheaters increase the approach temperature difference between the steam drum and economizer and decrease the final temperature of flue gases. However, the approach temperature difference should be kept close to 10K and the final temperature of flue gases should not be decreased under the dew point of flue gases. In addition, while operating without solar field, the larger heat surfaces increase the spray water mass flows.

However, the maximum amount of spray water is usually limited in order to reduce thermal shock on steam pipes and to ensure the full vaporization of the water droplets before HP turbine. Moreover, in NC boilers the ratio of different heat surfaces of steam boiler is fixed, whereas in OT boilers the ratio of different heat surfaces can be changed, as the end point of evaporation is changed according to the load of the steam boiler. Thus, the design and optimization of heat surfaces is different for NC and OT boilers, as the operation of heat surfaces is more flexible in OT boilers than in NC boilers. As a conclusion, the optimum design for the heat surfaces is a complex combination of different details, especially if a larger solar field is connected to the steam cycle. In future work, the optimization of heat surfaces should be investigated as well as the operation of the hybrid system should be investigated with different kinds of steam boilers.

The last main result is related to the transient situations, in which the main transients of solar field are steam mass flow gradients and temperature gradients, as the outlet steam pressure of solar field is kept close to its design value due to the control of the main steam valve. The steam mass flow is decreased directly proportional to the change of DNI level. Thus, 50% decrease of effective DNI level on collectors decreases the outlet steam mass flow from solar field approximately 50% within 4 minutes after the step change. Compared to Figure 18, the steam mass flow gradient of the model after the step change is more radical than in the Figure 18. This is possibly due to the different control of the model as well as the modelling of the entire solar field with multiplication coefficients. In Figure 18, the control method is modified sliding pressure control, whereas the model is operated on fixed pressure control method. Furthermore, as the entire solar field is modelled with multiplication coefficients, the mass flow through the actual dynamic process is related to only one collector row. The coefficients are now used in the solar field model in order to multiply the outlet steam mass flow and thermal power of one collector row. Thus, the thermal inertia of the dynamic process is also related to only one collector row instead of entire solar field. As a result, the change of steam mass flow from solar field might be less radical, as the entire solar field is modelled without multiplication coefficients and the thermal inertia of the process corresponds to entire solar field instead of one collector row. In addition to steam mass flow gradients, the outlet steam temperature of solar field is affected especially in the larger step change. As the effective DNI level is decreased -50%, the outlet steam temperature of solar field decreases 29 K within 2 minutes. Compared to Figure 19, the steam temperature gradient of the model after the step change is more radical than in Figure 19. This is possibly due to the design and dimensioning of the solar field model. By redimensioning the solar field, the spray water mass flows can be increased, and more buffer can be applied against steam temperature changes.

Despite of the fluctuations of steam mass flow and outlet steam temperature of the solar field, the load and temperature gradients of the -10% and -50% step changes are manageable by the steam boiler, as the hybrid plant is operated on power boost mode, in

which the power output of the turbines is increased by 10%. Thus, the largest modelled temperature gradient is 2.5K/min with -50% step change, which is acceptable for turbines, as the rule of thumb is 5K/min. Furthermore, the largest modelled power output gradient of the turbines is 1%/min, which can be controlled with the steam boiler (Figure 30) if a sophisticated and coordinative control system is applied to the hybrid system and the steam boiler is used to compensate the fluctuations. In order to apply steam boiler to compensate the fluctuations, control engineering of the hybrid system should be improved. For example, feed forward control loop has to be implemented between the fuel supply and steam generation of steam boiler, since it would speed up the control by measuring the change of steam mass flow, which indicates the change of live steam pressure (Joronen et al. 2007, p.158). In addition, the control loops of fuel and air supply in the steam boiler should be done as parallel loops, since it would assure adequate air supply during large load changes (Joronen et al. 2007, p.159). Furthermore, the already applied control loops needs to be more carefully tuned. Moreover, feedforward control loops between the solar field, steam boiler and joint turbine should be developed in order to add predictability to the hybrid system. Therefore, one feed forward control loop can be possibly implemented between the effective DNI on collectors and main controller of the steam boiler. As a conclusion, the control engineering in the hybrid system should be developed in order to use actual fluctuating DNI data for the simulation of the transient situations and simulate the start-ups and shutdowns of the hybrid system. Thus, the transient situations can be observed more realistic than with step changes. Furthermore, the transients affecting only to a part of the solar field should be researched, since the evaporator section defines the amount of produced steam mass flow, whereas the superheating section defines the outlet steam temperature of the solar field.

A challenge during transient situations is the steam mass flow gradients from solar field, which cause pressure gradients within the joint steam cycle. The operation of steam drum is sensitive to pressure variations, as pressure decrease releases energy from the steam drum and vice versa. As a result, a challenge with steam drum boilers is to keep the live steam pressure as close to the design value as possible while doing fast load changes, as the load of the solar field fluctuates. On the other hand, if the steam boiler is designed to be once-through boiler, the boiler is usually operated on modified sliding pressure mode. Thus, the steam boiler has to be capable of doing fast load changes, but the steam pressure can vary according to the load of the turbines. Another problem with the steam boiler is the heat stress on components during fluctuating solar irradiation conditions. The heat stress reduces the lifetime of components, such as superheaters and reheaters. In addition, the transient simulations are conducted with a power boost hybrid, in which solar steam increases the power output of the turbines by 10%. Thus, the transients within the joint steam cycle are going to be greater with larger solar share, as the steam mass flow from solar field is increased and the steam mass flow from steam boiler is decreased. Furthermore, the transient simulations of this thesis are rough esti-

mations of the fluctuations of DNI level and its impacts on the hybrid system, as the conducted transients are step changes instead of actual fluctuating DNI, the effective DNI on collectors is decreased only -50%, and the fuel supply of the steam boiler is not used in order to compensate the fluctuations. As a conclusion, larger DNI variations combined with larger solar share can be a limiting factor to the maximum solar share due to pressure gradients, load gradients and durability of heat surfaces. Thus, more detailed information of the durability of steam boilers and turbines need to be obtained from the manufacturers in order to research the impacts within the joint steam cycle during larger transients as well as during the start-ups and shutdowns of the solar field.

As a conclusion, the main challenges and future development requirements are gathered from the previous discussions. There are at least five main challenges in the hybrid system based on the theory and simulation results in this thesis:

- Attainable solar shares compared to the operation of the hybrid system and required greenhouse gas emission reductions.
- Design of the steam parameters in solar field and in steam boiler and combination of the two steam lines before HP turbine.
- Imbalance between heat surfaces and turbine sections.
- Optimization of heat surfaces in steam boiler for different loads of solar field and steam boiler.
- Operation of steam boiler under fluctuating solar irradiation conditions with larger solar shares.

In addition, there are at least five development requirements based on the simulation results as well as on the challenges of the hybrid system:

- Research of the optimal hybrid system for the local conditions in terms of different operation modes, different process arrangements, different steam boilers with different control strategies, optimization of heat surfaces and year-round operation.
- Possibilities to reach higher solar share should be investigated in terms of lower greenhouse gas emission levels, efficiency of the hybrid plant, optimization of heat surfaces and transient simulations.
- Design and dimensioning of the solar field model should be improved, and the entire solar field should be modelled without using multiplication coefficients in order to investigate its impacts to the transients of the solar field.
- Control engineering of the hybrid system should be improved in order to simulate transient situations with higher solar shares using actual measured DNI as well as the start-ups and shutdowns of the hybrid plant.
- An exergy and economic analysis should be conducted to hybrid system in order to find reasons for increased efficiency and investigate economic feasibility of the hybrid system.

6. CONCLUSIONS

This Master thesis "Development of concentrated solar power and conventional power plant hybrids" is conducted as part of the studies in the Master's Degree Programme of Environmental and Energy Engineering at Tampere University of technology. The research of the thesis is conducted from June 2015 to December 2015 for VTT Technical Research Centre of Finland, and the thesis can be seen as continuation for the research of concentrated solar power technology, which is quite new research area at VTT. The main objectives of the thesis are to research the state-of-the-art technologies in CSP and in conventional steam power plants, to comprehensively study the different process arrangements for the hybrid systems, to work out one hybrid configuration for Apros simulations, to develop control mechanism for the hybrid plant, to demonstrate the operation of the hybrid system under typical boundary conditions and to find challenges, process requirements and restrictions within the hybrid system. One of the difficulties countered during the thesis is the lack of theoretical and operational data of CSP hybrids, as only a few are operational and the applied solar share is small. Thus, some new information about the operation of CSP hybrids is achieved in this thesis, as one hybrid system is dynamically modelled and simulated by using Apros software, which is a dynamic modelling and simulation tool for industrial processes.

The development of CSP and conventional power plant hybrids aims to generate dispatchable renewable energy while lowering the LCOE of CSP, the greenhouse gas emission levels and fuel consumption. In addition, the goal is to increase the solar share of the installed capacity, as it is typically below 10%. The integration of CSP and steam power plant can be readily achieved by applying a solar field with direct steam generation, as there is no need for additional heat transfer fluid and heat exchanger between the power plants. In addition, there is no need for energy storage equipment if the fuel supply of the steam boiler can be adjusted to compensate the intermittency of solar irradiation. However, the ease of the integration depends on the operation mode, the selected process arrangement, and the development of coordinative control system. Furthermore, there are numerous of other details to be considered, such as age of the host plant, fuel expenses, CO_2 emission level, and local consumption curve for electricity.

As a conclusion of the state-of-the-art technologies and different process arrangements, high steam temperatures up to 550 °C are achieved with current state-of-the-art line-focusing collectors with DSG, but high pressure up to 160 bar sets challenges for the durability of absorber tubes and joint between collectors. In steam power plants, the combustion process is improved and steam parameters are increased in order to reach higher efficiency and lower greenhouse gas emission levels and fuel consumption rates.

As the steam parameters of the state-of-the-art line-focusing collectors with DSG are close to the live steam parameters of subcritical conventional steam power plants, the solar field can either produce heated feedwater, saturated steam or superheated steam for the steam power plant. A total of seven process arrangements and their advantages and disadvantages are introduced in this thesis. The options are:

- Feedwater heating, in which solar field produces heated feedwater to the feedwater line of steam boiler.
- Feedwater heating, in which superheated steam from solar field is fed into bled off steam line.
- Superheated steam from solar field is fed into cold reheat line after HP turbine.
- Superheated steam from solar field is fed into the inlet of HP turbine.
- Superheated steam from solar field is fed into the inlet of IP turbine.
- Saturated steam from solar field is fed into boiler drum.
- Saturated steam from solar field is fed into boiler drum combined with feedwater heating.

Feedwater heating is the most researched and easiest to implement from the process arrangements. However, based on the conducted energy analysis, higher solar shares can be achieved with injection of solar steam into the cold reheating line of steam boiler or to joint turbine. Furthermore, if feedwater is extracted for the solar field after the condensate pump, the thermal solar share is greater than if feedwater is extracted after the deaerator or before economizer. In addition, these process arrangements promote more the development of affordable stand-alone CSP plants than the feedwater heating process arrangement. Thus, the technical solution of today would be feedwater heating, whereas it is more likely in the future to feed high temperature and high pressure solar steam to the joint steam cycle if it can be proven to be feasible. In this thesis, the selected process arrangement is the injection of solar steam to the joint HP turbine, since it applies full potential of the line-focusing solar fields with DSG, promotes the most of the development of affordable stand-alone CSP plants, and it can be seen as long-term goal for CSP hybrids. Despite of the process arrangement, the parameters of the heated feedwater or steam of solar field should match with the feedwater or steam parameters in the steam power plant. Furthermore, sophisticated control system has to be developed for the co-operation of solar field, steam boiler and turbines.

The selected hybrid configuration is modelled in Apros based on theory and previously developed models for solar field and conventional steam power plant. In addition, the hybrid model is simulated under several steady state and transient conditions. Based on the steady state simulations, thermal efficiency is increased, thermal balance within the steam boiler is changed and higher solar shares are achieved with power boost hybrid than fuel saving hybrid. The increased efficiency is possibly due to the higher load of turbines compared to lower load of steam boiler and higher isentropic efficiency of HP turbine compared to other turbines. Higher load of turbine decreases throttling losses,

whereas lower load of steam boiler decreases exergy losses in the boiler and FWHs. Furthermore, steam mass flow increases relatively more through HP turbine than other turbines, which increases the overall efficiency of the turbines, but creates imbalance between the turbines. Higher solar shares are achieved in power boost mode due to higher load of turbines. Based on the transient simulations, the largest modelled transients with -50% step change of effective DNI level are acceptable for steam boiler and turbines, as the hybrid system is operated on power boost mode, in which the load of the turbines is increased by 10%. The largest power output gradient of turbines is 1%/min whereas the largest modelled temperature gradient is 2.5K/min.

Based on the conducted research, the main challenges of the hybrid system are identified. These are attainable solar shares, design of the steam parameters and the combination of the two steam lines, imbalance between turbines and heat surfaces, optimization of heat surfaces, and operation of steam boiler under fluctuating solar irradiation conditions with larger solar shares. However, the simulation results only provide initial information about the challenges of hybrid system, which should be researched more comprehensively in the future. Furthermore, multiple process requirements and restrictions should be considered. These are operational limitations of FWHs, turbines and boiler as well as local conditions, such as available DNI level, climate, topography and restrictions of use of land and water. Based on the simulations, the operational limitations include minimum superheating of steam, moisture content of the expanded steam, dew point of flue gases, maximum amount of spray water, maximum load of turbines as well as steam temperature, steam pressure and power output gradients. As a conclusion, the hybrid system includes a lot of challenges, process requirements and restrictions, and the development of CSP hybrids requires expertise of different fields.

The developed and modelled CSP and conventional steam power plant hybrid seems to be technically feasible at least with smaller solar shares. In addition, the achieved results and the developed model provide viable information for the future development of CSP hybrids. Furthermore, Apros has proven to be a very capable tool in order to develop hybrid models and study their dynamic behaviour. However, the results of the thesis are strongly based on the Apros model, which validity and uncertainty should be thoroughly investigated in future work. The validation of the model is difficult, as there is little available information for the comparison of the achieved results even though the calculation and component modules of Apros have been validated with several cases. Moreover, multiple development requirements are also found for the hybrid, as the development of large power plant models is quite demanding and time-consuming work. These are research of optimal hybrid system and possibilities to reach higher solar shares, improvement of the control engineering, transient simulations with higher solar shares and exergy and economic analyses. Therefore, the work on the hybrid systems is suggested to be continued in the future, as the hybrid systems are one possible way in order to increase the share of renewable energy and prevent climate change.

REFERENCES

Alguacil, M., Prieto, C., Rodriguez, A. & Lohr, J. (2014). Direct steam generation in parabolic trough collectors, Energy Procedia, pp.21-29.

Apros Training Course Material. (2015). Apros Training Course, Espoo, May 4th – 6th 2015.

Barlev, D., Vidu, R. & Stroeve, P. (2011). Innovation in concentrated solar power, Solar Energy Materials and Solar Cells, Vol. 95(10), pp.2703-2725.

Basu, S. & Debnath, A.K. (2015). Power Plant Instrumentation and Control Handbook: A Guide to Thermal Power Plants, Academic Press, 937p.

Behar, O., Khellaf, A. & Mohammedi, K. (2013). A review of studies on central receiver solar thermal power plants, Renewable and Sustainable Energy Reviews, Vol. 23, pp.12-39.

Birnbaum, J., Feldhoff, Eck, M., Fichtner, M., Hirsch, T., Lehmann, D. & Zimmermann, G. (2010). A direct steam generation solar power plant with integrated thermal storage, Journal of Solar Energy Engineering, Vol. 132(3), p.1-9.

Birnbaum, J., Feldhoff, J.F., Fichtner, M., Hirsch, T., Jöcker, M., Pitz-Paal, R. & Zimmermann, G. (2011). Steam temperature stability in a direct steam generation solar power plant, Solar Energy, Vol. 85(4), pp.660-668.

Bugge, J., Kjær, S. & Blum, R. (2006). High-efficiency coal-fired power plants development and perspectives, Energy, Vol. 31(10–11), pp.1437-1445.

Eck, M., Zarza, E., Eickhoff, M., Rheinländer, J. & Valenzuela, L. (2003). Applied research concerning the direct steam generation in parabolic troughs, Solar Energy, Vol. 74(4), pp.341-351.

Eck, M. & Zarza, E. (2006). Saturated steam process with direct steam generating parabolic troughs, Solar Energy, Vol. 80(11), pp.1424-1433.

Eck, M. & Hirsch, T. (2007a). Dynamics and control of parabolic trough collector loops with direct steam generation, Solar Energy, Vol. 81(2), pp.268-279.

Eck, M., Schmidt, H., Eickhoff, M. & Hirsch, T. (2007b). Field Test of Water-Steam Separators for Direct Steam Generation in Parabolic Troughs, Journal of Solar Energy Engineering, Vol. 130(1), pp.1-9.

Farhad, S., Saffar-Avval, M. & Younessi-Sinaki, M. (2008) Efficient design of feedwater heaters network in steam power plants using pinch technology and exergy analysis, International Journal of Energy Research, Vol 8, pp.1-11.

Feldhoff, J.F., Benitez, D., Eck, M. & Riffelmann, K. (2010). Economic Potential of Solar Thermal Power Plants With Direct Steam Generation Compared With HTF Plants, Journal of Solar Energy Engineering, Vol. 132(4), pp.41001-41009.

Feldhoff, J.F., Schmitz, K., Eck, M., Schnatbaum-Laumann, L., Laing, D., Ortiz-Vives, F. & Schulte-Fischedick, J. (2012). Comparative system analysis of direct steam generation and synthetic oil parabolic trough power plants with integrated thermal storage, Solar Energy, Vol. 86(1), pp.520-530.

Feldhoff, J.F., Eickhoff, M., Keller, L., Alonso, J.L., Meyer-Grünefeldt, M., Valenzuela, L., Pernpeintner, J. & Hirsch, T. (2014). Status and First Results of the DUKE Project – Component Qualification of New Receivers and Collectors, Energy Procedia, Vol. 49(0), pp.1766-1776.

Fernández-García, A., Zarza, E., Valenzuela, L. & Pérez, M. (2010). Parabolic-trough solar collectors and their applications, Renewable and Sustainable Energy Reviews, Vol. 14(7), pp.1695-1721.

Franco, A. & Diaz, A.R. (2009). The future challenges for "clean coal technologies": Joining efficiency increase and pollutant emission control, Energy, Vol. 34(3), pp.348-354.

Giostri, A., Binotti, M., Silva, P., Macchi, E. & Manzolini, G. (2011). Comparison of two linear collectors in solar thermal plants: parabolic trough vs Fresnel, Proceedings of the ASME 2011 5th International Conference on Energy Sustainability, ES2011, August 7-10, Washington DC, USA.

Gupta, M.K. & Kaushik, S.C. (2009). Exergetic utilization of solar energy for feedwater preheating in a conventional thermal power plant, International Journal of Energy Research, Vol. 33, pp.593-604.

Gupta, M.K. & Kaushik, S.C. (2010). Exergy analysis and investigation for various feed water heaters of direct steam generation solar–thermal power plant, Renewable Energy, Vol. 35(6), pp.1228-1235.

Gupta, M.K., Kaushik, S.C., Ranjan, K.R., Panwar, N.L., Siva Reddy, V. & Tyagi, S.K. (2015). Thermodynamic performance evaluation of solar and other thermal power generation system: A review, Renewable and Sustainable Energy Reviews, Vol. 50, pp.567-582.

Hirsch, T. & Eck, M. (2006). Simulation of the start-up procedure of a parabolic trough collector field with direct solar steam generation, The Modellica Association, Modellica 2006 September 4^{th} – 5^{th}, pp.135-143.

Hirsch, T., Feldhoff, J.F., Hennecke, K. & Pitz-Paal, R. (2014). Advancements in the field of direct steam generation in linear solar concentrators-a review, Heat Transfer Engineering, Vol. 35(3), pp.258-271.

Hong-juan, H., Zhen-yue, Y., Yong-ping, Y., Si, C., Na, L. & Junjie, W. (2013). Performance evaluation of solar aided feedwater heating of coal-fired power generation (SAFHCPG) system under different operating conditions, Applied Energy, Vol. 112(0), pp.710-718.

Hu, E., Mills, D., Morrison, G. & Lievre, P. (2003). Solar power boosting of fossil fuelled power plants. Proceedings ISES, Goteborg 2003, pp.14-19.

Hu, E., Yang, Y., Nishimura, A., Yilmaz, F. & Kouzani, A. (2010). Solar thermal aided power generation, Applied Energy, Vol. 87(9), pp.2881-2885.

Huhtinen, M., Kettunen, A., Nurminen, P. & Pakkanen, H. (1994). Höyrykattilatekniikka, 2nd ed., Painatuskeskus Oy, Helsinki, s.315.

Joronen, T., Kovács, J. & Majanne, Y. (2007). Voimalaitosautomaatio, 2nd ed., Suomen Automaatioseura ry, Helsinki. s.263.

Kalogirou, S.A. (2014). Solar Energy Engineering - Processes and Systems, 2nd ed., Elsevier, p.762.

Kaushik, S.C., Siva Reddy, V. & Tyagi, S.K. (2011). Energy and exergy analyses of thermal power plants: A review, Renewable and Sustainable Energy Reviews, Vol 15 (4), pp.1857-1872.

Khenissi, A., Krüger, D., Hirsch, T. & Hennecke, K. (2015). Return of Experience on Transient Behaviour at the DSG Solar Thermal Power Plant in Kanchanaburi, Thailand, Energy Procedia, Vol. 69(0), pp.1603-1612.

Koornneff, J., Junginger, M. & Faaij, A. (2007). Development of fluidized bed combustion – An overview of trends, performance and cost, Progress in Energy and Combustion Science, Vol 33(0), pp.19-55.

Krüger, D., Krüger, J., Pandian, Y., O'Connell, B., Feldhoff, J.F., Karthikeyan, R., Hempel, S., Muniasamy, K., Hirsch, T., Eickhoff, M. & Hennecke, K. (2012). Experiences with Direct Steam Generation at the Kanchanaburi Solar Thermal Power Plant, SolarPACES 2012, Marrakesch, Marokko, 11^{th} – 14^{th} Sept. 2012, p.7.

Laing, D., Bahl, C., Bauer, T., Lehmann, D. & Steinmann, W. (2011). Thermal energy storage for direct steam generation, Solar Energy, Vol. 85(4), pp.627-633.

Lappalainen, J., Blom, H. & Juslin, K. (2012). Dynamic process simulation as an engineering tool – A case of analysing a coal plant evaporator, VGB Powertech, Vol. 92(1-2), pp. 62-68.

Lovegrove, K. & Stein, W. (2012). Concentrating solar power technology. Principles, developments and applications, Woodhead Publishing Limited, Cambridge, p.674.

Miller, B. (2011). Clean Coal Engineering Technology, 1st ed., Butterworth-Heinemann, USA, p.681.

Muñoz-Antón, J., Abbas, R., Martínez-Val, J. & Montes, M. (2014). Going further with Fresnel Receiver: New Design Window for Direct Steam Generation, Energy Procedia, Vol. 49(0), pp.184-192.

Parvareh, F., Milani, D., Sharma, M., Chiesa, M. & Abbas, A. (2015). Solar repowering of PCC-retrofitted power plants; solar thermal plant dynamic modelling and control strategies, Solar Energy, Vol. 119, pp.507-530.

Peng, S., Wang, Z., Hong, H., Xu, D. & Jin, H. (2014). Exergy evaluation of a typical 330 MW solar-hybrid coal-fired power plant in China, Energy Conversion and Management, Vol. 85, pp.848-855.

Peterseim, J.H., White, S., Tadros, A. & Hellwig, U. (2013). Concentrated solar power hybrid plants, which technologies are best suited for hybridisation?, Renewable Energy, Vol. 57(0), pp.520-532.

Peterseim, J.H., White, S., Tadros, A. & Hellwig, U. (2014). Concentrating solar power hybrid plants – Enabling cost effective synergies, Renewable Energy, Vol. 67(0), pp.178-185.

Petrov, M., Salómon, M. & Fransson, T. (2012). Solar Augmentation of Conventional steam plants: From system studies to reality, World Renewable Energy Forum, Denver, Colorado, USA, p.8.

Pierce, W., Gauché, P., von Backström, T., Brent, A.C. & Tadros, A. (2013). A comparison of solar aided power generation (SAPG) and stand-alone concentrating solar power (CSP): A South African case study, Applied Thermal Engineering, Vol. 61(2), pp.657-662.

Popov, D. (2011). An option for solar thermal repowering of fossil fuel fired power plants, Solar Energy, Vol. 85(2), pp.344-349.

Raiko, R., Tolvanen, H. & Pääkkönen A. (2014). Energiatalous, Luentomoniste, Tampereen teknillinen yliopisto, Kemian ja biotekniikan laitos, 149s.

Raiko, R. & Saarenpää, I. (2013). Höyrytekniikka, Luentomoniste, Tampereen teknillinen yliopisto, Voimalaitos ja polttotekniikan laitos, 254s.

Rayaprolu, K. (2009). Boiler for Power and Process, CRC Press, USA, p.694.

Ruspini, L.C., Marcel, C.P. & Clausse, A. (2014). Two-phase flow instabilities: A review, International Journal of Heat and Mass Transfer, Vol. 71, pp.521-548.

Schenk, H. & Eck, M. (2012). Yield analysis for parabolic trough solar thermal power plants – A basic approach, Deutsches Zentrum fûr Luft- und Raumfahrt, Germany, 82p.

Selig, M. & Mertins, M. (2010). From saturated to superheated direct solar steam generation – technical challenges and economical benefits, Novatec BioSol AG, Karlsruhe, 8p.

Sengupta, S., Datta, A. & Duttagupta, S. (2007). Exergy analysis of a coal-based 210 MW thermal power plant, International Journal of Energy Research, Vol. 31(1), pp.14-28.

Sharma, M., Parvareh, F. & Abbas, A. (2015). Highly integrated post-combustion carbon capture process in a coal-fired power plant with solar repowering, International Journal of Energy Research, Vol. 39(0) pp.1623-1635.

Siva Reddy, V., Kaushik, S.C., Tyagi, S.K. (2013). Exergetic analysis of solar concentrator aided coal fired super critical thermal power plant (SACSCTPT), Clean technologies and Environmental Policy, Vol 15(1), pp.133-145.

Spliethoff, H. (2010). Power Generation for Solid Fuels, Springer-Verlag Berlin Heidelberg, Germany, p.672.

Suresh, M.V.J.J., Reddy, K.S. & Kolar, A.K. (2010). 4-E (Energy, Exergy, Environment, and Economic) analysis of solar thermal aided coal-fired power plants, Energy for Sustainable Development, Vol. 14(4), pp.267-279.

Teir, S. (2002). Modern boiler types and applications, Steam boiler technology, Energy Engineering and Environmental Protection Publications, Department of Mechanical Engineering, Helsinki University of Technology, Espoo, p.15.

Teir, S. & Kulla, A. (2002). Steam/Water Circulation Design, Steam boiler technology, Energy Engineering and Environmental Protection Publications, Department of Mechanical Engineering, Helsinki University of Technology, Espoo, p.15.

Valenzuela, L., Zarza, E., Berenguel, M. & Camacho, E.F. (2005). Control concepts for direct steam generation in parabolic troughs, Solar Energy, Vol. 78(2), pp.301-311.

Valenzuela, L., Zarza, E., Berenguel, M. & Camacho, E.F. (2006). Control scheme for direct steam generation in parabolic troughs under recirculation operation mode, Solar Energy, Vol. 80(1), pp.1-17.

Vignarooban, K., Xu, X., Arvay, A., Hsu, K. & Kannan, A.M. (2015). Heat transfer fluids for concentrating solar power systems - A review, Applied Energy, Vol. 146, pp.383-396.

VTT. (2014). Project plan for Combination of Concentrated Solar Power with Circulating Fluidized Bed Power Plants – COMBO-CFB, p.26.

Wu, J., Hou, H., Yang, Y. & Hu, E. (2015). Annual performance of a solar aided coal-fired power generation system (SACPG) with various solar field areas and thermal energy storage capacity, Applied Energy, Vol. 157, pp.123-133.

Yan, Q., Yang, Y., Nishimura, A., Kouzani, A. & Hu, E. (2010). Multi-point and multi-level solar integration into a conventional coal-fired power plant, Energy and Fuels, Vol. 24(7), pp.3733-3738.

Yan, Q., Hu, E., Yang, Y. & Zhai, R. (2011). Evaluation of solar aided thermal power generation with various power plants, International Journal of Energy Research, Vol. 35(10), pp.909-922.

Yang, Y., Cui, Y., Hou, H., Guo, X., Yang, Z. & Wang, N. (2008). Research on solar aided coal-fired power generation system and performance analysis, Science in China Series E: Technological Sciences, Vol. 51(8), pp.1211-1221.

Yinghong, C., Yongping, Y. & Juan, C. (2007). Utilization of Solar Energy in a Coal-fired Plant, in: Cen, K., Chi, Y. & Wang, F. (ed.), Springer Berlin Heidelberg, pp.1207-1212.

Zarza, E., Valenzuela, L., León, J., Hennecke, K., Eck, M., Weyers, H.-. & Eickhoff, M. (2004). Direct steam generation in parabolic troughs: Final results and conclusions of the DISS project, Energy, Vol. 29(5-6), pp.635-644.

Zarza, E., Rojas, M.E., González, L., Caballero, J.M. & Rueda, F. (2006). INDITEP: The first pre-commercial DSG solar power plant, Solar Energy, Vol. 80(10), pp.1270-1276.

Zhang, H.L., Baeyens, J., Degrève, J. & Cacères, G. (2013). Concentrated solar power plants: Review and design methodology, Renewable and Sustainable Energy Reviews, Vol. 22(0), pp 466-481.

Zhu, G., Wendelin, T., Wagner, M.J. & Kutscher, C. (2014). History, current state, and future of linear Fresnel concentrating solar collectors, Solar Energy, Vol. 103(0), pp.639-652.

Web publications and web pages

Apros. (2015a). Apros in brief, web page. Available from (cited 21.7.2015): http://www.apros.fi/en/apros_in_brief_2

Apros. (2015b). Apros Overview, web publication. Available from (cited 21.07.2015): http://www.apros.fi/filebank/68-Apros_overview.pdf

Apros. (2015c). Apros for the Combustion Power Industry, web page. Available from (cited 25.09.2015): http://www.apros.fi/en/industries/combustion_power

Apros. (2015d). Apros quality and validation, web page. Available from (cited 07.01.2016): http://www.apros.fi/en/quality_validation

AREVA India. (2013). Projects, web page. Available from (cited 30.06.2015): http://india.areva.com/EN/home-1057/areva-s-solar-projects-in-india-areva-india.html

AREVA Solar. (2015a). Solar-Generated Superheated Steam for Clean, Reliable Electricity, web publication. Available from (cited 01.07.2015): http://www.areva.com/arevasolar/liblocal/docs/clean_reliable_electricity_072710.pdf

AREVA Solar. (2015b). Sundt Solar Boost Project, web publication. Available from (cited 06.07.2015): http://www.areva.com/mediatheque/liblocal/docs/activites/energ-renouvelables/pdf-TEP-ProjectSheet-Final.pdf

AREVA Solar. (2015c). Kogan Creek Solar Boost Project, web publication. Available from (cited 01.07.2015): http://www.areva.com/mediatheque/liblocal/docs/activites/energ-renouvelables/pdf-solar-kogan-creek-2011-va.pdf

Canadian Environmental Protection Act. (2012). Reduction of Carbon Dioxide Emissions from Coal-fired Generation of Electricity Regulations, 73 p, web publication. Available from (cited 10.06.2015): http://lois.justice.gc.ca/PDF/SOR-2012-167.pdf

CRA-CIN. (2009). Linke turbidity factor, web page. Available from (cited 30.11.2015): http://agsys.cra-cin.it/tools/solarradiation/help/Linke_turbidity_factor.html

CS Energy. (2015). Kogan Creek Solar Boost Project, web page. Available from (cited 14.07.2015): http://kogansolarboost.com.au/

CSP World. (2015). CSP World Map, web page. Available (cited 26.06.2015): http://www.cspworld.org/cspworldmap

DLR. (2014). The German Aerospace Center, Deutsches Zentrum für Luft- und Raumfahrt, Cologne, Germany, web publication. Available from (cited 24.07.2015): http://www.dlr.de/dlr/en/Portaldata/1/Resources/documents/2012_1/The_DLR_GB.pdf

European Commission. (2015). Climate Change, 6 p, web publication. Available from (cited 29.09.2015): http://ec.europa.eu/clima/publications/docs/factsheet_climate_change_2014_en.pdf

European Investment Bank. (2013). EIB Emission performance standard, web publication. Available from (cited 11.06.2015):http://www.eib.org/attachments/consultations/elp_methodology_emission_performance_standard_20130722_en.pdf

FRENELL. (2015). Company, web page. Available from (cited 01.01.2016): http://frenell.de/index.php?article_id=1&clang=1

Hittite Solar Energy. (2015). Power applications, web page. Available from (cited 16.07.2015): http://hittitesolarenergy.com/?page=applications

Institut für Solarforschung. (2015). Aktuelle Projekte der Abteilung Linienfokussierende Systeme DUKE, DLR, web site. Available from (cited 13.12.2015): http://www.dlr.de/sf/en/desktopdefault.aspx/tabid-7088/18782_read-43608/

Institute of Solar Research. (2015). Concentrating Solar Systems for Power, Heat and Fuel Generation, DLR, p.6, web publication. Available from (cited 24.07.2015): http://www.dlr.de/sf/en/Portaldata/73/Resources/dokumente/folder_flyer__sf/Folder_DLR_Solar_Research-EN-0814-online.pdf

International Energy Agency. (2015a). A Snapshot of global PV markets, International Energy Agency Photovoltaic Power Systems Programme (IEA PVPS), p. 16, web publication. Available from (cited 13.07.2015): http://www.iea-pvps.org/fileadmin/dam/public/report/technical/PVPS_report_-_A_Snapshot_of_Global_PV_-_1992-2014.pdf

International Energy Agency. (2015b). Technology Roadmap: Nuclear Energy – 2015 edition, International Energy Agency (IEA), France, p. 57, web publication. Available from (cited 13.8.2015): https://www.iea.org/publications/freepublications/publication/TechnologyRoadmapNuclearEnergy.pdf

International Energy Agency (2014a). Technology Roadmap: Solar Thermal Electricity - 2014 edition, International Energy Agency (IEA), France, p. 52, web publication. Available from (cited 08.07.2015): https://www.iea.org/publications/freepublications/publication/TechnologyRoadmapSolarThermalElectricity_2014edition.pdf

International Energy Agency. (2014b). Key World Energy Statistics, International Energy Agency (IEA), France, p. 81, web publication. Available from (cited 11.06.2015): http://www.iea.org/publications/freepublications/publication/KeyWorld2014.pdf

International Energy Agency. (2012). Technology Roadmap: High-efficiency, Low-Emissions Coal-Fired Power Generation, International Energy Agency (IEA), France, p. 48, web publication. Available from (cited 13.07.2015): http://www.iea.org/publications/freepublications/publication/TechnologyRoadmapHighEfficiencyLowEmissionsCoalFiredPowerGeneration_WEB_Updated_March2013.pdf

IRENA. (2015). Renewable Power Generation Costs in 2014, International Renewable Energy Agency, Germany, p. 161, web publication. Available from (cited 13.07.2015): http://www.irena.org/DocumentDownloads/Publications/IRENA_RE_Power_Costs_2014_report.pdf

Metayer, M., Breyer, C. & Fell, H.J. (2015). The projections for the future and quality in the past of the World Energy Outlook for solar PV and other renewable energy technologies, web publication. Available from (cited 01.01.2016): http://www.lut.fi/documents/10633/70751/The-projections-for-the-future-and-quality-in-the-past-of-the-World-Energy-Outlook-for-solar-PV-and-other-renewable-energy-technologies-EWG-WEO-Study-2015.pdf

National Renewable Energy Laboratory. (2013). Concentrating Solar Power Projects, web page. Available from (cited 30.06.2015): http://www.nrel.gov/csp/solarpaces/by_project.cfm

Novatec Solar. (2015a). Technology offering, web page. Available from (cited 30.06.2015): http://www.novatecsolar.com/113-1-Technology-Offering.html

Novatec Solar. (2015b). Projects, web page. Available from (cited 30.06.2015): http://www.novatecsolar.com/8-1-Projects.html

Novatec Solar. (2015c). Concentrated Solar Power by Novatec Solar, web publication. Available from (cited 05.01.2016): http://www.novatecsolar.com/40-1-Download-Centre.html

Novatec Solar. (2015d). Main webpage. Available from (cited 13.12.2015): http://www.novatecsolar.com/106-1-Start.html

Reuters. (2014). Areva's stock plunges on sales warning, solar exit, web page. Available from (cited 03.08.2015): http://in.reuters.com/article/2014/08/01/areva-results-idINL6N0Q71IK20140801

Siemens. (2011). Steam turbines for CSP plants, web publication. Available from (cited 14.12.2015): http://www.energy.siemens.com/hq/pool/hq/power-generation/steam-turbines/downloads/steam-turbine-for-csp-plants-siemens.pdf

Solar Euromed. (2015a). LFR500, web page. Available from (cited 03.07.2015): http://www.solareuromed.com/en/lfr-500

Solar Euromed. (2015b). Alba Nova 1, web page. Available from (cited 05.01.2016): http://www.solareuromed.com/en/alba-nova-1

SolarGIS. (2013). World map of direct normal irradiation, GeoModel Solar, web page. Available from (cited 16.06.2015): http://solargis.info/doc/_pics/freemaps/1000px/dni/SolarGIS-Solar-map-DNI-World-map-en.png

SolarPACES. (2015). CSP Projects Around the World, web page. Available from (cited 26.6.2015): http://www.solarpaces.org/csp-technology/csp-projects-around-the-world

The United States Environmental Protection Agency. (2014a). Carbon Pollution Emission Guidelines for Existing Stationary Sources: Electric Utility Generating Units, pp. 34829-34958, web publication. Available from (cited 09.06.2015): http://www.gpo.gov/fdsys/pkg/FR-2014-06-18/pdf/2014-13726.pdf

The United States Environmental Protection Agency. (2014b). Standards of Performance for Greenhouse Gas Emissions From New Stationary Sources: Electric Utility Generating Units, pp. 1429-1519, web publication. Available from (cited 10.06.2015): http://www.gpo.gov/fdsys/pkg/FR-2014-01-08/pdf/2013-28668.pdf

United Nations. (2015). Historic Paris Agreement on Climate Change, Framework Convention on Climate Change, web page. Available from (cited 21.12.2015): http://newsroom.unfccc.int/unfccc-newsroom/finale-cop21/

Tucson. (2014). TEP's Sundt power plant getting 'solar boost', web page. Available from (cited 01.01.2016): http://tucson.com/business/local/tep-s-sundt-power-plant-getting-solar-boost/article_7d74b3f6-b5bb-57a4-b7f6-876ff31d965f.html

Tucson Electric Power. (2016). AREVA System to Boost TEP’s Solar Portfolio, web page. Available from (cited 01.01.2016): https://www.tep.com/news/pluggedin/areva/

Tucson local media. (2014). TEP steam booster nears completion with installation of ‘solar receiver’, web page. Available from (cited 04.01.2016): http://www.tucsonlocalmedia.com/business/article_40465470-3dfa-11e4-94a3-970b49dc68e8.html

VTT. (2015a). VTT in figures, web page. Available from (cited 24.07.2015): http://www.vttresearch.com/about-us

VTT. (2015b). General brouchure, web publication. Available from (cited 24.07.2015): http://www.vttresearch.com/Documents/vtt_about_us/presentation_material/vtt_general_brochure_english.pdf

VTT. (2015c). Future technologies and systems for renewable energy, web page. Available from (cited 24.07.2015): http://www.vttresearch.com/services/low-carbon-energy/future-energy-systems/future-technologies-and-systems-for-renewable-energy

World Energy Council. (2013). World Energy Perspective Cost of Energy Technologies. World Energy Council, London, United Kingdom, p. 48, web publication. Available from (cited 25.6.2015): http://www.worldenergy.org/publications/2013/world-energy-perspective-cost-of-energy-technologies/

APPENDIX A: THE CHARACTERISTICS OF CSP AND CONVENTIONAL POWER PLANT HYBRIDS 1/2 (ADAPTED FROM CSP WORLD 2015)

Name	Status	Power (MW_e)	Technology	Purpose	Country	Usage	HTF
Agua Prieta II ISCC	Under construction	12.0	Parabolic trough - ISCC	Commercial	Mexico	Electricity	Thermal Oil
Aïn Beni Mathar ISCC	Operational	20.0	Parabolic trough - ISCC	Commercial	Morocco	Electricity	Thermal Oil
Al Abdaliyah Integrated Solar Combined Cycle (ISCC)	Development	60.0	Parabolic trough - ISCC	Commercial	Kuwait	Electricity	N/A
Archimede	Operational	5.0	Parabolic trough - ISCC	Research & Development	Italy	Electricity	Molten Salt
Cameo	Decommissioned	2.0	Parabolic trough - Coal	Commercial	US	Steam generation	Thermal Oil
Collinsville Hybrid CSP-gas project	Planned	30.0	Linear Fresnel - ISCC	Commercial	Australia	Elecricity	N/A
El Borma ISCC	Planned	5.0	Tower - ISCC	Commercial	Tunisia	Electricity	N/A
Hassi R'mel ISCC	Operational	25.0	Parabolic trough - ISCC	Commercial	Algeria	Electricity	Thermal Oil
Kogan Creek	Under construction	44.0	Linear Fresnel - Coal	Commercial	Australia	Steam generation	Water
Kuraymat ISCC	Operational	20.0	Parabolic trough - ISCC	Commercial	Egypt	Electricity	Thermal Oil
Liddell Power Station	Operational	6.0	Linear Fresnel - Coal	Commercial	Australia	Steam generation	Water

APPENDIX A: THE CHARACTERISTICS OF CSP AND CONVENTIONAL POWER PLANT HYBRIDS 2/2 (ADAPTED FROM CSP WORLD 2015)

Name	Status	Power (MW_e)	Technology	Purpose	Country	Usage	HTF
Martin Next Generation Solar Energy Center	Operational	75.0	Parabolic trough - ISCC	Commercial	US	Electricity	Thermal Oil
Medicine Hat ISCC	Operational	1.0	Parabolic trough - ISCC	Commercial	Canada	Electricity	N/A
Ningxia ISCC	Under construction	92.0	Parabolic trough - ISCC	Commercial	China	Electricity	N/A
Palmdale Hybrid Power Plant	Planned	50.0	Parabolic trough - ISCC	Commercial	US	Electricity	Thermal Oil
PTC50 Alvarado	Development	50.0	Central receiver (power tower) - Biomass	Demonstration	Spain	Electricity	Water
Sundt Solar Boost	Development	5.0	Linear Fresnel – ISCC/Coal [1,2]	Commercial	US	Electricity	Water [1,2]
Termosolar Borges	Operational	22.5	Parabolic trough - Biomass	Commercial	Spain	Electricity	Thermal Oil
Victorville 2 Hybrid Power Plant	Planned	50.0	Parabolic trough - ISCC	Commercial	US	Electricity	N/A
Yazd ISCC	Operational	17.0	Parabolic trough - ISCC	Commercial	Iran	Electricity	N/A

[1] (AREVA Solar 2015b)

[2] (Tucson 2014)

APPENDIX B: WORLD MAP OF DIRECT NORMAL IRRADIATION (SOLARGIS 2013)

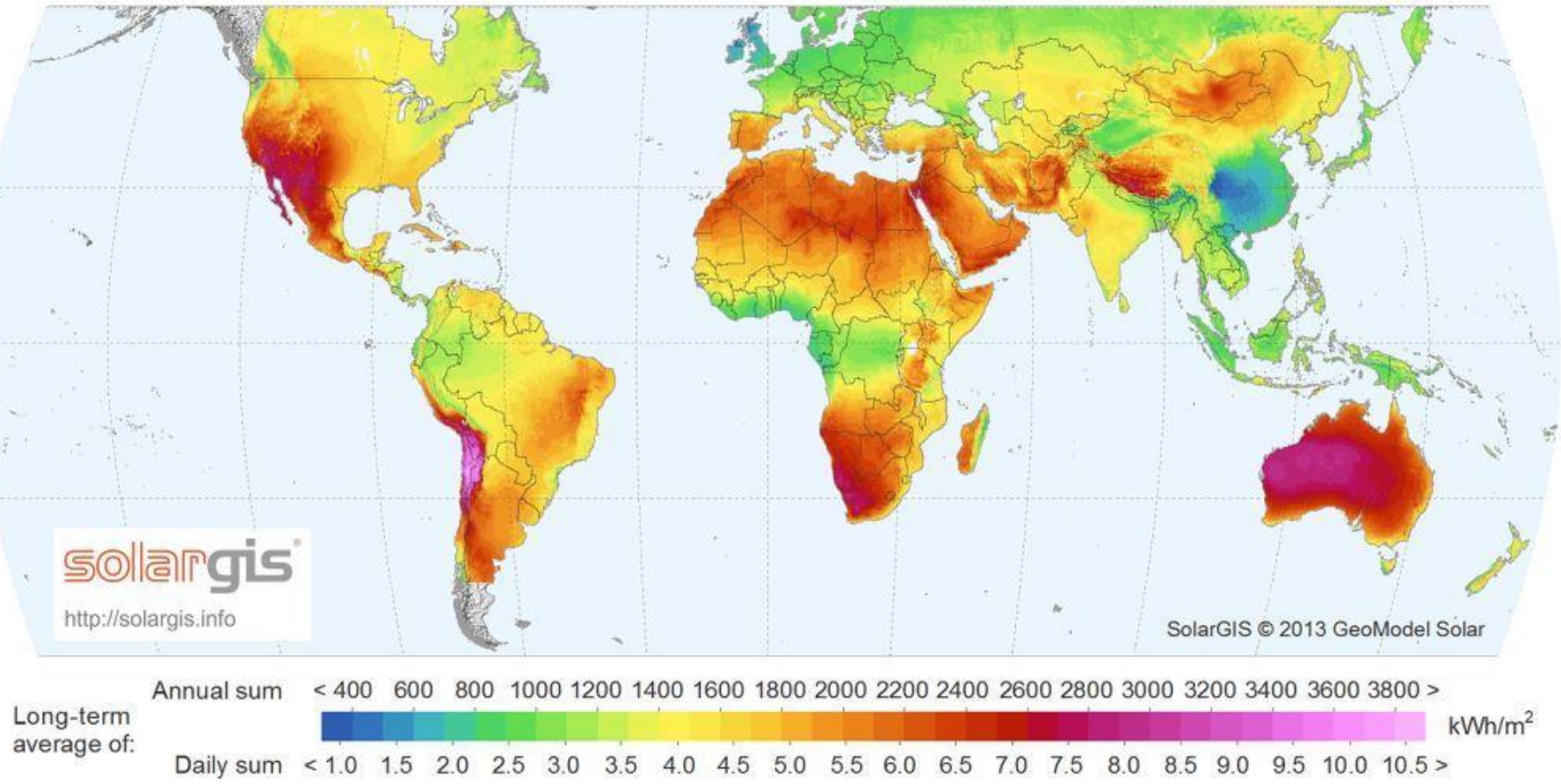

APPENDIX C: WORLD MAP OF CSP PROJECTS IN JUNE 2015 (SOLARPACES 2015)

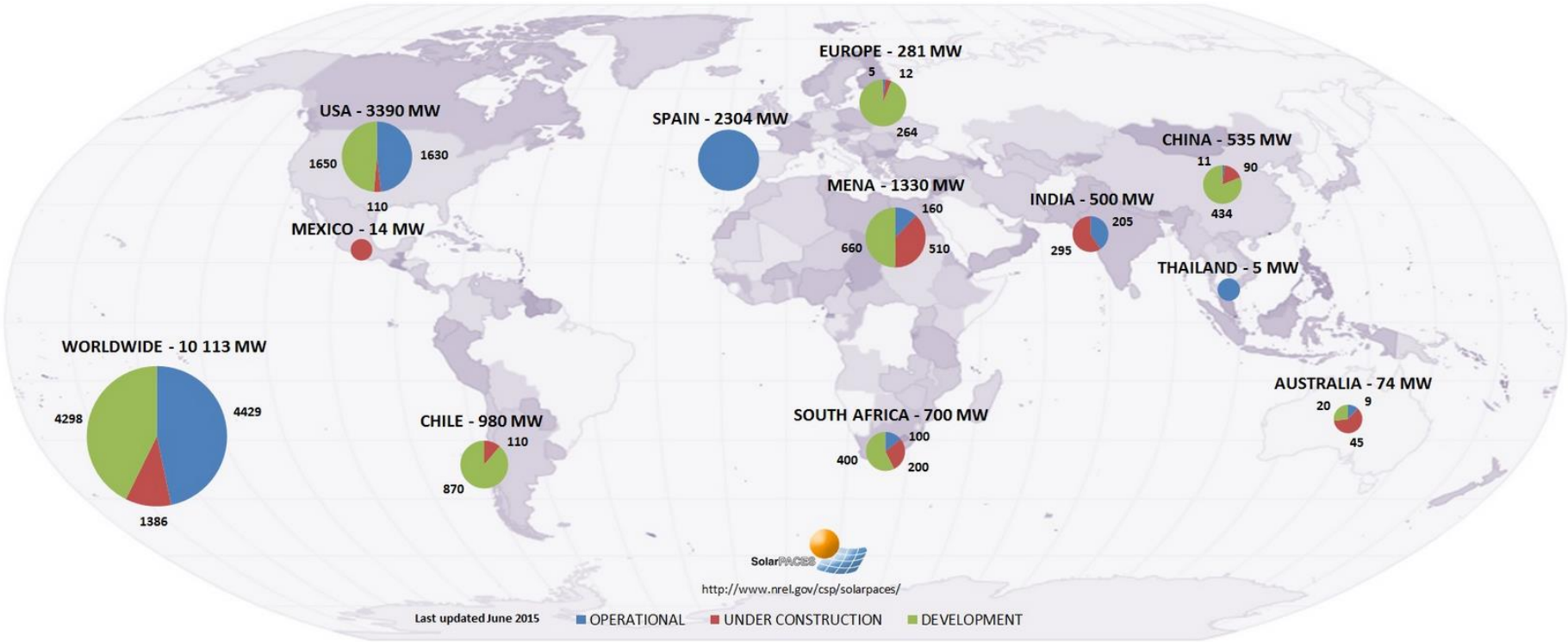

APPENDIX D: THE CHARACTERISTICS OF OPERATIONAL DSG PLANTS WITH PTC COLLECTORS (ADAPTED FROM CSP WORLD 2015)

Name	**Status**	**Power (MW_e)**	**Application**	**Country**	**Usage**	**Solar Field Inlet Temperature (°C)**	**Solar Field Outlet Temperature (°C)**	**Power cycle pressure (bar)**	**Electricity generation (MWh/year)**	**Storage and capacity**	**Cooling**
DISS facility [1]	Operational [1]	-	Research & Development [1]	Spain [1]	Test facility	260	500 [1]	110 [1]	-	-	Dry
Eureka GDV	Operational	8	Research & Development	Spain	Electricity	N/A	550	N/A	N/A	N/A	N/A
TSE1	Operational	5	Commercial	Thailand	Electricity	201 [2]	340 [2]	30 [2]	8 000 [2]	No [2]	Wet

[1] (Feldhoff et al. 2014)

[2] (National Renewable Energy Laboratory 2013)

APPENDIX E: THE CHARACTERISTICS OF OPERATIONAL AND UNDER CONSTRUCTION DSG PLANTS WITH LFR COLLECTORS. ADAPTED FROM NATIONAL RENEWABLE ENERGY LABORATORY 2013

Name	Status	Power (MW_e)	Application	Country	Usage	Feedwater Inlet Temperature (°C)	Solar Field Outlet Temperature (°C)	Power cycle pressure (bar)	Electricity generation (MWh/year)	Storage and capacity	Cooling
Alba Nova 1	Under construction	12	Commercial	France	Electricity	N/A	500	65	25 000 (Estimated)	Ruths Tank, 1h	Dry
Dhursar	Under construction	250 [1]	Commercial	India	Electricity	N/A	390 [1]	90 [1]	280 000 (Expected)	No	Wet
Kimberlina	Operational	5	Demonstration	US	Electricity	N/A	300	40	N/A	No	N/A
Kogan Creek	Under construction	44	Commercial	Australia	Steam generation	186	370	60	440	No	Dry
Liddell Power Station	Operational	6 [2]	Commercial	Australia	Steam generation	140	270	55	13 550	No	Dry
Puerto Errado 1	Operational	1	Prototype [2]	Spain	Electricity	140	500 [3]	55 [3]	2 000	Ruths Tank, 0.5h [4]	Dry [3]
Puerto Errado 2	Operational	30	Commercial	Spain	Electricity	140	270 [3]	55 [3]	50 000	Ruths Tank, 0.5h [4]	Dry [3]

[1] (AREVA India 2013)

[2] (CSP World 2015)

[3](Novatec Solar 2015b)

APPENDIX F: THE THERMAL BALANCE INFORMATION OF SUBCRITICAL 210 MW_e, 330 MW_e 500 MW_e UNITS (SENGUPTA ET AL. 2007, p.19; PENG ET AL. 2014, p.850; SURESH ET AL. 2010, p.272)

Size of the unit	**210 MW_e**	**330 MW_e**	**500 MW_e**	**210 MW_e**	**330 MW_e**	**500 MW_e**
Stream	**Pressure (bar)**			**Temperature (°C)**		
Live steam	150.00	167.00	166.70	537.00	538.00	537.00
After HP turbine	39.20	38.57	44.10	342.66	329.70	339.40
Reheated steam	34.94	34.72	39.70	537.00	538.00	537.00
After IP turbine	6.84	N/A	7.30	307.31	N/A	303.30
After LP turbine	0.10	0.15	0.10	46.39	53.97	46.40
Bled steam into HP FWH3	-	57.11	-	-	380.10	-
Bled steam into HP FWH2	39.20	38.57	44.10	342.66	329.70	339.40
Bled steam into HP FWH1	16.23	19.56	17.40	424.10	451.00	416.10
Bled steam into LP FWH3	2.30	5.90	2.60	192.20	290.80	192.60
Bled steam into LP FWH2	0.84	2.56	1.30	102.07	208.00	132.10
Bled steam into LP FWH1	0.22	0.80	0.26	61.63	106.00	65.80
After the condensate pump	16.07	17.24	7.30	46.15	54.00	46.50
After the feedwater pump	170.00	167.00 [1]	193.70	161.86	182.70	170.20
Before the economizer	168	167.00 [1]	193.70 [1]	244.98	272.1	253.2

Size of the unit	**210 MW_e**	**330 MW_e**	**500 MW_e**	**210 MW_e**	**330 MW_e**	**500 MW_e**
Stream	**Enthalpy (kJ/kg)**			**Mass flow (kg/s)**		
Live steam	3414.99	3398.62	3396.13	173.00	287.39	425.80
After HP turbine	3076.84	3045.53	3056.20	173.00	270.21	380.50
Reheated steam	3535.45	3537.94	3530.77	155.38	243.28	380.50
After IP turbine	3075.20	N/A	3065.66	524.69	N/A	316.90
After LP turbine	2465.62	2441.80	194.29	120.23	191.35	271.25
Bled steam into HP FWH3	-	3132.44	-	-	17.18	-
Bled steam into HP FWH2	3076.84	3045.53	3056.20	17.62	26.94	45.30
Bled steam into HP FWH1	3306.72	3360.83	3287.57	9.63	10.05	21.00
Bled steam into LP FWH3	2853.53	3043.19	2852.80	7.33	11.16	12.20
Bled steam into LP FWH2	2682.14	2884.37	2738.22	7.87	12.00	23.30
Bled steam into LP FWH1	2494.23	2690.61	2618.96	8.23	13.44	10.20
After the condensate pump	194.63	227.52	195.33	137.93	228.34	335.50
After the feedwater pump	693.30	783.10 [2]	730.51	173.28	287.39	425.80
Before the economizer	1062.65	1192.76 [2]	1101.55 [2]	173.28	287.39	425.80

[1] The value should be higher because of the pressure loss in the FWHs and boiler.

[2] The value should be lower due to higher pressure.

APPENDIX G: THE ADVANTAGES AND DISADVANTAGES OF DIFFERENT PROCESS ARRENGEMENTS 1/2

Process arrangement	Advantages	Disadvantages
FWHFL	- Most studied process arrangement - Flexible - Least invasive, no complex boiler integration and associated extra costs - Guarantees the steady function of power plant if existing FWHs are operated parallel	- Only heated water can be injected - Full potential of the state-of-the-art line-focusing collectors with DSG is not fulfilled. - Promotes the least steps towards stand-alone CSP plants - In the power boost mode the maximum solar share is limited by the maximum capacities of turbines and FWHs - In the fuel saving mode, the maximum solar share is limited by the capacities of FWHs
FWHBOS	- Same advantages as above - Applied at Liddell Power Station - Superheated steam can be injected	- Full potential of the state-of-the-art line-focusing collectors with DSG is not fulfilled - If multiple FWHs are replaced, the solar field has to produce steam at multiple enthalpy levels - In the power boost mode the maximum solar share is limited by the maximum capacities of turbines and FWHs - In the fuel saving mode, the maximum solar share is limited by the capacities of FWHs
SuSCRH	- The steam parameters are readily achievable with current line-focusing collectors with DSG - Applied at Kogan Creek - Short term goal for CSP and steam power plant hybrids	- Full potential of the state-of-the-art line-focusing collectors with DSG is not fulfilled In the power boost mode, the maximum solar share is limited by the capacities of the reheaters and turbine - In the fuel saving mode the maximum solar share is limited by the partial load of the boiler, which guarantees the operation of the HP turbine and reheaters and by maximum load of the IP and LP turbine sections - The net efficiency of the power plant is lower than if the solar steam is expanded in the HP turbine - Increased or decreased mass flow through part of the system can result a disturbance in balance between different heating surfaces and between the HP and other turbine sections
SuSHP	- Full potential of state-of the-art line-focusing collectors with DSG can be fulfilled in near future - Long term goal in the development of CSP and steam power plant hybrids - Promotes the most steps towards the stand-alone CSP power plants	- The quality of solar steam needs to be assured. - Development of sophisticated control strategy for the solar field and steam power plant. - In power boost mode, the maximum solar share is limited by the capacities of turbine sections and the reheaters - In fuel saving mode, the maximum solar share is limited by the partial load of the boiler, which guarantees the thermal performance of the reheaters

APPENDIX G: THE ADVANTAGES AND DISADVANTAGES OF DIFFERENT PROCESS ARRENGEMENTS 2/2

Process arrangement	Advantages	Disadvantages
SuSIP	- The steam parameters are achievable with PTCs - Maybe better balance for boiler compared to SuSCRH and SuSHP as the solar steam is injected after the boiler and reheater - Medium term goal in the development of CSP and steam power plant hybrids	- Maybe a little bit disadvantageous for solar field as the superheating of solar steam is around 290 °C - In power boost mode the maximum solar share is limited by the maximum capacities of IP and LP turbine sections - In the fuel saving mode, the maximum solar share is limited by the minimum partial load of the boiler and by the possible balance limit between HP and other turbine sections. - The net efficiency of the power plant is decreased, as the solar steam is not expanded in the HP turbine
SaSBD	- Superheater assures the quality of live steam if the boiler is operated with adequate load	- Full potential of the state-of-the-art line-focusing collectors with DSG is not fulfilled - Only saturated steam is produced - In the power boost mode, the maximum solar share is limited by the maximum capacities of turbine. - In the fuel saving mode, the maximum solar share is limited by the minimum partial load of the boiler, which guarantees the thermal performance of superheater and reheater.
SaSBDFWH	- Superheater assures the quality of live steam if the boiler is operated with adequate load	- Full potential of the state-of-the-art line-focusing collectors with DSG is not fulfilled - Only saturated steam is produced - In the power boost mode, the maximum solar share is limited by the maximum capacities of the turbines - In the fuel saving mode, the maximum solar share is limited by the minimum partial load of the boiler which guarantees the thermal performance of superheater and reheater

APPENDIX H: STATE POINT DATA OF FWHs AND STEAM BOILER AND SCHEMATIC OF THE STEAM CYCLE IN 150 MW_e POWER PLANT

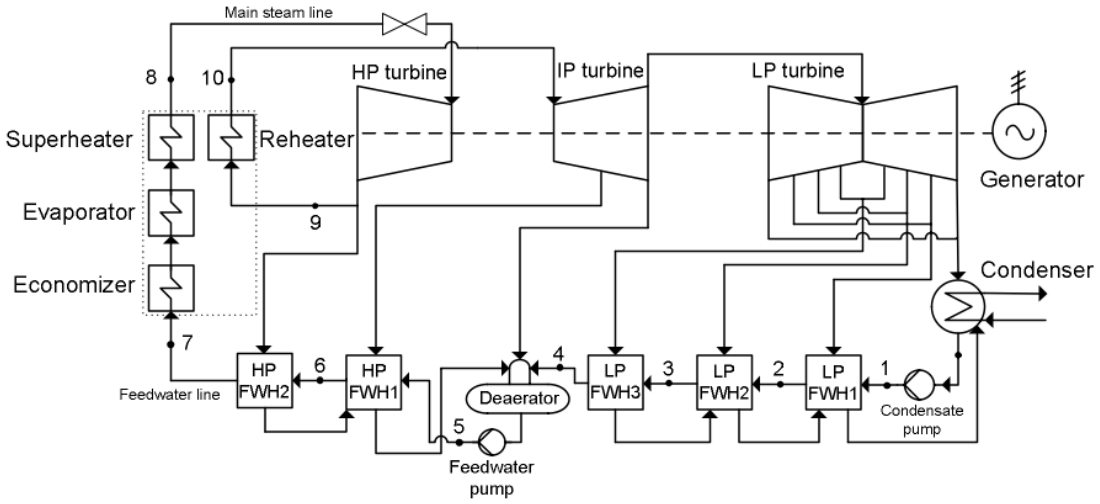

Figure 69. *Schematic of 150 MW_e Touss steam power plant.*

Table 29. *State point data of 150 MW_e Touss steam power plant and calculated thermal powers. Adapted from Farhad et al. 2008, p.6-7.*

State point [Figure 69]	Pressure [bar]	Temperature [°C]	Enthalpy [kJ/kg]	Mass flow [kg/s]	Energy flow [MW]
1	10.0	67.6	283.8	112.9	32.0
2	8.7	92.6	388.5	112.9	43.9
3	7.3	132.4	556.9	112.9	62.9
4	7.3	166.8	705.2	112.9	79.6
5	174.9	170.3	729.9	137.4	100.3
6	173.4	206.8	889.3	137.4	122.2
7	172.0	240.5	1041.9	137.4	143.2
8	127.5	538.0	3442.5	137.4	473.0
9	36.5	361.7	3129.9	127.9	400.3
10	32.5	537.4	3538.8	127.9	452.6

Component	Energy flow in [MW]	Energy flow out [MW]	Thermal power [MW_{th}]
Economizer + evaporator + superheater	143.2	473.0	329.8
Reheaters	400.3	452.6	52.3
Total steam boiler			382.1
LP FWH1	32.0	43.9	11.83
LP FWH2	43.9	62.9	19.01
LP FWH3	62.9	79.6	16.74
HP FWH1	100.3	122.2	21.90
HP FWH2	122.2	143.2	20.97

APPENDIX I: EXAMPLE OF THE PROCESS COMPONENT LEVEL AND CALCULATION LEVEL IN APROS (APROS TRAINING COURSE MATERIAL 2015)

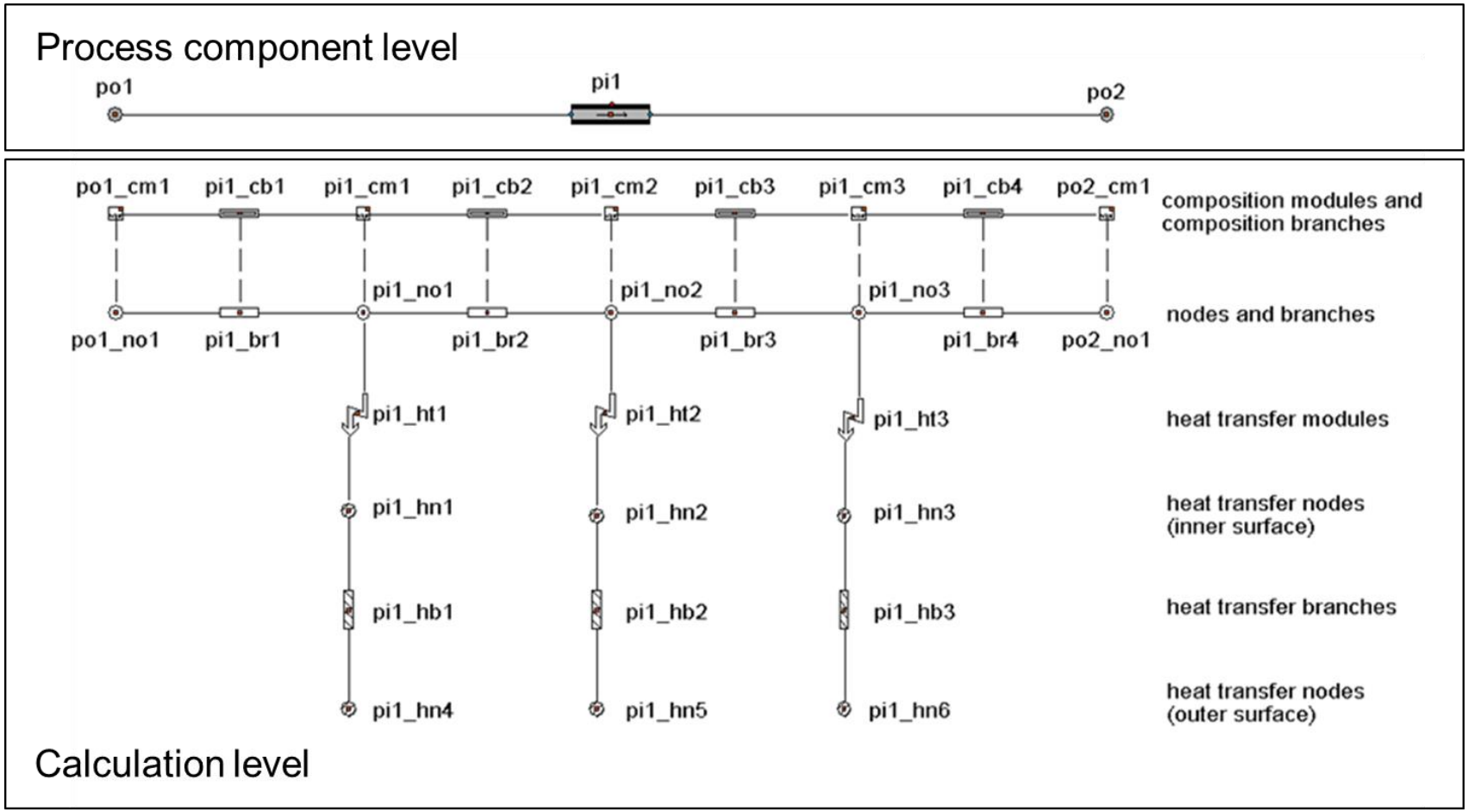

APPENDIX J: RESULTS OF FOUR STEADY STATE SIMULATION CASES CONDUCTED WITH APROS 1/2

Table 30. *Steady state results of the overall operation of the hybrid.*

Case number	**1**	**2**	**3**	**4**
Number of collector rows	7	15	7	10
Thermal solar share [%]	9.5	21.2	11.3	15.4
Power output of the turbines [MW]	147.6	147.6	124.6	134.2
Turbine load [%]	110.0	110.0	92.9	100.0
Steam boiler load [%]	96.6	80.9	79.4	79.6
Fuel power of steam boiler [MW]	392.9	328.8	322.7	323.6
Thermal power of solar field [MW_{th}]	41.3	88.5	41.3	59.0
Total heat input to hybrid plant [MW]	434.3	417.3	364.1	382.6
Thermal efficiency [%]	34.0	35.4	34.2	35.1

Table 31. *Steady state results from the combustion process.*

Case number	**1**	**2**	**3**	**4**
Fuel mass flow [kg/s]	28.4	23.9	23.5	23.6
Primary air flow [kg/s]	190.2	159.2	156.3	156.7
Secondary air flow [kg/s]	65.6	54.9	53.9	54.0
Flue gases mass flow [kg/s]	284.4	238.1	233.7	234.3
Flue gases initial temperature [°C]	889.7	834.8	828.3	829.6
Flue gases final temperature [°C]	171.9	164.6	162.7	163.7

Table 32. *Steady state results from the operation of superheaters and HP turbine.*

Case number	**1**	**2**	**3**	**4**
Live steam temperature of steam boiler [°C]	550.0	550.0	550.0	548.4
Live steam pressure of steam boiler [bar]	145.1	145.1	145.1	145.1
Live steam temperature of solar field [°C]	550.0	550.0	550.0	550.0
Live steam pressure of solar field [bar]	160.0	160.0	160.0	160.0
Steam temperature after outlet throttle of solar field [°C]	541.3	542.4	533.7	542.5
Steam pressure after outlet throttle of solar field [bar]	138.9	141.8	120.5	142.3
Steam temperature at connection point before HP turbine [°C]	546.6	546.9	539.0	547.4
Steam pressure at connection point before HP turbine [bar]	138.8	141.8	120.4	141.8
Steam mass flow from solar field [kg/s]	14.7	31.4	14.7	21.0
Steam mass flow from steam drum [kg/s]	101.4	92.8	90.7	91.7
Superheating spray water mass flow of steam boiler [kg/s]	5.1	0.1	0.1	0.0
Overall steam mass flow to HP turbine [kg/s]	121.3	124.3	105.4	112.7

APPENDIX I: RESULTS OF FOUR STEADY STATE SIMULATION CASES CONDUCTED WITH APROS 2/2

Table 33. *Steady state results from the operation of reheaters and IP turbine.*

Case number	**1**	**2**	**3**	**4**
Steam temperature before reheaters [°C]	362.6	357.8	354.6	352.6
Steam pressure before reheaters [bar]	40.1	39.5	33.9	37.8
Reheated steam temperature [°C]	549.7	549.7	549.7	549.7
Reheated steam pressure [bar]	37.9	37.1	32.0	36.0
Reheated steam mass flow to IP turbine [kg/s]	123.8	121.0	104.0	109.8
Steam mass flow from HP turbine [kg/s]	116.7	120.6	101.8	108.7
Reheating spray water mass flow [kg/s]	7.1	0.4	2.2	1.1

Table 34. *Steady state results from the operation of steam drum, economizer, HP FWHs, deaerator, LP FWHs and condenser.*

Case	**1**	**2**	**3**	**4**
Steam temperature at steam drum [°C]	347.3	346.5	346.4	346.4
Steam pressure at steam drum [bar]	153.9	152.2	151.9	152.0
Steam fraction at the end of steam drum	0.20	0.18	0.18	0.18
Feedwater temperature after economizer [°C]	320.7	312.2	308.9	310.8
Feedwater pressure after economizer [bar]	154.1	152.4	152.1	152.2
Feedwater temperature before economizer [°C]	245.4	245.6	237.1	243.2
Feedwater pressure before economizer [bar]	164.1	160.9	160.2	160.5
Feedwater temperature before HP FWHs [°C]	141.6	140.9	140.9	144.4
Feedwater pressure before HP FWHs [bar]	168.7	164.9	164.1	164.5
Feedwater temperature after deaerator [°C]	138.8	138.2	138.2	141.6
Feedwater pressure after deaerator [bar]	10.2	10.2	9.2	10.2
Overall mass flow from deaerator [kg/s]	128.3	125.1	107.6	113.9
Feedwater mass flow to solar field [kg/s]	14.7	31.8	14.7	21.1
Feedwater mass flow to attemperators [kg/s]	12.2	0.5	2.3	1.1
Feedwater mass flow to HP FWHs [kg/s]	101.4	92.8	90.7	91.7
Feedwater temperature before LP FWHs [°C]	44.5	44.5	45.1	44.8
Feedwater pressure before LP FWHs [bar]	13.3	13.2	12.0	12.7
Feedwater mass flow to LP FWHs [kg/s]	110.4	108.6	93.3	98.8
Steam temperature before condenser [°C]	54.0	54.0	54.1	54.0
Steam pressure before condenser [bar]	0.15	0.15	0.15	0.15
Steam mass flow to condenser [kg/s]	94.0	92.9	80.0	84.0
Steam fraction before condenser [-]	0.961	0.962	0.970	0.963